Dalton Transactions

PERSPECTIVE

Cite this: *Dalton Trans.*, 2016, **45**, 4935

The main progress over the past decade and future outlook on high-nuclear transition-metal substituted polyoxotungstates: from synthetic strategies, structural features to functional properties

Xing Ma, Hailou Li, Lijuan Chen* and Junwei Zhao*

Received 25th December 2015,
Accepted 6th February 2016

DOI: 10.1039/c5dt05020k

www.rsc.org/dalton

Currently, transition-metal substituted polyoxotungstates (TMSPTs) have developed as a fast growing and challengeable subfamily of polyoxometalates (POMs). Before 2005, the number of TM cores in TMSPTs was mostly lower than five. Since 2005, numerous inorganic or organic–inorganic TMSPTs with more than five TM cores (denoted as high-nuclear TMSPTs) have continuously been excavated and investigated. In this perspective, we endeavor to discuss the synthetic methodologies, structural diversities and relevant properties of the high-nuclear TMSPTs reported in the past decade. Future perspectives and opportunities on TMSPTs are included in the last section. This review is meant to provide fodder and guidance for further exploration and discovery of more high-nuclear TMSPTs with innovative architectures and remarkable functionality.

1. Introduction

The gate of polyoxometalate (POM) chemistry was first opened by a groundbreaking discovery of molybdenum blue that was obtained by the famous Swedish chemist Scheele in 1778.[1] Then after nearly half a century, the discovery of the first textbook example $(NH_4)_3[P\ Mo_{12}O_{40}]\cdot nH_2O$ greatly stimulated the developmental pace of POM chemistry, which is one of the most significant milestones in the history of POM discipline.[2] POMs, an unique and remarkable class of anionic metal–oxide clusters, are generated from the condensation of $\{MO_x\}$ polyhedra in the edge-, corner-, face-sharing fashions, where M generally represents the early transition-metal (TM) atoms in their d^0 or d^1 electronic configurations (usually Mo^V, Mo^{VI}, W^{VI}, V^V, Nb^V or Ta^V).[3]

The oxygen-enriched surfaces of POMs especially for lacunary POM fragments endow them with excellent nucleophilic

Henan Key Laboratory of Polyoxometalate Chemistry, Institute of Molecular and Crystal Engineering, College of Chemistry and Chemical Engineering, Henan University, Kaifeng, Henan 475004, P. R. China. E-mail: ljchen@henu.edu.cn, zhaojunwei@henu.edu.cn; Fax: (+86) 371 23881589

Xing Ma

Xing Ma was born in Anhui, China in 1995 and is pursuing her BS degree in chemistry at Henan University. In 2013, she began to conduct the scientific research in the group of Prof. Junwei Zhao in Henan Key Laboratory of Polyoxometalate Chemistry. Her current research interest is focused on the preparation, luminescent and magnetic properties of lanthanide-containing polyoxotungstate materials.

Hailou Li

Hailou Li was born in Henan Province, China. Currently, he is pursuing his MS degree at Henan University under the supervision of Prof. Junwei Zhao in Henan Key Laboratory of Polyoxometalate Chemistry. His research interest is focused on the synthesis, structures and relevant properties of high-nuclear transition-metal and multi-nuclear rare-earth encapsulated nanosized poly(polyoxotungstate) aggregates.

ability to chelate and capture extraneous metal ions constructing new materials with different structural dimensionality and potential functionality in various fields such as catalysis, magnetism, medicine, photochemistry and materials science.[4] In the meantime, POM chemistry can also integrate with other disciplines (such as nanotechnology,[5a] colloid science,[5b] supramolecular materials,[5c,d] electronic materials,[5e] molecular materials,[5f] biology,[5g] surfaces,[5h] sensors,[5i–j] *etc.*), giving rise to new multi-discipline areas of research.[6] Among the library of the second metal substituted POMs, TM substituted polyoxotungstates (TMSPTs) have become an important subclass since a mono-Co^{II} substituted Keggin tungstosilicate was firstly reported by Baker and co-workers at the 1962 (Stockholm) International Conference on Coordination Chemistry.[7] Therewith, intensive and extensive research interests were persistently devoted to this field because of the size, shape, composition, solubility, magnetism, catalysis and redox potential of TMSPTs are relatively flexible and easily fine-tuned by the elaborate design and selection of TM cations and polyoxotungstate (POT) building units. The constantly emerging large number of novel TMSPT species entails that studies on TMSPTs always occupy the forefront of research in the POM discipline.[8]

The conventional aqueous solution synthesis method (CASSM) (ambient pressure, $T < 100$ °C) and the hydrothermal synthesis method (HSM) are two major synthetic methodologies in the design and synthesis of intriguing TMSPTs. Undoubtedly, CASSM have won researchers' favor in the preparation of TMSPTs due to its numerous merits such as the lower requirements of temperature and pressure, higher collision probability of chemical components in such homogeneous system and high-quality crystals generated from the slow evaporation process. Simultaneously, HSM also displays uncompromising momentum in synthetic chemistry as the high temperature and pressure could not only increase the solubility of chemical components but also drive the shift of a chemical reaction from a thermodynamically-controlled process to a dynamically-controlled process and facilitate the desired products. Thus, HSM has been developed as a very effective method in synthesizing novel inorganic–organic hybrid TMSPTs since Yang *et al.* communicated the first series of inorganic–organic hybrid Ni_6-substituted POTs through HSM in 2007.[9] Apart from the outlining aspects, some reaction variables are of great importance during the synthetic processes: (a) the molar ratio of reactants, (b) pH, (c) ionic strength, (d) reducing agent, (e) inducing of functional organic ligands, (f) temperature of reaction and crystallization.[10] From the viewpoint of synthetic strategies, two types of main synthetic strategies can be used during the course of exploring TMSPTs: (a) the step-by-step reaction strategy of preformed lacunary POM precursors reacting with TM ions or preformed TM clusters reacting with simple oxometalate (Na_2WO_4) or preformed lacunary POM precursors reacting with preformed TM clusters; (b) the one-pot self-assembly reaction strategy of simple Na_2WO_4, TM ions and other components. In the exploration of TMSPTs, the step-by-step reaction strategy is principally chosen by researchers because the preformed POM clusters or TM clusters can work as templates and induce the construction of TMSPTs although some TMSPTs were obtained through a one-pot self-assembly strategy. Here, some typical stable and metastable lacunary POTs precursors are worthy of listing: (a) monolacunary precursors: $[\alpha\text{-}XW_{11}O_{39}]^{7/8-}$ (X = P^V, Si^{IV}, Ge^{IV}) and $[\alpha\text{-}P_2W_{17}O_{61}]^{10-}$;[11a] (b) dilacunary precursors: $[\gamma\text{-}XW_{10}O_{36}]^{7/8-}$ (X = P^V, Si^{IV}, Ge^{IV}),[11b–d] $[As_2W_{19}O_{67}(H_2O)]^{14-}$;[11e] (c) trilacunary precursors: $[\alpha\text{-}XW_9O_{34}]^{9/10-}$ (X = P^V, As^V, Si^{IV}, Ge^{IV}),[11f,g] $[\alpha\text{-}XW_9O_{33}]^{8/9-}$ (X = Te^{IV}, As^{III}, Sb^{III}, Bi^{III}),[11h–k] and $[\alpha\text{-}P_2W_{15}O_{56}]^{12-}$;[11l] (d) multilacunary precursors: the metastable

Lijuan Chen

Lijuan Chen was born in Henan, China. She gained her BS and MS degrees in chemistry from Henan University (2005) and obtained her PhD under the supervision of Prof. Jianmin Chen at Lanzhou Institute of Chemical Physics, Chinese Academy of Sciences (2009). In 2009, she joined Henan University and was appointed as a lecturer. In 2013, she was promoted to an associate professor. Since April 2014, she has been working with Prof. Jingyang Niu as a postdoctoral fellow in Henan University. Her research interest is focused on coordination chemistry and photophysical properties of polyoxometalate-based materials.

Junwei Zhao

Junwei Zhao obtained the BS degree in chemistry in 2002 and gained his MS degree under the supervision of Prof. Jingyang Niu in 2005 from Henan University. In 2008, he received his PhD under the supervision of Prof. Guo-Yu Yang at Fujian Institute of Research on the Structure of Matter, Chinese Academy of Sciences. After that, he joined the faculty of Henan University, was promoted to a full professor in chemistry in 2014 and was ranked as an academic leader of Department of Education of Henan Province and a Science & Technology Innovation Talent in the universities of Henan Province in 2015. He is mainly engaged in the synthesis and preparative chemistry of polyoxometalate-based functional materials and the relevant optical, electrical, magnetic and medical properties.

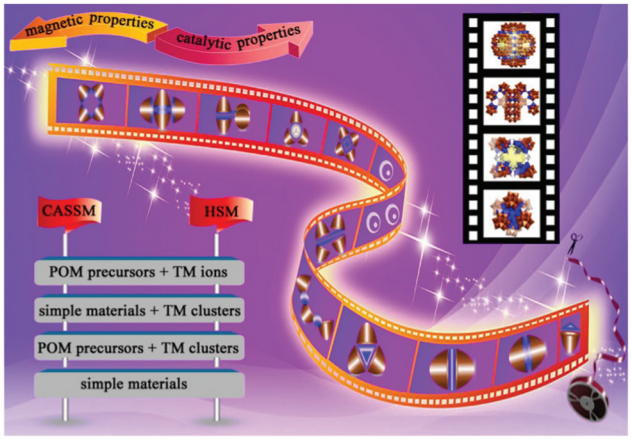

Fig. 1 Schematic summary of TMSPTs involving the main synthetic methodologies, structural diversities and relevant properties.

hexalacunary Wells–Dawson polyoxoanion (POA) $[\alpha\text{-}H_2P_2W_{12}O_{48}]^{12-}$;[11m] the D_{4h} symmetric $[H_7P_8W_{48}O_{184}]^{33-}$ POA,[11n] and the D_{3h} symmetric $[NaSb_9W_{21}O_{86}]^{18-}$ POA.[11o] Moreover, the above mentioned lacunary POT precursors can further isomerize and degrade to their derivative fragments to participate in the construction of TMSPTs. The most changeable precursor is the dilacunary precursor $[\gamma\text{-}XW_{10}O_{36}]^{8-}$ (X = Si^{IV}, Ge^{IV}) and a detailed discussion will be involved in the following part.

Before 2005, the number of TM cores encapsulated in TMSPTs was mostly lower than five, which can be named as low-nuclear TMSPTs. Here, these research achievements on low-nuclear TMSPTs are not repeated. After 2005, numerous TMSPTs with the number of TM cores greater than five were constantly discovered, which can be denoted as high-nuclear TMSPTs. In this review, we will concentrate on elaborating the main development of high-nuclear TMSPTs made between 2005 and 2015 involving synthetic strategies, structural features and potential applications. In order to better understand their structural correlations, we expand our intensive statements on high-nuclear TMSPTs according to the number of POT fragments per molecular unit. The major structural types of high-nuclear TMSPTs include monomer, dimer, trimer, tetramer, hexamer, octamer, hexadecamer and tetracosamer (Fig. 1). In the third section, we will emphatically discuss magnetic properties and catalytic properties of some representative high-nuclear TMSPTs. Some personal viewpoints will be presented in the last section and we hope to offer some highlights that many more chemists can be actively devoted to this domain and discover innovative high-nuclear TMSPTs with desired properties and potential applications.

2. Representative structure types of high-nuclear TMSPTs

2.1 Monomeric high-nuclear TMSPTs

During the course of exploring hexa-nuclear TMSPTs, trilacunary Keggin-type precursors $[\alpha\text{-}XW_9O_{34}]^{9/10-}$ (X = P^V, As^V, Si^{IV}, Ge^{IV}) play an irreplaceable role and consequently trigger a series of important discoveries, which can be ascribed to the following reasons: (a) trilacunary Keggin-type $[\alpha\text{-}XW_9O_{34}]^{9/10-}$ fragments are accessible and have relatively higher stability among diverse lacunary POT fragments; (b) abundant lacunary sites and exposed surface oxygen atoms endow trilacunary $[\alpha\text{-}XW_9O_{34}]^{9/10-}$ fragments with high reaction ability to incorporate TM ions, therefore, $[\alpha\text{-}XW_9O_{34}]^{9/10-}$ fragments can serve as structure-directing agents (SDAs) to induce the aggregation of TM ions in the lacunary sites; (c) since the extra exposed oxygen atom from XO_4 units can be also combined with TM ions, $[B\text{-}\alpha\text{-}XW_9O_{34}]^{9/10-}$ fragments generally show higher reactivity than $[A\text{-}\alpha\text{-}XW_9O_{34}]^{9/10-}$ fragments and thus the isomerization of $[A\text{-}\alpha\text{-}XW_9O_{34}]^{9/10-} \rightarrow [B\text{-}\alpha\text{-}XW_9O_{34}]^{9/10-}$ can easily occur in the process of reaction; (d) under hydrothermal environments, trilacunary Keggin-type $[\alpha\text{-}XW_9O_{34}]^{9/10-}$ fragments sometimes can be transformed to other lacunary POT building blocks. Based on the aforementioned design philosophy and synthesis concepts, Yang's group developed an effective strategy of utilizing the highly active $[A\text{-}\alpha\text{-}XW_9O_{34}]^{9/10-}$ fragments as SDAs and the multidentate N-ligands as structure-stabilizing agents (SSAs) to capture *in situ* formed TM clusters, giving rise to novel high-nuclear TMSPTs with isolated, finite polymeric and extended structures (Fig. 2a). For example, in 2007, they communicated the first series of Ni_6-substituted trilacunary Keggin POTs $[Ni(H_2O)_6][Ni_6(\mu_3\text{-}OH)_3(H_2O)_6(enMe)_3(B\text{-}\alpha\text{-}SiW_9O_{34})]_2\cdot 8H_2O$, $[Ni(enMe)_2][Ni_6(\mu_3\text{-}OH)_3(H_2O)_6(enMe)_3(B\text{-}\alpha\text{-}SiW_9O_{34})]_2\cdot 10H_2O$ and $[Ni_6(\mu_3\text{-}OH)_3(H_2O)_2(dien)_3(B\text{-}\alpha\text{-}PW_9O_{34})]\cdot 4H_2O$ (enMe = 1,2-diaminopropane, dien = diethylenetriamine), which represent the first lacunary Keggin monomeric POTs incorporating the highest number of Ni^{II} ions at that time.[12a] The fundamental skeleton of $\{Ni_6(\mu_3\text{-}OH)_3(H_2O)_n(L)_3(B\text{-}\alpha\text{-}XW_9O_{34})\}$ (X = Si^{IV}, P^V; n = 5, 6; L = enMe, dien) fragment (Fig. 2b) is constructed from a trilacunary Keggin $\{B\text{-}\alpha\text{-}XW_9O_{34}\}$ unit and a capping hexa-Ni^{II} $\{Ni_6(\mu_3\text{-}OH)_3(H_2O)_n(L)_3\}$ cluster. The hexa-Ni^{II} cluster is constituted by six nearly co-planar Ni^{II} ions in a triangular fashion combined together through three μ_3-OH groups and stabilized by six μ_3-O atoms from six $\{WO_6\}$ octahedra and one μ_4-O atom from the $\{XO_4\}$ tetrahedron, finally, the octahedral coordination sphere of each Ni^{II} ion is accomplished by water, enMe or dien ligands. The reactive activity of water ligands on the hexa-Ni^{II} clusters and different orientations of enMe (di-amines), dien (tri-amine) and water ligands on the hexa-Ni^{II} clusters should be highlighted here. In $[Ni(H_2O)_6][Ni_6(\mu_3\text{-}OH)_3(H_2O)_6(enMe)_3(B\text{-}\alpha\text{-}SiW_9O_{34})]_2\cdot 8H_2O$ and $[Ni(enMe)_2][Ni_6(\mu_3\text{-}OH)_3(H_2O)_6(enMe)_3(B\text{-}\alpha\text{-}SiW_9O_{34})]_2\cdot 10H_2O$, two isomeric $\{Ni_6(\mu_3\text{-}OH)_3(H_2O)_6(enMe)_3(B\text{-}\alpha\text{-}SiW_9O_{34})\}$ clusters can be seen as the derivatives of the hypothetical $\{Ni_6(\mu_3\text{-}OH)_3(H_2O)_{12}(B\text{-}\alpha\text{-}SiW_9O_{34})\}$ unit by replacing six water ligands on the exterior Ni^{II} ions with three bidentate enMe ligands (Fig. 2c and d).[12a] Intriguingly, two water ligands on adjacent interior and exterior Ni^{II} ions in the hexa-Ni^{II} $\{Ni_6(\mu_3\text{-}OH)_3(H_2O)_n(L)_3\}$ cluster can also be simultaneously replaced by a bidentate acetate anion, resulting in the production of the $\{Ni_6(\mu_3\text{-}OH)_3(H_2O)_4(enMe)_3(CH_3COO)(B\text{-}\alpha\text{-}PW_9O_{34})\}$ unit (Fig. 2e) in

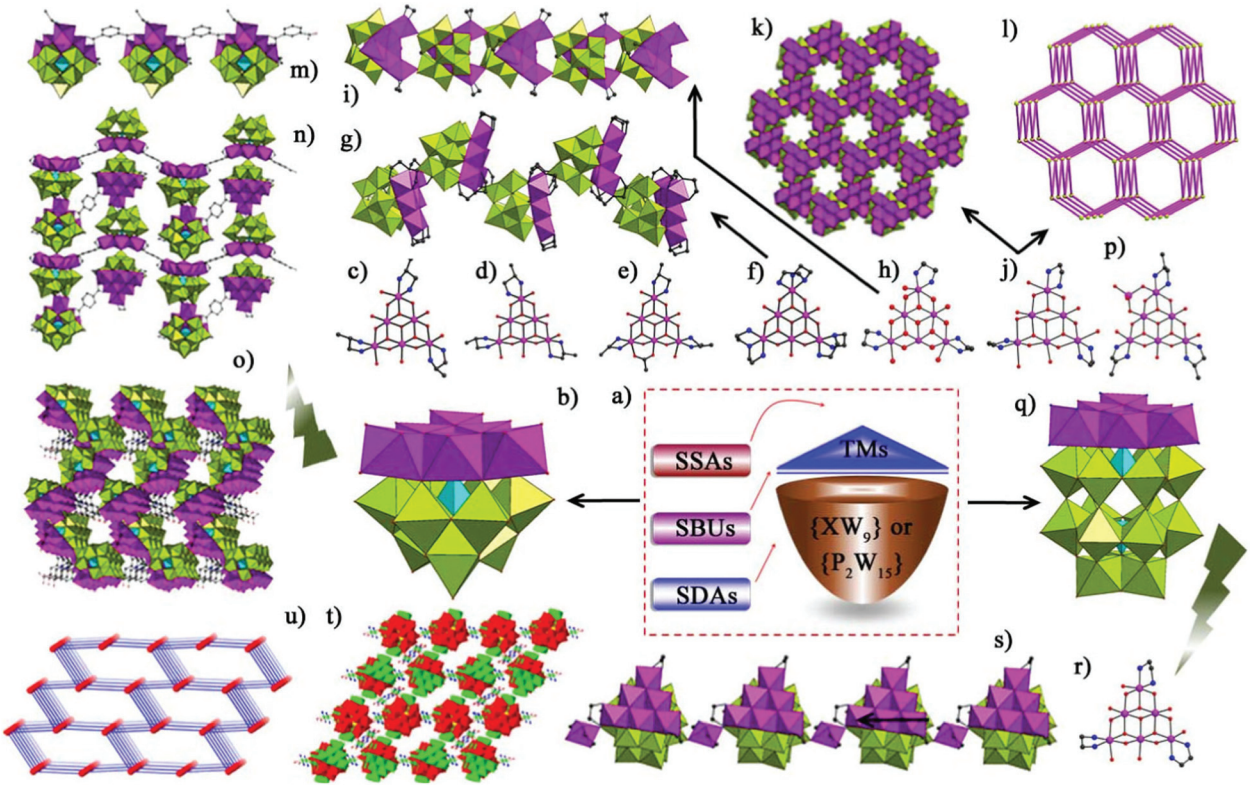

Fig. 2 (a) A schematic synthetic strategy in preparing high-nuclear TMSPTs. (b) View of the TM_6-substituted trilacunary Keggin $\{TM_6(\mu_3\text{-}OH)_3(H_2O)_n(L)_3(B\text{-}\alpha\text{-}XW_9O_{34})\}$ monomeric unit. (c, d) View of Ni_6-cores in two isomeric units $\{Ni_6(\mu_3\text{-}OH)_3(H_2O)_6(enMe)_3(B\text{-}\alpha\text{-}SiW_9O_{34})\}$. (e) View of the Ni_6-core in $\{Ni_6(\mu_3\text{-}OH)_3(H_2O)_4\ (enMe)_3(CH_3COO)(B\text{-}\alpha\text{-}PW_9O_{34})\}$. (f, g) View of the Ni_6-core in $\{Ni_6(\mu_3\text{-}OH)_3(H_2O)_2(dien)_3(B\text{-}\alpha\text{-}PW_9O_{34})\}$ and the 1-D chain structure of $[Ni_6(\mu_3\text{-}OH)_3(H_2O)_2(dien)_3(B\text{-}\alpha\text{-}PW_9O_{34})]\cdot 4H_2O$. (h, i) View of the Cu_6-core in $\{Cu_6(\mu_3\text{-}OH)_3(en)_3(H_2O)_3(B\text{-}\alpha\text{-}PW_9O_{34})\}$ and the 1-D chain structure of $[Cu_6(\mu_3\text{-}OH)_3(en)_3(H_2O)_3(B\text{-}\alpha\text{-}PW_9O_{34})]\cdot 4H_2O$. (j) View of the Cu_6-core in $\{Cu_6(\mu_3\text{-}OH)_3(en)_3(H_2O)_3(B\text{-}\alpha\text{-}PW_9O_{34})\}$. (k, l) View of the 3-D framework and "Archimedean-type" topology view of $[Cu_6(\mu_3\text{-}OH)_3(en)_3(H_2O)_3(B\text{-}\alpha\text{-}PW_9O_{34})]\cdot 7H_2O$ [the lime balls are six-connected nodes on behalf of $\{Cu_6(\mu_3\text{-}OH)_3(en)_3(H_2O)_3(B\text{-}\alpha\text{-}PW_9O_{34})\}$ units]. (m) The 1-D chain of $\{[Ni_6(OH)_3(H_2O)_2\ (enMe)_3(PW_9O_{34})](1,3\text{-}bdc)\}[Ni(enMe)_2]\cdot 4H_2O$. (n) View of the 2-D layer of $\{[Ni_6(OH)_3(H_2O)(en)_3(PW_9O_{34})][Ni_6(OH)_3(H_2O)_4(en)_3(PW_9O_{34})](1,4\text{-}bdc)_{1.5}\}[Ni(en)(H_2O)_4]\cdot H_3O$. (o) The 3-D architecture of $\{[Ni_6(OH)_3(H_2O)_5(PW_9O_{34})](1,2,4\text{-}Hbtc)\}\cdot H_2enMe\cdot 5H_2O$. (p) View of the Ni_7-core in $\{\{Ni_7(\mu_3\text{-}OH)_3O_2(dap)_3(H_2O)_6\}(B\text{-}\alpha\text{-}PW_9O_{34})\}$. (q) View of the TM_6-substituted trilacunary Dawson $\{TM_6(\mu_3\text{-}OH)_3(\alpha\text{-}P_2W_{15}O_{56})\}$ monomeric unit. (r, s) View of the Ni_6-core in $\{Ni_6(\mu_3\text{-}OH)_3(H_2O)_6(en)_3H(\alpha\text{-}P_2W_{15}O_{56})\}$ and the 1-D chain structure of $[Ni(en)_2][Ni_6(\mu_3\text{-}OH)_3(H_2O)_6(en)_3H(\alpha\text{-}P_2W_{15}O_{56})]\cdot 5.5H_2O$. (t, u) View of the 3-D framework and the $SrAl_2$ topology of $[Ni(enMe)_2]_3[Ni(enMe)_2(H_2O)]\ [Ni(enMe)(H_2O)_2][Ni_6(enMe)_3(\mu_3\text{-}OH)_3(Ac)_2(H_2O)(P_2W_{15}O_{56})]_2\cdot 6H_2O$. [Copied from ref. 14*b*]. [$\{WO_6\}$: lime, $\{XO_4\}$: turquoise, TM and $\{TMO_xN_y\}$: light lavender, O: red, C: cray-80%, N: blue]. (t) and (u) are reprinted with permission from ref. 14*b*. Copyright 2014 Wiley-VCH Verlag GmbH&Co. KGaA, Weinheim.

$[Ni(enMe)_2(H_2O)_2][Ni_6(\mu_3\text{-}OH)_3(H_2O)_4(enMe)_3(CH_3COO)\ (B\text{-}\alpha\text{-}PW_9O_{34})]_2\cdot 10H_2O$.[12a] More interestingly, nine water ligands on all exterior Ni^{II} ions in the hypothetical $\{Ni_6(\mu_3\text{-}OH)_3(H_2O)_{12}\text{-}(B\text{-}\alpha\text{-}PW_9O_{34})\}$ unit can be substituted by three tridentate dien ligands, leading to the generation of the $\{Ni_6(\mu_3\text{-}OH)_3(H_2O)_2\text{-}(dien)_3(B\text{-}\alpha\text{-}PW_9O_{34})\}$ unit (Fig. 2f) in $[Ni_6(\mu_3\text{-}OH)_3(H_2O)_2\text{-}(dien)_3(B\text{-}\alpha\text{-}PW_9O_{34})]\cdot 4H_2O$.[17a] It should be pointed out that water ligands on interior Ni^{II} ions can be further superseded by terminal oxygen atoms on the $[B\text{-}\alpha\text{-}PW_9O_{34}]^{9-}$ fragments to form the first 1-D infinite TM_6-substituted POT (Fig. 2g).[12a] In the copper–en–phosphotungstate (PT) system (en = ethylenediamine), another novel double-bridging 1-D chain architecture based on $[Cu_6(\mu_3\text{-}OH)_3(en)_3(H_2O)_3(B\text{-}\alpha\text{-}PW_9O_{34})]$ units was also obtained by Yang's group, in which two water ligands on two adjacent exterior Cu^{II} ions are simultaneously substituted by two terminal oxygen atoms from adjacent $[B\text{-}\alpha\text{-}PW_9O_{34}]^{9-}$ fragments (Fig. 2h and i).[12b] Notably, one $\{CuO_5\}$ square pyramid, two $\{CuO_6\}$ octahedra and three $\{CuN_2O_4\}$ octahedra coexist in $[Cu_6(\mu_3\text{-}OH)_3(en)_3(H_2O)_3(B\text{-}\alpha\text{-}PW_9O_{34})]$. The synergistic effect between the pseudo-Jahn–Teller effect of the square pyramid and the Jahn–Teller effect of the octahedra with the axial elongation reducing large steric hindrance could be the main reason for the formation of such double-bridging 1-D chain architecture.[12b] Subsequently, the first 3-D extended architecture $[Cu_6(\mu_3\text{-}OH)_3(en)_3(H_2O)_3(B\text{-}\alpha\text{-}PW_9O_{34})]\cdot 7H_2O$ was also discovered by Yang's group, in which three water ligands on three exterior Cu^{II} ions in the $\{Cu_6(\mu_3\text{-}OH)_3(en)_3(H_2O)_3\text{-}(B\text{-}\alpha\text{-}PW_9O_{34})\}$ unit are simultaneously substituted by three terminal oxygen atoms from three adjacent $[B\text{-}\alpha\text{-}PW_9O_{34}]^{9-}$ fragments. It not only illustrates an unprecedented 3-D framework constructed from $\{Cu_6(\mu_3\text{-}OH)_3(en)_3(H_2O)_3(B\text{-}\alpha\text{-}PW_9O_{34})\}$ units with hexagonal channels, but also displays an interesting

"Archimedean-type" three-dimensional network with the Schäfli symbol of $4^9 6^6$ (Fig. 2j–l).[12c] Above all, active water ligands on exterior and interior Ni^{II} ions in the hexa-Ni^{II} $\{Ni_6(\mu_3\text{-}OH)_3(H_2O)_n(L)_3\}$ cluster not only can be substituted by nitrogen atoms from organoamine ligands or terminal oxygen atoms from adjacent POM fragments, but can also be replaced by carboxylate oxygen atoms from functional organic ligands. Yang's discovery of a class of POM–organic frameworks (POMOFs) based on $\{Ni_6(\mu_3\text{-}OH)_3(H_2O)_6(L)_3(B\text{-}\alpha\text{-}PW_9O_{34})\}$ units and rigid carboxylate ligands exemplified this standpoint.[12d] For example, the introduction of V-type 1,3-benzene dicarboxylate (1,3-bdc) ligand led to an interesting 1-D straight chain $\{[Ni_6(OH)_3(H_2O)_2(enMe)_3(PW_9O_{34})](1,3\text{-}bdc)\}[Ni(enMe)_2]\cdot 4H_2O$, in which neighboring $\{Ni_6(OH)_3(H_2O)_2(enMe)_3(PW_9O_{34})\}$ units are connected together in a shoulder-to-shoulder mode by 1,3-bdc ligands (Fig. 2m).[12d] Based on V-type thiophene-2,5-dicarboxylic acid (Htda), a 1-D zigzag chain $\{[Ni_6(OH)_3(H_2O)(en)_4(PW_9O_{34})](Htda)\}\cdot H_3O\cdot 4H_2O$ was also isolated, in which neighboring $\{Ni_6(OH)_3(H_2O)(en)_4(PW_9O_{34})\}$ units are interlinked in a face-to-face mode through Htda ligands.[12d] By making use of the linear 1,4-benzene dicarboxylate (1,4-bdc) ligand, a unique 2-D network $\{[Ni_6(OH)_3(H_2O)(en)_3(PW_9O_{34})][Ni_6(OH)_3(H_2O)_4(en)_3(PW_9O_{34})](1,4\text{-}bdc)_{1.5}\}[Ni(en)(H_2O)_4]\cdot H_3O$ was made (Fig. 2n), in which each $\{[Ni_6(OH)_3(H_2O)(en)_3(PW_9O_{34})][Ni_6(OH)_3(H_2O)_4(en)_3(PW_9O_{34})]\}$ moiety firstly links to adjacent ones by 1,4-bdc ligands, forming the infinite 1-D chain, and $\{Ni_6(OH)_3(H_2O)_4(en)_3(PW_9O_{34})\}$ units in the 1-D chains can be further linked by other 1,4-bdc ligands to finish the 2-D layer.[12d] It is most intriguing that an unseen 3-D framework $\{[Ni_6(OH)_3(H_2O)_5(PW_9O_{34})](1,2,4\text{-}Hbtc)\}\cdot H_2enMe\cdot 5H_2O$ was also obtained by means of 1,3,5-benzene tricarboxylate (1,3,5-btc) ligand, in which each $\{Ni_6(OH)_3(H_2O)_5\ (PW_9O_{34})\}$ unit is combined with two others *via* four W═O–Ni linkages to form the right-handed helical chain along the *c* axis and then Y-type 1,2,4-Hbtc ligands connect all the right-handed helical chains along the *a* and *b* axes to construct the 3-D framework (Fig. 2o).[12d] During the course of exploring the Ni_6-substituted Keggin-type monomers, a neoteric high-nuclear TMSPT $\{[Ni_7(\mu_3\text{-}OH)_3O_2(dap)_3(H_2O)_6(B\text{-}\alpha\text{-}PW_9O_{34})][Ni_6(\mu_3\text{-}OH)_3(dap)_3(H_2O)_6(B\text{-}\alpha\text{-}PWO_{34})]\}[Ni(dap)_2(H_2O)_2]\cdot 4.5H_2O$ with a Ni_6-substituted POT fragment and a Ni_7-substituted POT fragment was discovered for the first time.[12c] From the structural viewpoint, such previously unseen Ni_7-substituted POT $[Ni_7(\mu_3\text{-}OH)_3O_2(dap)_3(H_2O)_6(B\text{-}\alpha\text{-}PW_9O_{34})]^{2-}$ fragment can be viewed as a derivative of one $\{NiO_2(H_2O)_2\}$ tetrahedron replacing terminal water ligands on two adjacent interior and exterior Ni^{II} ions in the $\{Ni_6(\mu_3\text{-}OH)_3(dap)_3(H_2O)_6(B\text{-}\alpha\text{-}PW_9O_{34})\}$ fragment (Fig. 2p).[12c] To date, various TM_6-substituted trilacunary Keggin POT monomers have been isolated in differing systems such as dap-containing PTs (dap = 1,2-diaminopropane),[12c,13a] en-containing silicotungstates (PTs),[12c] en-containing germanotungstates (GTs),[13b] dap-containing GTs,[13b] en and tris-containing PTs (tris1 = tris(hydroxymethyl)aminomethane; tris2 = pentaerythritol; tris3 = dipentaerythritol; tris4 = tripentaerythritol),[13c] oeen-containing PTs (oeen = *N*-(2-hydroxyethyl)enediamine),[13d] oeen and tran-containing PTs (tran = 1,4,7-triazonane)[13d] and en-containing arsenotungstates (ATs).[13e] Due to the similarity of coordination chemistry and structural chemistry between trilacunary Keggin-type and Dawson-type POT fragments, it can be speculated that the Ni_6-substituted trilacunary Dawson-type TMSPTs (Fig. 2q) should exist. By hydrothermal reaction of lacunary precursor $[\alpha\text{-}H_2P_2W_{12}O_{48}]^{12-}$, $Ni(CH_3COO)_2\cdot 4H_2O$ and dien or en, Yang *et al.* obtained the first series of Ni_6-substituted trilacunary Dawson-type TMSPTs $[Ni_6(\mu_3\text{-}OH)_3(H_2O)_3(dien)_3H_3(\alpha\text{-}P_2W_{15}O_{56})]\cdot 4.5H_2O$ and $[Ni(en)_2][Ni_6(\mu_3\text{-}OH)_3(H_2O)_6(en)_3H(\alpha\text{-}P_2W_{15}O_{56})]\cdot 5.5H_2O$ (Fig. 2r) in 2013.[14a] In the latter, $[Ni_6(\mu_3\text{-}OH)_3(H_2O)_6(en)_3H(\alpha\text{-}P_2W_{15}O_{56})]^{2-}$ units can be further linked together by the extraneous $\{NiO_2(en)_2\}$ units *via* W═O–Ni linkages to form a novel 1-D chain architecture (Fig. 2s). Subsequently, they discovered the first 3-D framework $[Ni(enMe)_2]_3[Ni(enMe)_2(H_2O)][Ni(enMe)(H_2O)_2][Ni_6(enMe)_3(\mu_3\text{-}OH)_3(CH_3COO)_2(H_2O)(P_2W_{15}O_{56})]_2\cdot 6H_2O$ based on Dawson-type Ni_6-substituted POT units $\{Ni_6(enMe)_3(\mu_3\text{-}OH)_3(CH_3COO)_2(H_2O)(P_2W_{15}O_{56})\}$, which displays a four-connected $(4^2\cdot 6^3\cdot 8)$ $SrAl_2$ topology (Fig. 2t and u).[14b] In this 3-D architecture, one water ligand on the exterior Ni^{II} ion of the hexa-Ni^{II} $\{Ni_6(enMe)_3(\mu_3\text{-}OH)_3(CH_3COO)_2(H_2O)\}$ cluster is replaced by one terminal oxygen atom on one WO_6 group from a neighboring $\{Ni_6(enMe)_3(\mu_3\text{-}OH)_3(CH_3COO)_2(H_2O)(P_2W_{15}O_{56})\}$ unit, forming the 1-D zigzag chain. And then adjacent 1-D zigzag chains are bridged together through $[Ni(enMe)_2]^{2+}$ ions to create the 2-D layer. Finally, adjacent 2-D layers are further joined by $\{Ni(enMe)(H_2O)_2\}^{2+}$ ions to construct the 3-D architecture.[14b] The synthesis of these hexa-Ni^{II}/Cu^{II} substituted POTs not only illustrate that triangle hexa-Ni^{II}/Cu^{II} clusters are very stable in trilacunary Keggin and trivacant Dawson POT systems, but also prove that the hydrothermal reaction can serve as an efficient approach for synthesizing and developing novel TMSPTs through combination chemistry of lacunary POT precursors with high-nuclear TM clusters.

Additionally, in 2005, Gouzerh and co-workers communicated a novel Fe_9-substituted Dawson TMSPT monomer $[H_4P_2W_{12}Fe_9O_{56}(CH_3COO)_7]^{6-}$ (Fig. 3). In this structure, six Fe^{III} ions firstly fill in the vacancies of the hexavacant Dawson $[\alpha\text{-}H_2P_2W_{12}O_{48}]^{12-}$ fragment, forming the $\{P_2W_{12}Fe_6\}$ subunit. Two additional Fe^{III} ions graft to three contiguous bridging oxo ligands of the formed $\{P_2W_{12}Fe_6\}$ subunit and the last Fe^{III} ion links to four bridging oxo ligands, giving rise to the $\{P_2W_{12}Fe_9\}$ skeleton. Finally, the octahedral coordination

Fig. 3 View of $[H_4P_2W_{12}Fe_9O_{56}(CH_3COO)_7]^{6-}$. [{$WO_6$}: lime, {$PO_4$}: turquoise, {$FeO_6$}: light lavender].

sphere of each Fe^{III} center is finished by acetate ligands.[15a] The preparation of this Dawson TMSPT monomer not only contradicts the previous (false) judgment that the metastable hexalacunary fragment $[\alpha\text{-}H_2P_2W_{12}O_{48}]^{12-}$ can be not combined with divalent or trivalent TM ions to form TMSPTs,[15b] but also can be viewed as bridging the gap between TMSPTs such as $[\alpha\text{-}P_2W_{15}O_{59}(FeCl)_2\ (FeOH_2)]^{11-}$ and classic complex clusters such as $[Fe_3O(CH_3COO)_6(H_2O)_3]^{+}$.[15c–e]

2.2 Dimeric high-nuclear TMSPTs

Admittedly, the sandwich-type TMSPTs consisting of two lacunary Keggin or Dawson-type building blocks incorporating kaleidoscopic TM cores have developed as the most typical subfamily of TMSPTs, since the first sandwich-type TMSTPs $[Co_4(H_2O)_2(PW_9O_{34})_2]^{10-}$ containing a rhomb-like tetra-Co^{II} core was reported by Weakley *et al.* in 1973.[16] According to the embedded mode of TM ions located on the sandwich belt, sandwich-type TMSPTs can be divided into two types: (a) some TM ions substitute some W atoms to complete saturated Keggin or Dawson fragments $\{XW_{12-n}M_n\}$ or $\{X_2W_{18-n}M_n\}$, and then the resulting two $\{XW_{12-n}M_n\}$ or $\{X_2W_{18-n}M_n\}$ fragments are fused together giving rise to the embedded sandwich-type structure assembly (Fig. 4a); (b) instead of TM ions substituting some W atoms to complete saturated Keggin or Dawson fragments, TM ions are merely fixed by the exposed surface oxygen atoms of two lacunary POT fragments, and then TM ions bridge two lacunary POT fragments together, producing the filled sandwich-type structure assembly (Fig. 5a). In the following discussion, we describe in detail these two sandwich-type TMSPTs according to the above classification. Moreover, several non-sandwich-type dimeric TMSPTs have been involved.

Systematic researches indicate that almost all embedded sandwich-type TMSPTs were obtained by reaction of TM ions with preformed lacunary precursors in aqueous solution with appropriate pH value and reaction temperature while a few exceptions were generated from the self-assembly reaction of simple starting materials. In 2005, Kortz *et al.* reported a Fe_6-substituted embedded-sandwich-type Keggin GT $[Fe_6(OH)_3(A\text{-}\alpha\text{-}GeW_9O_{34}(OH)_3)_2]^{11-}$ by CASSM. The insertion of six Fe^{III} centers to the lacunary sites of two trivacant $[A\text{-}\alpha\text{-}GeW_9O_{34}]^{10-}$ moieties leads to two hypothetical saturated $[Fe_3(OH_2)_3(A\text{-}\alpha\text{-}GeW_9O_{34}(OH)_3)]^{4-}$ units that connect together through three Fe–O–Fe linkers in the corner-shared fashion (Fig. 4b). Obviously, the trigonal prismatic arrangement of six equivalent Fe^{III} centers (Fig. 4c) results in the virtual D_{3h} symmetry of $[Fe^{III}_6(OH)_3(A\text{-}\alpha\text{-}GeW_9O_{34}(OH)_3)_2]^{11-}$.[17a] In 2014, by reaction of WO_4^{2-}, SeO_3^{2-}, dimethylamine hydrochloride and Fe^{3+} ions in acidic aqueous solution (pH = 5.5), Wang and co-workers obtained an intriguing Fe_6-substituted Dawson selenotungstate $[Fe_6Se_6W_{34}O_{124}(OH)_{16}]^{18-}$ (Fig. 4d), in which two tetravacant Dawson-type $\{\alpha\text{-}Se_2W_{14}\}$ moieties are linked by an almost regular cube $\{Fe_4W_4O_{12}\}$ unit.[17b] In addition, four extra sites located at both wings of the $\{Fe_4W_4O_{12}\}$ unit are taken up by two Fe^{III} and two W^{VI} atoms, forming the disordered

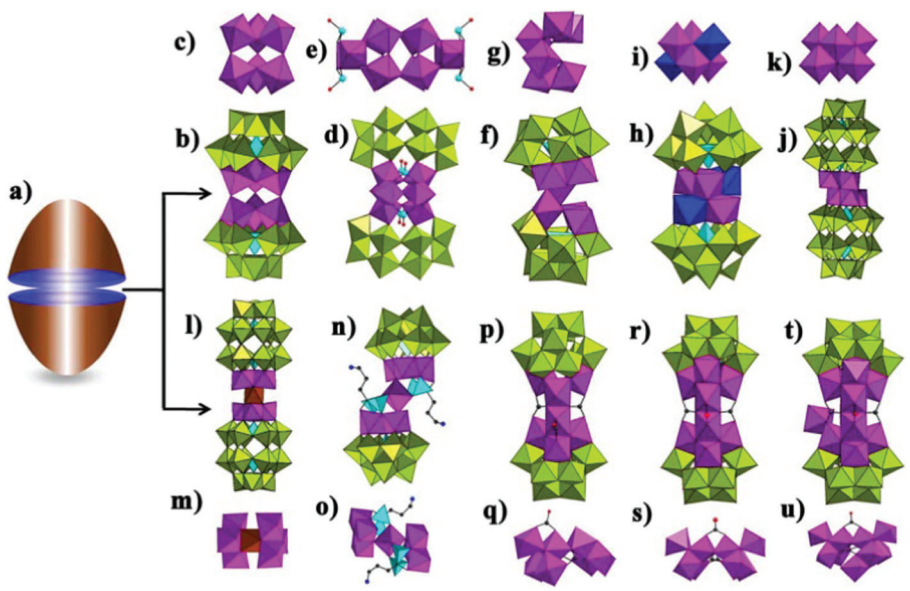

Fig. 4 (a) The schematic mode of embedded-sandwich-type TMSPTs. (b, c) View of $[Fe_6(OH)_3(A\text{-}\alpha\text{-}GeW_9\ O_{34}(OH)_3)_2]^{11-}$ and its trigonal prismatic core $\{Fe_6(OH)_9\}$. (d, e) View of $[Fe_6Se_6W_{34}O_{124}(OH)_{16}]^{18-}$ and its central core $\{Fe_6W_6\}$. (f, g) View of $[\{Ni_6(H_2O)_4(\mu_2\text{-}H_2O)_4(\mu_3\text{-}OH)_2\}(SiW_9O_{34})_2]^{10-}$ and its central core $\{Ni_6(H_2O)_4(\mu_2\text{-}H_2O)_4(\mu_3\text{-}OH)_2\}$. (h, i) View of $[\{B\text{-}\alpha\text{-}GeW_9O_{34}\}_2\{Mn^{III}_4Mn^{II}_2O_4(H_2O)_4\}]^{12-}$ and its mixed-valence double-cubane core $\{Mn^{II}_4(H_2O)_2\ Mn^{II}_2O_4(H_2O)_2\}$ [Mn^{II}: blue]. (j) View of the POA in $[P_4V_6W_{30}O_{120}]^{10-}$. (k) The double-cubane $\{V_6O_8\}$ core in $[P_4V_6W_{30}O_{120}]^{10-}$. (l, m) View of $[(\alpha\text{-}P_2W_{15}O_{56})_2Mn^{III}_6\ Mn^{IV}O_6(H_2O)_6]^{14-}$ and its double-cubane core $\{Mn^{III}_6Mn^{IV}O_8\}$ [Mn^{IV}: brown]. (n, o) View of $[\{(B\text{-}\alpha\text{-}PW_9O_{34})Co_3(OH)(H_2O)_2(Ale)\}_2Co]^{14-}$ and its Co_7-core [P: turquoise]. (p, q) View of $[Ni_7(OH)_4(H_2O)(CO_3)_2(HCO_3)(A\text{-}\alpha\text{-}SiW_9O_{34})(\beta\text{-}SiW_{10}O_{37})]^{10-}$ and its central core $\{Ni_7(OH)_4(H_2O)(CO_3)_2(HCO_3)\}$. (r, s) View of $[(A\text{-}\alpha\text{-}SiW_9O_{34})_2Co_8(OH)_6(H_2O)_2(CO_3)_3]^{16-}$ and its central core $\{Co_8(OH)_6(H_2O)_2\ (CO_3)_3\}$. (t, u) View of $[(A\text{-}\alpha\text{-}SiW_9O_{34})_2Ni_9(OH)_6(H_2O)_6(CO_3)_3]^{14-}$ and its central core $\{Ni_9(OH)_6\ (H_2O)_6(CO_3)_3\}$. [$\{WO_6\}$: lime, $\{XO_4\}$: turquoise, TM and $\{TMO_x\}$: light lavender, O: red, C: cray-80%, N: blue].

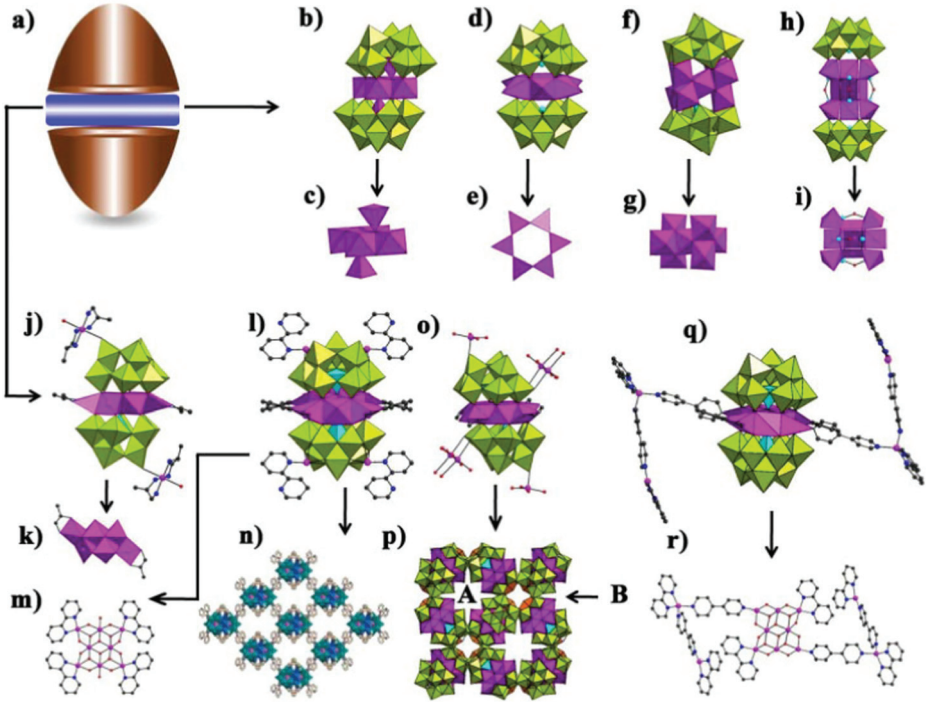

Fig. 5 (a) The schematic mode of filled-sandwich type TMSPTs. (b, c) View of $[Ni_4(H_2O)_2(\alpha\text{-}NiW_9O_{34})_2]^{16-}$ and its the $\{Ni_6O_{22}\}$ core. (d, e) View of $[(CuCl)_6(AsW_9O_{33})_2]^{12-}$ and it's the hexagonal $\{(CuCl)_6\}$ core. (f, g) View of $[(\beta\text{-}SiW_8O_{31})_2Ni_7(H_2O)_4(OH)_6]^{12-}$ and its double-cubane $\{Ni_7O_8\}$ core. (h, i) View of $[H_4\{Cu_9As_6O_{15}(H_2O)_6\}(\alpha\text{-}AsW_9O_{33})_2]^{8-}$ and its central cylindrical $[Cu^{II}_9As^{III}_6O_{15}(H_2O)_6]^{6+}$ core. (j, k) View of $\{[Cu(enMe)_2(H_2O)]_2[Cu_6(enMe)_2(B\text{-}\alpha\text{-}SiW_9O_{34})_2]\}^{4-}$ and its belt $\{Cu_6(enMe)_2\}$ core. (l, m) View of $\{[Cu(bdyl)]_2[Cu_8(2,2'\text{-}bpy)_4(H_2O)_2\ (B\text{-}\alpha\text{-}GeW_9O_{34})_2]\}^{4-}$ and its $\{Cu^{II}_8(2,2'\text{-}bpy)_4(H_2O)_2\}$ core. (n) The 2-D sheet of $\{[Cu^{II}(bdyl)]_2[Cu^{II}_8(2,2'\text{-}bpy)_4(H_2O)_2(B\text{-}\alpha\text{-}GeW_9O_{34})_2]\}^{4-}$ [copied from ref. 22*a*]. (o, p) View of $[Cu(H_2O)_2]H_2[Cu_8(en)_4(H_2O)_2(B\text{-}\alpha\text{-}SiW_9O_{34})_2]$ and its 3-D framework. (q, r) View of $\{[Cu^{I}_2(2,2'\text{-}bpy)_2(4,4'\text{-}bpy)]_2[Cu^{I}_2Cu^{II}_6(2,2'\text{-}bpy)_2(4,4'\text{-}bpy)_2(B\text{-}\alpha\text{-}GeW_9O_{34})_2]\}^{2-}$ and its mixed-valence $\{Cu^{I}_2Cu^{II}_6(2,2'\text{-}bpy)_2(4,4'\text{-}bpy)_2\}$ core. [{WO_6}: lime, {XO_4}: turquoise, TM, {TMO_x} and {TMO_xN_y}: light lavender, O: red, C: cray-80%, N: blue].

$\{Fe_6W_6\}$ core with each Fe/W position half site-occupancy disorder. Interestingly, four Se^{IV} atoms with half site-occupancy disorder attach to both terminals of the disordered $\{Fe_6W_6\}$ core (Fig. 4e). Reaction of $[\gamma\text{-}SiW_{10}O_{36}]^{8-}$ with Ni^{2+} in the 80 °C, pH = 8.2 aqueous solution afforded a Ni_6-substituted ST $[\{Ni_6(H_2O)_4(\mu_2\text{-}H_2O)_4(\mu_3\text{-}OH)_2\}(SiW_9O_{34})_2]^{10-}$ with embedded sandwich-type skeleton (Fig. 4f),[17c] which can be deemed as a dimer formed by two well-defined Ni_3-substituted moieties $\{\beta\text{-}Ni_3SiW_9O_{40}\}$ through two μ_3-OH groups.[17c] The two $\{Ni_3O_{13}\}$ trimers embedded in $\{\beta\text{-}Ni_3SiW_9O_{40}\}$ moieties are linked in an edge-sharing fashion to form an unobserved "Z" type $\{Ni_6(H_2O)_4(\mu_2\text{-}H_2O)_4(\mu_3\text{-}OH)_2\}$ core (Fig. 4g).[17c] Historically, the $\{Mn^{III}_4Mn^{II}_2\}$-embedded sandwich-type GT $[\{B\text{-}\alpha\text{-}GeW_9O_{34}\}_2\{Mn^{III}_4Mn^{II}_2\ O_4(H_2O)_4\}]^{12-}$ with two saturated Keggin $\{TM_3XW_9\}$ units contacting through the face-sharing mode was also observed (Fig. 4h).[17d] The face-sharing mode of $\{\alpha\text{-}GeW_9\text{-}Mn^{III}_2Mn^{II}\}$ benefited from the insertion of the double-cubane $\{Mn^{III}_4Mn^{II}_2O_4(H_2O)_4\}$ core (Fig. 4i) in the lacunae of two trilacunary $\{B\text{-}\alpha\text{-}GeW_9O_{34}\}$ moieties,[17d] while the corner-shared mode of $\{\alpha\text{-}GeW_9Fe_3\}$ fragments in $[Fe_6(OH)_3(A\text{-}\alpha\text{-}GeW_9O_{34}\text{-}(OH)_3)_2]^{11-}$ is attributed to the insertion of a trigonal prismatic core $\{Fe_6(OH)_9\}$ in the lacunae of two trilacunary $\{A\text{-}\alpha\text{-}GeW_9O_{34}\}$ moieties.[17a] Through the assembly of trivanadium capped Dawson clusters $(TBA)_5H_4[P_2W_{15}V_3O_{62}]$ in organic solvent under simple reflux conditions, Cronin *et al.* separated an embedded-sandwich Dawson-type POT $(TBA)_{10}[P_4V_6W_{30}O_{120}]$ that consists of two $\{\alpha\text{-}P_2W_{15}V_3\}$ units related together with one $\{\alpha\text{-}P_2W_{15}V_3\}$ unit rotated by 180°, displaying the stagger appearance of the two $\{\alpha\text{-}P_2W_{15}V_3\}$ units (Fig. 4j).[17e] The $\{V_6O_8\}$ core sandwiched by two $\{\alpha\text{-}P_2W_{15}O_{56}\}$ fragments exhibits a vanadium face-sharing double cubane architecture (Fig. 4k). With continued effort towards this branch, some embedded-sandwich-type TMSPTs with more nuclearity of TM ions were found by different synthetic approaches. For instance, Fang *et al.* developed an effective strategy of combining preformed high-nuclear manganese clusters with lacunary POT precursors to search for novel magnetic TMSPTs.[18a–c] Thus, by reaction of the preformed Mn_{12}-acetate cluster $[Mn^{III}_8Mn^{IV}_4(CH_3COO)_{16}(H_2O)_4O_{12}]$ with the trivacant Dawson precursor $[\alpha\text{-}P_2W_{15}O_{56}]^{12-}$, they synthesized a Dawson-type heptanuclear $\{Mn^{III}_6Mn^{IV}\}$ substituted POT $[(\alpha\text{-}P_2W_{15}O_{56})_2Mn^{III}_6\ Mn^{IV}O_6(H_2O)_6]^{14-}$ (Fig. 4l), which contains two $[\alpha\text{-}P_2W_{15}O_{56}]^{12-}$ fragments encapsulating a double-cubane $\{Mn^{III}_6Mn^{IV}O_8\}$ core (Fig. 4m).[18d] The $\{Mn^{III}_6Mn^{IV}O_8\}$ core is similar to two corner-sharing cubanes and can be regarded as a fusion of two $\{Mn^{III}_3Mn^{IV}O_4\}$ subunits *via* sharing a common Mn^{IV} vertex. Worthy of mention is that the Mn_{12}-acetate cluster is degraded to the $\{Mn^{III}_6Mn^{IV}O_8\}$ core and the bridging acetate

groups move away from the manganese cluster in the process of the reaction. As we know, functional organic ligands can be introduced to capture TM ions to enhance the possibility of constructing high-nuclear TMSPTs since the deprotonation of organic ligands under suitable conditions can increase the negative charge of the reaction system. Thereby, in the presence of alendronic acid [H_5Ale = $H_2O_3PC(OH)$ ($C_3H_6NH_3$) PO_3H_2], Mialane *et al.* made a novel Co_7-substituted POT hybrid $[\{(B\text{-}\alpha\text{-}PW_9O_{34})Co_3(OH)(H_2O)_2(Ale)\}_2Co]^{14-}$ (Fig. 4n) that is composed of two $\{B\text{-}\alpha\text{-}PW_9O_{34}Co_3\}$ subunits sandwiching a central Co^{II} ion (Fig. 4o).[18e] In this structure, the central Co^{II} ion is combined with two $\{B\text{-}\alpha\text{-}PW_9O_{34}Co_3\}$ subunits through two μ_3-OH groups and two alendronate groups with the $\eta^1{:}\eta^1{:}\eta^1{:}\eta^3{:}\eta^3{:}\mu_4$ coordination mode, and finally the octahedral coordination spheres of the cobalt atoms are accomplished by terminal aqueous ligands. Notably, the hydroxyl group of the bisphosphonato ligand has been deprotonated, which caters to the requirement of increasing the negative charge of the reaction system. In addition, the utilization of some inorganic acid anions can also increase the negative charge of the reaction system and further induce the aggregation of more TM ions in the lacunary sites of POM fragments to manufacture higher nuclear TMSPTs, which is exemplified by three carbonates includingTMSPTs: a Ni_7^{II}-substituted ST $\{[Ni_7(OH)_4(H_2O)(CO_3)_2(HCO_3)(A\text{-}\alpha\text{-}SiW_9O_{34})(\beta\text{-}SiW_{10}O_{37})]\}^{10-}$ (Fig. 4p), a Co_8^{II}-substituted ST $[(A\text{-}\alpha\text{-}SiW_9O_{34})_2Co_8(OH)_6(H_2O)_2(CO_3)_3]^{16-}$ (Fig. 4r) and a Ni_9^{II}-substituted ST $[(A\text{-}\alpha\text{-}SiW_9O_{34})_2Ni_9(OH)_6(H_2O)_6(CO_3)_3]^{14-}$ (Fig. 4t).[17c,19] In the first POA skeleton, two Ni^{II}-substituted Keggin $\{\alpha\text{-}Ni_3SiW_9O_{40}\}$ and $\{\beta\text{-}Ni_2SiW_{10}O_{40}\}$ fragments connect together through the $\{Ni_2(H_2O)\}$ group and are further consolidated by two tridentate carbonate ligands and one bidentate carbonate ligand (Fig. 4q). Although two identical $\{\alpha\text{-}Co_3SiW_9O_{40}\}$ units in the second are also bridged together *via* two edge-sharing Co ions, two tridentate carbonate ligands and one bidentate carbonate ligand (Fig. 4s),[19a] the bidentate carbonate ligand in the first one coordinates to an exotic Ni^{II} ion and a Ni^{II} ion from a $\{\alpha\text{-}Ni_3SiW_9O_{40}\}$ fragment on one side while the bidentate carbonate ligand in the second skeleton only bind two exotic Co^{II} ions. Based on the POA skeleton of the second, the ninth Ni^{II} ion can be further encapsulated to the POA skeleton leading to the appearance of the third, in which the ninth Ni^{II} ion joins one $\{\alpha\text{-}Ni_3SiW_9O_{40}\}$ subunit *via* the $\mu_5\text{-}\eta^1{:}\eta^2{:}\eta^2$ CO_3^{2-} ligand and one terminal oxygen atom of the $[A\text{-}\alpha\text{-}SiW_9O_{34}]^{10-}$ fragment (Fig. 4u).[19b]

In the following section, we will discuss the filled-sandwich-type TMSPTs (Fig. 5a). Niu's creative work of a Weakley-type TMSPT $[Ni_4(H_2O)_2(\alpha\text{-}NiW_9O_{34})_2]^{16-}$ (Fig. 5b) made up of two $\{\alpha\text{-}NiW_9O_{34}\}$ building blocks and a rhomb-like Ni_4-core should be highlighted because it represents the first Ni_6^{II}-containing TMSPTs with four-coordinate Ni^{II} centers as heteroatoms and two unusual tetra-coordinate Ni^{II} heteroatoms residing in two $\{\alpha\text{-}NiW_9O_{34}\}$ fragments are jointly combined with the central, rhomb-like Ni_4-core (Fig. 5c).[20a] Surprisingly, although the Dawson-type $[P_2W_{15}O_{56}]^{12-}$ precursor was employed as the raw material in the preparation of $[Ni_4(H_2O)_2(\alpha\text{-}NiW_9O_{34})_2]^{16-}$, the Keggin-type $\{\alpha\text{-}NiW_9O_{34}\}$ fragments rather than Dawson-type fragments are observed in the POA skeleton, which indicates the Dawson-type $[P_2W_{15}O_{56}]^{12-}$ anions can transform into the Keggin-type POT units, even the P^V heteroatoms can be substituted by TM ions under appropriate hydrothermal conditions. The other TM_6 filled sandwich-type TMSPT example is the unobserved Cu_6^{II}-hexagon sandwiched AT $[(CuCl)_6(AsW_9O_{33})_2]^{12-}$ (Fig. 5d) obtained by Yamase *et al.*, which can be visualized as two inorganic $\{B\text{-}\alpha\text{-}AsW_9O_{33}\}$ ligands chelating a Cu_6^{II}-hexagon moiety (Fig. 5e).[20b] Here, each Cu^{II} ion links four oxygen atoms from two inorganic $\{B\text{-}\alpha\text{-}AsW_9O_{33}\}$ ligands and an exterior Cl^- ion to finish the square pyramidal geometry. In 2007, Wang *et al.* discovered the first innovative double-cubane Ni_7^{II}-substituted ST $[(\beta\text{-}SiW_8O_{31})_2Ni_7(H_2O)_4(OH)_6]^{12-}$ (Fig. 5f),[20c] in which the adaptable precursor $[\gamma\text{-}SiW_{10}O_{36}]^{8-}$ transforms into tetralacunary $\{\beta\text{-}SiW_8O_{31}\}$ fragments for arresting more TM ions and the generation of double-cubane cluster $\{Ni_7O_8\}$ formed by two $\{Ni_3O_{13}\}$ triplets linked by a $\{NiO_6\}$ octahedron (Fig. 5g). Apparently, the reaction strategy of adaptable POM precursors reacting with TM ions to synthesize TMSPTs plays an important role in the development of TMSPT chemistry, but the one-pot reaction strategy of simple materials can also make some contribution. For instance, by reaction of WO_4^{2-}, AsO_2^- and Cu^{2+} in the presence of acetic acid, Niu's group communicated an unprecedented Cu_9-sandwiched AT $[H_4\{Cu_9As_6O_{15}(H_2O)_6\}(\alpha\text{-}AsW_9O_{33})_2]^{8-}$ (Fig. 5h) comprising of two trivacant $\{\alpha\text{-}AsW_9O_{33}\}$ fragments anchoring a central cylindrical $[Cu_9^{II}As_6^{III}O_{15}(H_2O)_6]^{6+}$ unit (Fig. 5i).[20d] The most remarkable innovation is highlighted on the central cylindrical $[Cu_9^{II}As_6^{III}O_{15}(H_2O)_6]^{6+}$ cluster in which three di-tripodal $\{As_2O_5\}$ units bridge nine Cu^{II} ions together accompanying six square-pyramid Cu^{II} ions and three square-planar Cu^{II} ions. Moreover, this Cu_9-sandwiched AT shows noteworthy activity against K562 leukaemia cells and induces HepG2 cell apoptosis and autophagy.[20d]

Apart from the above discussed purely inorganic filled-sandwich-type TMSPTs, several types of aliphatic or aromatic amine ligand stabilized organic–inorganic hybrid filled-sandwich-type copper-substituted POTs were also reported by Yang and co-workers by reaction of $[A\text{-}\alpha\text{-}XW_9O_{34}]^{10-}$ (X = Si^{IV} or Ge^{IV}) and Cu^{2+} ions under hydrothermal conditions, which not only can further promote the wide application of HSM in the synthesis of organic–inorganic hybrid TMSPTs, but also extend the research categories of TMSPTs to some degree.[12c,21] The organic–inorganic hybrid Cu_6-substituted filled-sandwich-type ST $\{[Cu(enMe)_2(H_2O)]_2[Cu_6(enMe)_2(B\text{-}\alpha\text{-}SiW_9O_{34})_2]\}^{4-}$ (Fig. 5j) was separated in 2007 and is constituted by a belt-like Cu_6-core (Fig. 5k) sandwiched by two stagger $\{B\text{-}\alpha\text{-}SiW_9O_{34}\}$ units.[21a] Subsequently, Cu_8-substituted filled-sandwich-type POTs with different organoamine ligands were obtained and they consist of the intriguing 3 : 2 : 3 distributed Cu_8-cores and two trilacunary POT fragments, such as 0-D $[Cu(dap)(H_2O)_3]_2\{Cu_8(dap)_4(H_2O)_2\}(B\text{-}\alpha\text{-}SiW_9O_{34})_2]$,[12c] $[Cu_8(en)_4(H_2O)_2(B\text{-}\alpha\text{-}SiW_9O_{34})_2]^{4-}$,[21b] $[Cu_8^{II}(dap)_4(H_2O)_2(B\text{-}\alpha\text{-}GeW_9O_{34})_2]^{4-}$,[21b] $[Cu_8(en)_4(H_2O)_2(B\text{-}\alpha\text{-}GeW_9O_{34})_2]^{4-}$,[21b] 2-D $\{[Cu(bdyl)]_2[Cu_8(2,2'\text{-}bpy)_4(H_2O)_2(B\text{-}\alpha\text{-}GeW_9O_{34})_2]\}^{4-}$,[21b] and 3-D $[Cu(H_2O)_2]H_2[Cu_8(en)_4(H_2O)_2(B\text{-}\alpha\text{-}SiW_9O_{34})_2]$ and $[Cu(H_2O)_2]H_2[Cu_8(dap)_4(H_2O)_2$-

(B-α-$GeW_9O_{34})_2$].[21b,c] It should be highlighted that the reliever metalation of 2,2′-bpy permits the bdyl group to work as a twofold-deprotonated anionic N,C^C,N ligand bridging two Cu centers in the unique *trans*-four-coordinate fashion for the construction of a novel 2-D architecture with a 2-D (4,4)-network topology of $\{[Cu(bdyl)]_2[Cu_8(2,2'\text{-bpy})_4(H_2O)_2(B\text{-}\alpha\text{-}GeW_9O_{34})_2]\}^{4-}$ (Fig. 5l–n), which represents the first reliever metalation of 2,2′-bpy in a copper complex system under hydrothermal conditions.[21b] The 3-D architecture of $[Cu(H_2O)_2]H_2[Cu_8(en)_4(H_2O)_2(B\text{-}\alpha\text{-}SiW_9O_{34})_2]$ (Fig. 5o) utilizes a 3-D (3,6)-connected framework with a $(4\cdot6^2)(4^2\cdot6^4\cdot8^7\cdot10^2)$ topology exhibiting two kinds of small helical channels along the *c*-axis (sizes of channel A: 2.5 × 2.5 Å and channel B: 1.3 × 1.3 Å) (Fig. 5p),[21b] which are generated from the regular arrangements of $\{Cu_8(en)_4(H_2O)_2(B\text{-}\alpha\text{-}SiW_9O_{34})_2\}$ units and $[Cu_4(H_2O)_2]^{2+}$ bridges along the 4_2 screw axis. Meanwhile, the employment of mixed ligands of 2,2′-bpy and 4,4′-bpy under hydrothermal conditions resulted in the first mixed-valence $\{Cu^I_4Cu^I_2Cu^{II}_6\}$ core sandwich-type GT hybrid $\{[Cu^I_2(2,2'\text{-bpy})_2(4,4'\text{-bpy})]_2[Cu^I_2Cu^{II}_6(2,2'\text{-bpy})_2(4,4'\text{-bpy})_2(B\text{-}\alpha\text{-}GeW_9O_{34})_2]\}^{2-}$ (Fig. 5q), which can be viewed as a derivative of two di-Cu^I $[Cu^I_2(2,2'\text{-bpy})_2(4,4'\text{-bpy})]^{2+}$ cations attaching to the mixed-valence octa-copper sandwiched dimer $[Cu^I_2Cu^{II}_6(2,2'\text{-bpy})_2(4,4'\text{-bpy})_2(B\text{-}\alpha\text{-}GeW_9O_{34})_2]^{14-}$ (Fig. 5r).[21b] Alternatively, to date, it still stands for the first organic–inorganic hybrid dodeca–copper cluster encapsulated sandwich-type TMSPT. In addition, Niu's group also reported three organic–inorganic hybrid filled-sandwich-type TM_6-substituted GTs $[Cu(2,2'\text{-bpy})]_2[Cu(2,2'\text{-bpy})_2]_2[Cu_6(2,2'\text{-bpy})_2(B\text{-}\alpha\text{-}GeW_9O_{34})_2]\cdot3H_2O$, $[Cu(phen)]_2[Cu(phen)_2]_2[Cu_6(phen)_2(B\text{-}\alpha\text{-}GeW_9O_{34})_2]\cdot2H_2O$ and $(C_6N_2H_{18})_3H_2[\{Co(2,2'\text{-bpy})\}_2\ Co_4(H_2O)_2\text{-}(B\text{-}\alpha\text{-}GeW_9O_{34})_2]\cdot4H_2O$ (phen = 1,10-phenanthroline), in which the TM_6-cores are functionalized by different aromatic N-ligands.[22] In the first two GTs, the belt-like Cu_6-cores are stabilized by two bidentate 2,2′-bpy or phen ligands whereas the third GT anchors a Co_6-core chelated by two bidentate 2,2′-bpy ligands.

Besides the above-mentioned sandwich-type TMSPTs, several kinds of non-sandwich-type dimeric TMSPTs with two malposed subunits have also been discovered. For instance, by reaction of trilacunary POM precursor $[\alpha\text{-}SiW_9O_{34}]^{10-}$ and Ni^{II} ions in aqueous solution, Hill *et al.* made a special Fe_6-substituted ST $[(\alpha\text{-}Si(FeOH_2)_2FeW_9(OH)_3O_{34})_2]^{8-}$ (Fig. 6a) with two saturated $[\alpha\text{-}Si(FeOH_2)_2FeW_9(OH)_3O_{34}]^{4-}$ Keggin units connected *via* a edge-sharing mode.[23a] Subsequently, Mialane *et al.* reported a 2-D azido-bridging Cu_6-substituted ST $[SiW_9O_{34}Cu_3(\mu_{1,1,3}\text{-}N_3)_2(OH)(H_2O)]_2^{14-}$ which represents the first 2-D TMSPT based on azido ligands (Fig. 6b and c).[23b] In the skeleton of the $[SiW_9O_{34}Cu_3(\mu_{1,1,3}\text{-}N_3)_2(OH)(H_2O)]^{7-}$ unit, each of both $\{A\text{-}\alpha\text{-}SiW_9O_{34}\}$ ligands chelates a triangular Cu_3 subunit affording two $[SiW_9O_{34}Cu_3(\mu_{1,1,3}\text{-}N_3)_2(OH)(H_2O)]^{7-}$ units, which are connected *via* two crystallographically independent basal–basal end-on azido ligands as well as a hydroxo bridge. Under the synergistic coordination of en and a polycarboxylate ligand of IDA^{2-} (H_2IDA = iminodiacetic acid), an unseen Ni_{11}-substituted PT combination of two Ni_6-substituted trilacunary Keggin or Dawson-type POT units can form another kind of dimeric TMSPTs that were mainly found under hydrothermal reaction conditions. For example, the reaction of a saturated Keggin precursor $[\alpha\text{-}SiW_{12}O_{40}]^{4-}$ and Ni^{II} ions resulted in the generation of a discrete dimer $[Ni_6(\mu_3\text{-}OH)_3(H_2O)_9\ SiW_9O_{34}]_2^{2-}$, in which two malposed $[Ni_6(\mu_3\text{-}OH)_3(H_2O)_9SiW_9O_{34}]^{22-}$ subunits in the opposite motif are connected by four Ni–O–W connectors (Fig. 6f).[23d] Analogously, the 1-D $[Ni(2,2'\text{-bpy})(H_2O)_2]_2[Ni_6(\mu_3\text{-}OH)_3(H_2O)_{11}H\text{-}(\alpha\text{-}P_2W_{15}O_{56})]\cdot H_2O$ (Fig. 6g) with two Ni^{II}_6-substituted Dawson-type $[Ni_6(\mu_3\text{-}OH)_3(H_2O)_{11}H(\alpha\text{-}P_2W_{15}O_{56})]^{2-}$ subunits was also isolated by reaction of $[\alpha\text{-}P_2W_{15}O_{56}]^{12-}$ and Ni^{II} ions, in which $[Ni(2,2'\text{-bpy})(H_2O)_2]^{2+}$ ions as linkages bridge $[Ni_6(\mu_3\text{-}OH)_3(H_2O)_{11}H(\alpha\text{-}P_2W_{15}O_{56})]^{2-}$ subunits together, giving rise to the 1-D ladder chain alignment (Fig. 6h).[14a] Although the above two examples represent the highest number of TM ions containing Keggin or Dawson-type dimers to date, much higher nuclear TM including POT dimeric species still need to be explored.

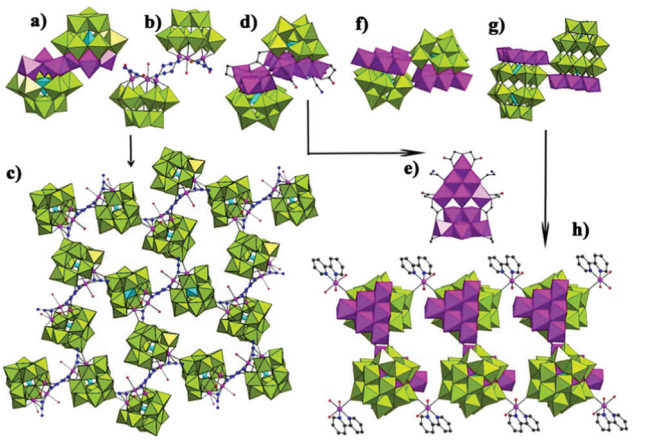

Fig. 6 (a) View of $[(\alpha\text{-}Si(FeOH_2)_2FeW_9(OH)_3O_{34})_2]^{8-}$. (b, c) View of $[SiW_9O_{34}Cu_3(\mu_{1,1,3}\text{-}N_3)_2(OH)(H_2O)]_2^{14-}$ and its 2-D layer architecture. (d, e) View of $[Ni_{11}(PW_9O_{34})_2(IDA)_3(en)_2(Hen)_2(OH)_6]^{13-}$ and its central Ni_{11} core. (f) The skeleton of $[Ni_6(\mu_3\text{-}OH)_3(H_2O)_9SiW_9O_{34}]_2^{2-}$. (g, h) View of $[Ni_6(\mu_3\text{-}OH)_3(H_2O)_{11}H(\alpha\text{-}P_2W_{15}O_{56})]_2^{4-}$ and its 1-D chain structure. [{WO_6}: lime, {XO_4}: turquoise, TM, {TMO_x} and {TMO_xN_y}: light lavender, O: red, C: cray-80%, N: blue].

2.3 Trimeric high-nuclear TMSPTs

The growing library of TMSPTs not only concentrates on monomeric sand dimeric species but also can be expanded into the trimeric triangle-shaped species (Fig. 7a). It is has been proven that the precursor $[\gamma\text{-}SiW_{10}O_{36}]^{8-}$ plays an indelible role in the exploration of triangle-shaped STs. Specifically, the metastable and labile dilacunary precursor $[\gamma\text{-}SiW_{10}O_{36}]^{8-}$ can not only retain its γ-configuration and isomerize to the α- and β-isomers, but also transform to plenary, mono-, tri- and tetralacunary Keggin POM units, which provides superior conditions for integrating TM centers to assemble novel high-nuclear TMSPT with unexpected architectures. For instance, based on the reactions of $[\gamma\text{-}SiW_{10}O_{36}]^{8-}$ and different TM ions

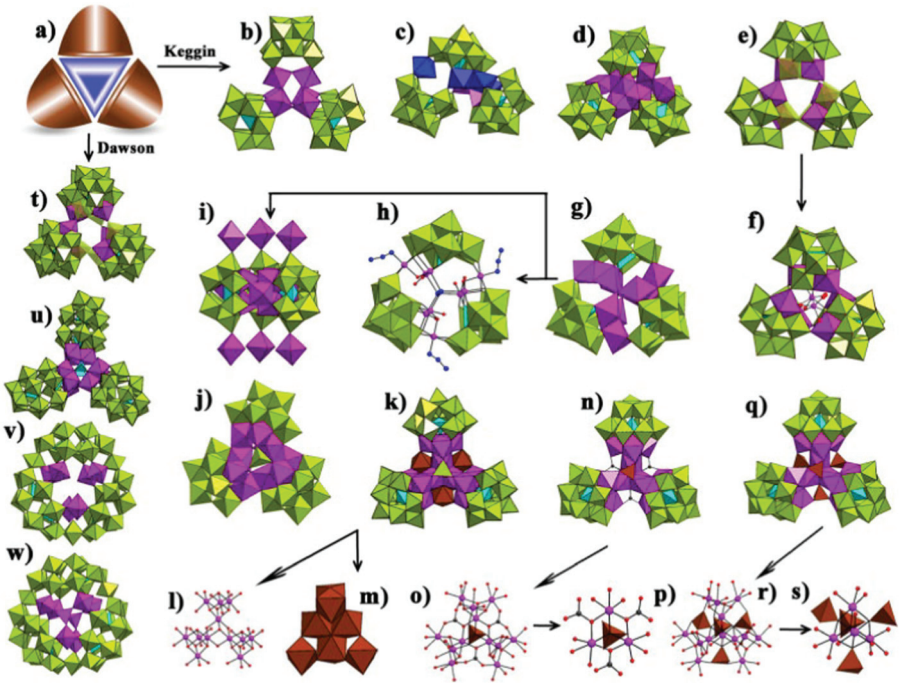

Fig. 7 (a) The schematic mode of triangle-shaped TMSPTs. (b) View of $[\{Fe_2(OH)_3(H_2O)_2\}_3(\gamma\text{-}SiW_{10}O_{36})_3]^{15-}$. (c) View of $[Mn^{III}_2Mn^{II}_4(\mu_3\text{-}O)_2(H_2O)_4(B\text{-}\beta\text{-}SiW_8O_{31})(B\text{-}\beta\text{-}SiW_9O_{34})(\gamma\text{-}SiW_{10}O_{36})]^{18-}$ [Mn^{II}: blue]. (d) $[Zr_6O_2(OH)_4(H_2O)_3\ (\beta\text{-}SiW_{10}O_{37})_3]^{14-}$. (e) View of $[Rb \subset (GeW_{10}Mn_2O_{38})_3]^{17-}$. (f) View of $[(Mn(H_2O)_3)_2(K \subset \{\alpha\text{-}GeW_{10}Mn_2O_{38}\}_3)]^{19-}$. (g) View of $[Co_9Cl_2(OH)_3(H_2O)_9(B\text{-}\beta\text{-}SiW_8O_{31})_3]^{19-}$. (h) View of $[\{SiW_8O_{31}Cu_3(OH)(H_2O)_2(N_3)\}_3(N_3)]^{17-}$. (i) View of $[Co_6(H_2O)_{30}\{Co_9Cl_2(OH)_3(H_2O)_9(\beta\text{-}SiW_8O_{31})_3\}]^{5-}$. (j) View of $[WFe_9(\mu_3\text{-}O)_3(\mu_2\text{-}OH)_6O_4H_2O(\alpha\text{-}SiW_9O_{34})_3]^{17-}$. (k, l, m) View of $[Ni_{12}(OH)_9WO_4(W_7O_{26}(OH))\ (PW_9O_{34})_3]^{25-}$, Ni^{II}_{12}-core $[Ni_{12}(OH)_9O_{13}]^{11-}$ and nona-dentate $[W_7O_{26}\ (OH)]^{11-}$ ligand [W centers in $[W_7O_{26}(OH)]^{11-}$ unit: brown]. (n, o, p) View of $[Ni_{12}(OH)_9(CO_3)_3(PO_4)(SiW_9O_{34})_3]^{24-}$ and its central $[Ni_{12}(OH)_9(CO_3)_3(PO_4)]^{6+}$ core as well as a $\{Ni_3(CO_3)_3(PO_4)\}$ quasi-cubane [P: brown]. (q, r, s) View of $[Ni_{13}(H_2O)_3(OH)_9(PO_4)_4(SiW_9O_{34})_3]^{25-}$ and its $[Ni_{13}(H_2O)_3\ (OH)_9(PO_4)_4]^{8+}$ as well as a $\{Ni_3(PO_4)_4\}$ quasi-cubane [P: brown]. (t) View of $[K \subset (P_2W_{16}Co_2O_{60})_3]^{23-}$. (u) View of $[Co_9P_8W_{45}O_{176}(OH)_3(H_2O)_6]^{27-}$. (v) View of $[Na_3 \subset \{M(H_2O)_4\}_6\{WO(H_2O)\}_3(P_2W_{12}O_{48})_3]^{15-}$. (w) View of $[Rb_3 \subset \{V^V\ V^{IV}_3O_7(H_2O)_6\}_2\{H_6P_6W_{39}O_{147}(H_2O)_3\}]^{15-}$. [$\{WO_6\}$: lime, $\{XO_4\}$: turquoise, TM and $\{TMO_x\}$: light lavender, O: red, C: cray-80%, N: blue].

by means of CASSM, three kinds of trimeric TM_6-substituted triangle-shaped STs have been obtained such as a $\{Fe^{III}_6\}$ containing $[\{Fe_2(OH)_3(H_2O)_2\}_3(\gamma\text{-}SiW_{10}O_{36})_3]^{15-}$ with a typical trianglar shape (Fig. 7b),[24a] a mixed-valence $\{Mn^{III}_2Mn^{II}_4\}$ including $[Mn^{III}_2Mn^{II}_4\ (\mu_3O)_2(H_2O)_4(B\text{-}\beta\text{-}SiW_8O_{31})(B\text{-}\beta\text{-}SiW_9O_{34})(\gamma\text{-}SiW_{10}O_{36})]^{18-}$ with an irregular triangular shape (Fig. 7c),[24b] and a $\{Zr^{IV}_6\}$ comprising $[Zr_6O_2(OH)_4(H_2O)_3\ (\beta\text{-}SiW_{10}O_{37})_3]^{14-}$ with a distorted triangle (Fig. 7d).[24c] Their structural differences are as follows: (a) although those structure building blocks are all derived from the $[\gamma\text{-}SiW_{10}O_{36}]^{8-}$ precursor, different reaction conditions stimulate the generation of $\{B\text{-}\beta\text{-}SiW_8O_{31}\}$ and $\{B\text{-}\beta\text{-}SiW_9O_{34}\}$ building blocks in the second and the $\{\beta\text{-}SiW_{10}O_{37}\}$ fragments in the third while the $\{\gamma\text{-}SiW_{10}O_{36}\}$ units are maintained in the first; (b) due to the existence of different building blocks, three TM_6-cores exhibit distinct arrangements and insertions, respectively. For the first one, six Fe^{III} centers are embedded in the binding pockets of three $\{\gamma\text{-}SiW_{10}O_{36}\}$ units, and then three formed $\{\gamma\text{-}SiW_{10}Fe_2O_{36}\}$ subunits are corner-shared with each other.[24a] In the second skeleton, an octahedral Mn^{II} ion is chelated by a $[B\text{-}\beta\text{-}SiW_8O_{31}]^{10-}$ ligand and a $[\gamma\text{-}SiW_{10}O_{36}]^{8-}$ ligand, and a mixed-valence appended cubane $\{Mn^{III}_2Mn^{II}_3\}$ is simultaneously ligated by all three lacunary Keggin moieties.[24b] Interestingly, the $\{Mn^{III}_2Mn^{II}_3\}$ group can be considered as a $\{Mn_4O_4\}$ cubane attached to a Mn^{II} atom through one of the oxygen atoms of the cube. Moreover, the Mn^{III} centers in the $\{Mn_5\}$ cubane are the generation of air oxidation of the Mn^{II} ions by vigorous stirring of the alkaline Mn^{II}-containing POM solution. Interestingly, a belt-like $\{Zr_6O_2(OH)_4(H_2O)_3\}$ cluster with three seven-coordinate Zr^{IV} centers and three eight-coordinate Zr^{IV} centers can be observed in the third skeleton.[24c] In the construction of trimeric triangle-shaped GTs, the $[\gamma\text{-}GeW_{10}O_{36}]^{8-}$ precursor usually chelates some TMs with its configuration and lacunary sites remaining unchanged, which is somewhat different from the variable $[\gamma\text{-}SiW_{10}O_{36}]^{8-}$ precursor. For instance, Cronin and collaborators synthesized a triangle-shaped Mn_6-substituted $[Rb \subset (GeW_{10}Mn_2O_{38})_3]^{17-}$ based on three Keggin-type building blocks $\{\gamma\text{-}GeW_{10}O_{36}\}$ (Fig. 7e).[24d] Different from the above discussed three triangle-shaped TM_6-substituted ST, six Mn^{III} ions are all filled in the lacunae of $\{\gamma\text{-}GeW_{10}O_{36}\}$ units to form three plenary Keggin-type units $\{\gamma\text{-}Mn_2GeW_{10}O_{36}\}$ in an approximately equilateral triangle distribution.[24d] When the molar ratio of $Mn^{II}/[\gamma\text{-}GeW_{10}O_{36}]^{8-}$ almost increases to 5, they also synthesized an intriguing triangle-shaped $Mn_8{}^{II}$-substituted GT $[(Mn(H_2O)_3)_2(K \subset \{\alpha\text{-}GeW_{10}Mn_2O_{38}\}_3)]^{19-}$ (Fig. 7f),[24e] which is structurally similar to the skeleton of

$[Rb \subset (GeW_{10}Mn_2O_{38})_3]^{17-}$.[24d] Significantly, the extra two Mn^{II} ions cap to two faces of the triangle through three bridging oxygen atoms on three $\{\alpha\text{-}GeW_{10}Mn_2O_{38}\}$ fragments, respectively. Under appropriate conditions, the $[\gamma\text{-}SiW_{10}O_{36}]^{8-}$ precursors can all transform into $\{SiW_8O_{31}\}$ fragments, facilitating the insertion of more TM centers. Thus, Cronin's group reported a triangle-shaped ST $[Co_9Cl_2(OH)_3(H_2O)_9(B\text{-}\beta\text{-}SiW_8O_{31})_3]^{17-}$, in which three $\{B\text{-}\beta\text{-}SiW_8O_{31}\}$ units anchor a central fan-shaped Co_9^{II}-core (Fig. 7g).[25a] Historically, two cases of azido ligand or additional TMs modified Co_9^{II}-substituted triangle-shaped STs $[\{SiW_8O_{31}Cu_3(OH)(H_2O)_2(N_3)\}_3(N_3)]^{19-}$ (Fig. 7h),[25b] and $[Co_6(H_2O)_{30}\{Co_9Cl_2(OH)_3(H_2O)_9(\beta\text{-}SiW_8O_{31})_3\}]^{5-}$ (Fig. 7i)[25c] with similar TM substituted modes to the $[Co_9Cl_2(OH)_3(H_2O)_9(B\text{-}\beta\text{-}SiW_8O_{31})_3]^{17-}$ unit[25a] have already reported. In the skeleton of $[\{SiW_8O_{31}Cu_3(OH)(H_2O)_2(N_3)\}_3(N_3)]^{19-}$, three equivalent $\{\gamma\text{-}SiW_8O_{31}Cu_2\}$ subunits are fused together by an encapsulated hexadentate μ-1,1,1,3,3,3-azido ligand. And three fringe $\{Cu(N_3)\}$ units with terminal azido ligands attaching to the Cu^{II} centers, link to adjacent $\{\gamma\text{-}SiW_8O_{31}Cu_2\}$ moieties *via* μ_3-OH ligands and Cu–O–W linkers.[25b] By reaction of Co^{II} ions and $[\gamma\text{-}SiW_{10}O_{36}]^{8-}$ precursor in aqueous acidic NaCl medium (pH = 5.4), six pendent Co^{II} ions can be grafted to the structure of $[Co_9Cl_2(OH)_3(H_2O)_9(B\text{-}\beta\text{-}SiW_8O_{31})_3]^{17-}$ through the terminal oxygen atoms of $\{B\text{-}\beta\text{-}SiW_8O_{31}\}$ subunits, leading to a satellite-shaped Co_{15} containing ST $[Co_6(H_2O)_{30}\{Co_9Cl_2(OH)_3(H_2O)_9(\beta\text{-}SiW_8O_{31})_3\}]^{5-}$.[25c] Notably, Wang *et al.* obtained a Fe_9-substituted ST $[WFe_9(\mu_3\text{-}O)_3(\mu_2\text{-}OH)_6O_4H_2O(\alpha\text{-}SiW_9O_{34})_3]^{17-}$ (Fig. 7j) in ionic liquids ([EMIM]Br, where EMIM = 1-ethyl-3-methylimidazolium) by an ionothermal synthesis method (ITSM).[25d] The skeleton of this triangle-shaped ST with C_3 symmetry, is constructed from three $[\alpha\text{-}SiW_9O_{34}]^{10-}$ unitsencapsulating a rare heterometallic $\{WFe_9(\mu_3\text{-}O)_3(\mu_2\text{-}OH)_6O_4H_2O\}$ core. Obviously, nine Fe^{III} ions can be viewed as the substitution of nine W centers in three trilacunary $[\alpha\text{-}SiW_9O_{34}]^{10-}$ units. Besides, the findings on triangle dodecanuclear TMSPTs were mainly carried out by Wang's group and their synthesis strategy concentrated on introducing acid anions (as WO_4^{2-}, PO_4^{3-} CO_3^{2-}) to increase the activity of the reaction system. Firstly, the reaction of $[A\text{-}PW_9O_{34}]^{9-}$, Ni^{2+} and WO_4^{2-} led to a triangle-shaped Ni_{12}-substituted PT $[Ni_{12}(OH)_9WO_4(W_7O_{26}(OH))(PW_9O_{34})_3]^{25-}$, which represents the first Ni_{12}-substituted POT (Fig. 7k).[26a] And then, with the introduction of PO_4^{3-} and CO_3^{2-} into the similar ST system, they obtained another triangle-shaped Ni_{12}-substituted ST $[Ni_{12}(OH)_9(CO_3)_3(PO_4)(SiW_9O_{34})_3]^{24-}$ (Fig. 7n).[26b] At first glance, both major skeletons are all composed of three trilacunary Keggin-type fragments anchoring a Ni_{12}-core. Nevertheless, by careful analysis of their building and the central cores, three structural distinctions can also be observed between them: (a) the $\{B\text{-}\alpha\text{-}PW_9O_{34}\}$ fragment in the former has seven exposed surface oxygen atoms while the $\{A\text{-}\alpha\text{-}SiW_9O_{34}\}$ fragment in the latter has six exposed surface oxygen atoms, which induce different substituted modes of Ni^{II} ions; (b) the $\{Ni_{12}(OH)_9O_{13}\}$ core (Fig. 7l) in the former can be viewed as the condensation of three distorted $\{Ni_4O(OH)_3\}$ cubane units. Moreover, each distorted cubane contributes three Ni^{II} ions as substitutions to form the saturated Keggin moieties $\{B\text{-}\alpha\text{-}PW_9O_{34}Ni_3\}$. However, for the latter, only one $\{Ni_3O_4\}$ quasi-cubane (Fig. 7p) unit decorated by a PO_4^{3-} and three CO_3^{2-} units can be arrested in the central $\{Ni_{12}(OH)_9(CO_3)_3(PO_4)\}$ core (Fig. 7o); (c) on both sides of the large $\{Ni_{12}(OH)_9O_{13}(PW_9O_{34})_3\}$ moiety, two extra tetradentate WO_4^{2-} and nonadentate $\{W_7O_{26}(OH)\}$ ligands (Fig. 7m) jointly chelate the $\{Ni_{12}(OH)_9O_{13}\}$ core. During the discovery of Ni_{12}-substituted ST $[Ni_{12}(OH)_9(CO_3)_3(PO_4)(SiW_9O_{34})_3]^{24-}$, an unique Ni_{13}-substituted ST $[Ni_{13}(H_2O)_3(OH)_9(PO_4)_4(SiW_9O_{34})_3]^{25-}$ (Fig. 7q) was captured by Wang and co-workers.[26b] The most obvious difference between them are their central cores $\{Ni_{12}(OH)_9(CO_3)_3(PO_4)\}$ and $\{Ni_{13}(H_2O)_3(OH)_9(PO_4)_3\}$ (Fig. 7r). Compared with the $\{Ni_{12}(OH)_9(CO_3)_3(PO_4)\}$ core, the thirteenth Ni^{II} ion in the $\{Ni_{13}(H_2O)_3(OH)_9(PO_4)_3\}$ core joins the $\{Ni_3O_4\}$ quasi-cubane (Fig. 7s) to construct a distorted cubane unit. Furthermore, owing to the absence of Na_2CO_3 in the reaction process, three PO_4^{3-} groups in the $\{Ni_{13}(H_2O)_3(OH)_9(PO_4)_3\}$ core occupy the positions of three CO_3^{2-} groups in the $\{Ni_{12}(OH)_9(CO_3)_3(PO_4)\}$ core. In the exploitation of trimeric TMSPTs, two triangle Dawson-type PTs were also discovered, such as the Co_6 substituted $[K \subset (P_2W_{16}Co_2O_{60})_3]^{23-}$ (Fig. 7t)[24d] and the Co_9 substituted $[Co_9P_8W_{45}O_{176}(OH)_3(H_2O)_6]^{27-}$ (Fig. 7u).[27] Obviously, the skeleton of $[K \subset (P_2W_{16}Co_2O_{60})_3]^{23-}$ is completed by three di-substituted Dawson units $\{P_2W_{16}Co_2O_{60}\}$ linked together through six Co–O–W bridges,[24d] whereas three tri-substituted Dawson-type fragments $\{P_2W_{15}Co_3O_{60}\}$ combine together *via* six Co–O–Co bridges and two μ_3-PO_4^{3-} groups to form the major skeleton of the latter.[27] Based on the crown-shaped trimeric $\{P_6W_{39}\}$ unit with three $\{P_2W_{12}O_{48}\}$ units connected by three $\{WO(H_2O)\}$ groups in the corner-sharing mode,[28a,b] Wang *et al.* also communicated a M_6^{II}-substituted PT $[Na_3 \subset \{M(H_2O)_4\}_6\{WO(H_2O)\}_3(P_2W_{12}O_{48})_3]^{15-}$ (M = Co^{II}, Ni^{II}) (Fig. 7v)[28c] and Kortz *et al.* isolated a mixed-valence $\{V_2^VV_6^{IV}\}$-substituted PT $[Rb_3 \subset \{V^VV_3^{IV}O_7(H_2O)_6\}_2\{H_6P_6W_{39}O_{147}(H_2O)_3\}]^{15-}$ (Fig. 7w).[28d] In the former, each of six hexa-coordinate M^{II} ions is encapsulated in the defect sites of the crown-type $\{P_6W_{39}\}$ shell by coordinating to two μ_2-oxygen atoms from two neighboring $\{P_2W_{12}O_{48}\}$ fragments in a trans mode.[28c] In the latter, six octahedral V^{IV} ions are firstly encapsulated in the defect sites of the crown-type $\{P_6W_{39}\}$ shell and then each of two tetrahedral V^V ions as a μ_3-bridge is combined with three octahedral V^{IV} ions.[28d]

In the arsenal of TMSPTs, banana-shaped species have been widely studied.[29a–c] In 2009, Mialane *et al.* also reported a banana-shaped trimeric Fe_9^{III}-substituted TMSPT $[(Fe_4W_9O_{34}(H_2O))_2(FeW_6O_{26})]^{19-}$ (Fig. 8a and b).[29d] Based on the different coordination environments, Fe^{III} ions can be classified into two types: (a) three tetrahedral Fe^{III} centers work as heteroatoms to establish tri- and hexa-vacant Keggin-type POT fragments: $\{FeW_9O_{34}\}$ and $\{FeW_6O_{26}\}$; (b) six octahedral Fe^{III} centers not only fill the lacunae of two tri-vacant POT fragments to constitute the saturated Keggin-type moieties, but also act as connectors to link $\{FeW_9O_{34}\}$ and $\{FeW_6O_{26}\}$ fragments together into a banana fashion.

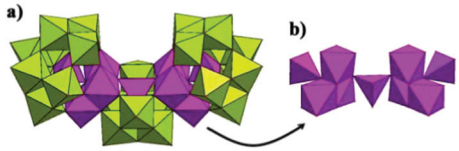

Fig. 8 (a, b) View of banana-shaped TMSPT $[(Fe_4W_9O_{34}(H_2O))_2(FeW_6O_{26})]^{19-}$ and its central Fe_9 core. [{WO_6}: lime, {TMO_x}: light lavender, O: red].

2.4 Tetrameric high-nuclear TMSPTs

Tetrameric species can be generally subdivided into the following categories: "S"-shaped tetramers (Fig. 9a), tetrahedral tetramers, wheel-shaped tetramers, stagger tetramers, cruciform tetramers and rectangle tetramers. In general, two dimeric TMSPT subunits are fused together by a TM ion, a {TM_n} cluster or a {TM_xW_y} hetreometallic cluster to form the "S"-shaped tetrameric TMSPTs. For instance, Mialane *et al.* made a typical "S"-shaped Co^{II}_7-substituted ST $[\{(B\text{-}\beta\text{-}SiW_9O_{33}(OH))(\beta\text{-}SiW_8O_{29}(OH)_2)Co_3(H_2O)\}_2Co(H_2O)_2]^{20-}$, in which two equivalent Co^{II}_3-substituted sandwich-type {$(B\text{-}\beta\text{-}SiW_9O_{33}(OH))(\beta\text{-}SiW_8O_{29}(OH)_2)Co_3(H_2O)$} subunits connected *via* a $[Co(H_2O)_2]^{2+}$ unit (Fig. 9b).[19a] The nearly equilateral triangular {Co_3} cluster in each sandwich-type subunit is encapsulated by a {$B\text{-}\beta\text{-}SiW_9O_{33}(OH)$} unit and a {$\beta\text{-}SiW_8O_{29}(OH)_2$} fragment, whereas the bridging $[Co(H_2O)_2]^{2+}$ unit is chelated by two {$\beta\text{-}SiW_8O_{29}(OH)_2$} fragments from two sandwich-type subunits. Similar work in Mn^{II}_7-substituted GT $[Mn(H_2O)_2\{Mn_3(H_2O)(B\text{-}\beta\text{-}GeW_9O_{33}(OH))(B\text{-}\beta\text{-}GeW_8O_{30}(OH))\}_2]^{22-}$ was reported by Kortz and co-workers in 2009.[30a] Recently, two "S"-shaped TM_8-substituted POTs constructed from two tri-TM sandwiched POT moieties and one {TM_2} unit also emerged in succession. Cronin *et al.* firstly reported a mixed-valence $\{Mn^{II}_2Mn^{III}_6\}$-substituted ST $[Mn^{II}_2\{Mn^{II}(H_2O)_5Mn^{III}_3(H_2O)(B\text{-}\beta\text{-}SiW_9O_{34})(B\text{-}\beta\text{-}SiW_6O_{26})\}_2]^{18-}$ with two supporting $[Mn^{II}(H_2O)_5]^{2+}$ cations (Fig. 9c), in which two sandwich-type $\{Mn^{II}(H_2O)_5Mn^{III}_3(H_2O)(B\text{-}\beta\text{-}SiW_9O_{34})(B\text{-}\beta\text{-}SiW_6O_{26})\}$ moieties are fused together by a $\{Mn_2^{II}\}$ linker.[30b] Two triangular $\{Mn^{III}_3\}$ units fill in the lacunae of two {$B\text{-}\beta\text{-}SiW_9O_{34}$} fragments while the $\{Mn_2^{II}\}$ unit is chelated by two hexa-vacant {$B\text{-}\beta\text{-}SiW_6O_{26}$} fragments. In 2011, a similar "S"-shaped Fe_8-substituted AT $\{[(\alpha\text{-}H_2AsW_6O_{26})Fe_3(H_2O)(B\text{-}\alpha\text{-}H_4AsW_9O_{34})]_2[Fe]_2\}^{4-}$ was reported by Zhao *et al.* utilizing the $[As_2^{III}W_{19}O_{67}(H_2O)]^{14-}$ precursor under hydrothermal conditions.[30c] In addition, an "S"-shaped nona-Mn^{II} encapsulated ST $\{[Mn(H_2O)_3]_2[Mn(H_2O)_2][(B\text{-}\beta\text{-}SiW_9O_{33}(OH))Mn_3(H_2O)(B\text{-}\beta\text{-}SiW_8O_{30}(OH))]_2\}^{18-}$ was discovered by Zhao and co-workers, which is constructed from two structurally equivalent asymmetric sandwich-type $[(B\text{-}\beta\text{-}SiW_9O_{33}(OH))Mn_3(H_2O)(B\text{-}\beta\text{-}SiW_8O_{30}(OH))]^{12-}$ moieties held together by two structurally equivalent $[Mn(H_2O)_3]^{2+}$ cations and an unique $[Mn(H_2O)_2]^{2+}$ cation (Fig. 9d).[31] The most intriguing feature is that adjacent tetrameric $\{[Mn(H_2O)_3]_2[Mn(H_2O)_2][(B\text{-}\beta\text{-}SiW_9O_{33}(OH))Mn_3(H_2O)(B\text{-}\beta\text{-}SiW_8O_{30}(OH))]_2\}^{18-}$ units are linked *via* two equivalent $[Mn(H_2O)_3]^{2+}$ cations constructing the infinite 1-D chain architecture (Fig. 9e).[31]

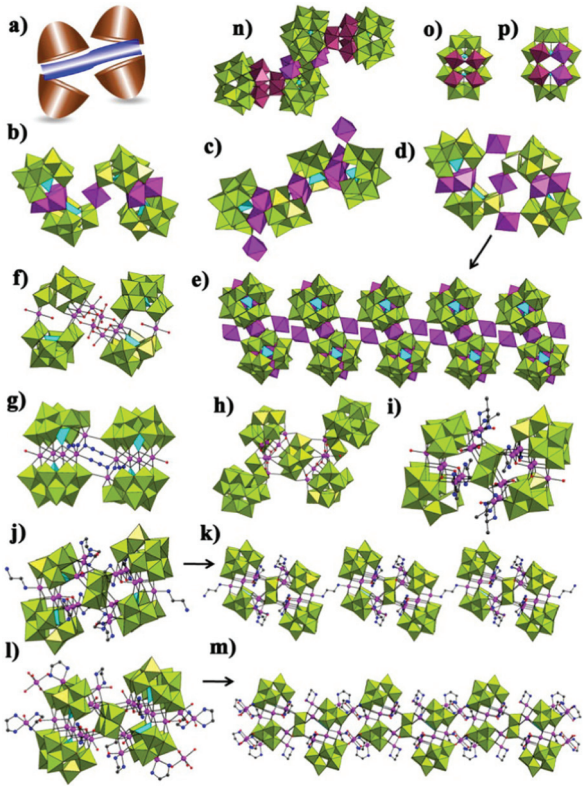

Fig. 9 (a) The schematic mode of "S"-shaped TMSPTs. (b) View of $[\{(B\text{-}\beta\text{-}SiW_9O_{33}(OH))(\beta\text{-}SiW_8O_{29}(OH)_2)Co_3(H_2O)\}_2Co(H_2O)_2]^{20-}$. (c) View of $[Mn^{II}_2\{Mn^{II}(H_2O)_5Mn^{III}_3(H_2O)(B\text{-}\beta\text{-}SiW_9O_{34})(B\text{-}\beta\text{-}SiW_6O_{26})\}_2]^{18-}$. (d, e) View of $\{[Mn(H_2O)_3]_2[Mn(H_2O)_2][(B\text{-}\beta\text{-}SiW_9O_{33}(OH))Mn_3(H_2O)(B\text{-}\beta\text{-}SiW_8O_{30}(OH))]_2\}^{18-}$ and its 1-D chain. (f) View of $[\{Fe(H_2O)_2(SiW_{10}O_{35})(SiFe_2W_8O_{35})\}_2(Fe_4O_4(H_2O)_6)]^{26-}$. (g) View of $[Cu_{10}(H_2O)_2(N_3)_4(GeW_9O_{34})_2(GeW_8O_{31})_2]^{24-}$. (h) View of $[\{Mn^{III}_3Mn^{IV}_4O_4(OH)_2(OH_2)\}_2(W_6O_{22})(H_2W_8O_{32})_2(H_4W_{13}O_{46})_2]^{26-}$. (i) View of $[H_6Ni_{20}P_4W_{34}(OH)_4O_{136}(enMe)_8(H_2O)_6]^{6-}$. (j, k) View of $[H_8Ni_{20}P_4W_{34}(OH)_4O_{136}(en)_9(H_2O)_4]^{4-}$ and its 1-D chain. (l, m) View of $\{[(\alpha\text{-}AsW_6O_{26})Ni_6(OH)_2(H_2O)_3(en)(B\text{-}\alpha\text{-}AsW_9O_{34})]_2[W_4O_{16}][Ni_3(H_2O)_2(en)]_2\}^{16-}$ and its 1-D chain. (n, o, p) View of $[Fe_{10}Se_8W_{62}O_{222}(OH)_{18}(H_2O)_4]^{28-}$ and two saturated $\{\alpha\text{-}Se_2W_{16}Fe_2\}$ and $\{\gamma\text{-}Se_2W_{15}Fe_3\}$ fragments [W/Fe: violet]. [{WO_6}: lime, {XO_4}: turquoise, TM and {TMO_x}: light lavender, O: red, C: cray-80%, N: blue].

Notably, a "S"-shaped Fe_{10}-substituted ST $[\{Fe(H_2O)_2(SiW_{10}O_{35})(SiFe_2W_8O_{35})\}_2(Fe_4O_4(H_2O)_6)]^{26-}$ (Fig. 9f) was firstly realized by Cronin and co-workers, which can be seen as a dimerization of $[Fe(H_2O)_2\{\gamma\text{-}Fe_2SiW_8O_{33}(H_2O)_2\}\{\gamma\text{-}SiW_{10}O_{35}\}]^{11-}$ joined by four additional Fe^{III} ions.[32a] Alternatively, $[\{Fe(H_2O)_2(SiW_{10}O_{35})(SiFe_2W_8O_{35})\}_2(Fe_4O_4(H_2O)_6)]^{26-}$ can also be regarded as an {Fe_8} core combined with two {$\gamma\text{-}SiW_{10}O_{36}$} and two {$B\text{-}\beta\text{-}SiW_8O_{31}$} moieties meanwhile each of the two additional $[Fe(H_2O)_2]^{3+}$ ions, respectively, connects a {$\gamma\text{-}SiW_{10}O_{36}$} and a {$B\text{-}\beta\text{-}SiW_8O_{31}$} together. Another "S"-shaped azido-bridging Cu_{10}-substituted GT $[Cu_{10}(H_2O)_2(N_3)_4(GeW_9O_{34})_2(GeW_8O_{31})_2]^{24-}$ (Fig. 9g) was also discovered by Wang's group by reaction of $[\gamma\text{-}GeW_{10}O_{36}]^{8-}$ with Cu^{2+} and the participation of N_3^- at room temperature, comprising a peculiar {$Cu_{10}(N_3)_4$} cluster linking two {$\beta\text{-}GeW_8O_{31}$} and two {$B\text{-}\alpha\text{-}GeW_9O_{34}$} fragments.[32b] It should be pointed out that the {$Cu_{10}(N_3)_4$} cluster can be

interpreted as four edge-sharing Cu^{II} ions firstly form a rhombus $\{Cu_4\}$ cluster, and then an extra Cu^{II} ion grafts to the rhombus $\{Cu_4\}$ cluster by two end-on azido ligands, forming the $\{Cu_5(N_3)_2\}$ cluster, and finally two $\{Cu_5(N_3)_2\}$ clusters are linked together through two $\mu_{1,1,3}$-azido ligands to create the $\{Cu_{10}(N_3)_4\}$ cluster.[32b] By acidifying and then refluxing a solution of WO_4^{2-} in the presence of Mn_{12}-acetate, Fang *et al.* discovered a tetradeca-manganese magnetic cluster $[\{Mn^{III}_3Mn^{IV}_4O_4(OH)_2(OH_2)\}_2(W_6O_{22})(H_2W_8O_{32})_2(H_4W_{13}O_{46})_2]^{26-}$ (Fig. 9h), the most apparent feature of which not only contains two high spin Mn_7 cores stabilized by isopolytungstate ligands, but also consists of three types of isopolytungstate units of one $\{W_6O_{22}\}$, two $\{W_8O_{32}\}$ and two $\{W_{13}O_{46}\}$.[33] The successful synthesis of this tetradeca-manganese POT illustrates the promising feasibility of utilizing defect isopolytungstate fragments as synthons to construct high nuclear TMSPT aggregates and model the surface deposition of molecular magnets.[33] Besides "S"-shaped multi-Co^{II}, $Mn^{II/III/IV}$ and Fe^{III} substituted tetrameric POTs, "S"-shaped multi-Ni^{II} substituted tetrameric POTs were also prepared by Yang's group and Zhao's group by the reaction strategy of utilizing the highly active $[A\text{-}\alpha\text{-}XW_9O_{34}]^{9-}$ ($X = P^V$, As^V) fragments as SDAs and the bidentate organoamine ligands as SSAs under hydrothermal conditions.[34,35] In 2009, Yang *et al.* creatively addressed a discrete Ni_{20}-including POT $[H_6Ni_{20}P_4W_{34}(OH)_4O_{136}(enMe)_8(H_2O)_6]^{6-}$ with two Ni_6-cores $\{Ni_6O_{15}(OH)_2(H_2O)(enMe)_2\}$ andtwo Ni_4-cores $\{Ni_4O_{10}(H_2O)_2(enMe)_2\}$ stabilized by three kinds lacunary PT fragments $\{B\text{-}\alpha\text{-}PW_9O_{34}\}$, $\{PW_6O_{26}\}$ and $\{W_4O_{16}\}$ (Fig. 9i).[34] It is noteworthy that this Ni_{20}-including POT can be further functionalized to generate new derivatives by removing or inserting Ni^{II} centers on the surface or can be linked together by employing organic amines or Ni^{II} complexes as connectors. For example, by removing two Ni^{II} ions from two Ni_4-cores, Zhao *et al.* isolated a novel Ni^{II}_{18}-substituted AT $\{[(\alpha\text{-}AsW_6O_{26})Ni_6(OH)_2(H_2O)_3(en)(B\text{-}\alpha\text{-}AsW_9O_{34})]_2[W_4O_{16}][Ni_3(H_2O)_2(en)]_2\}^{16-}$.[35a] By inserting two extraneous Ni^{II} ions to two Ni_4-cores, Yang *et al.* made a Ni_{22}-encapsulated POT $[Ni_{22}X_4W_{34}(OH)_4O_{136}(en)_{10}(H_2O)_5]^{12-}$ (X = 0.5P + 0.5Ge).[35b] More interestingly, the bridging function of the en ligand led to the formation of the 1-D infinite chain structure constructed from Ni_{20}-including POT $[H_8Ni_{20}P_4W_{34}(OH)_4O_{136}(en)_9(H_2O)_4]^{4-}$ building units (Fig. 9j and k).[34] Similar phenomenon was observed in Ni^{II}_{20}-substituted AT.[35a] Furthermore, the employment of Ni^{II} complexes resulted in the construction of the other 1-D chain For example, in $[enH_2]_2[Ni(H_2O)_4]_2[Ni(en)_2]_2[Ni(en)]_2\{[(\alpha\text{-}AsW_6O_{26})Ni_6(OH)_2(H_2O)_3(en)(B\text{-}\alpha\text{-}AsW_9O_{34})]_2[W_4O_{16}][Ni_3(H_2O)_2(en)]_2\}\cdot16H_2O$, the 1-D chain alignment is made up of eighteen Ni^{II}_{18}-substituted $\{[(\alpha\text{-}AsW_6O_{26})Ni_6(OH)_2(H_2O)_3(en)(B\text{-}\alpha\text{-}AsW_9O_{34})]_2[W_4O_{16}][Ni_3(H_2O)_2(en)]_2\}^{16-}$ units through two $[Ni(H_2O)_4]^{2+}$ and two $[Ni(en)_2]^{2+}$ bridges (Fig. 9l and m).[35a] The discovery of these multi-Ni^{II} substituted tetrameric POTs not only enriches the diversity of the structural chemistry and coordination chemistry of TM substituted ATs, but also provides inspiring directions to design and prepare many more high-nuclear TMSPTs. On the other hand, an unobserved "S"-shaped multi-Fe^{III} substituted Dawson-type tetrameric selenotungstate $[Fe_{10}Se_8W_{62}O_{222}(OH)_{18}(H_2O)_4]^{28-}$ (Fig. 9n) was also synthesized by Wang *et al.* from an acidified mixture of $[Se_6W_{39}O_{141}(H_2O)_3]^{24-}$ and Fe^{3+} ions in the presence of NH_4^+ media.[17b] In this skeleton, two di-Fe^{III} substituted Dawson ($\alpha\text{-}Se_2W_{16}Fe_2$) units (Fig. 9o) and two tri-Fe^{III} substituted Dawson $\{(\gamma\text{-}Se_2W_{15}Fe_3)\}$ units (Fig. 9p) connected *via* twelve μ_2-oxo bridges.

Now we start to talk about the wheel-shaped tetramers (Fig. 10a) based on $\{P_8W_{48}O_{184}\}$ ligands. In 1985, Tézé and Contant for the first time reported the preparation and structure of the wheel-shaped POT $[H_7P_8W_{48}O_{184}]^{33-}$ that was evolved from the corner-sharing end-to-end connection of four hexa-vacant Dawson $[H_2P_2W_{12}O_{48}]^{12-}$ fragments.[15b] Before that, the relevant investigation on $\{P_8W_{48}O_{184}\}$ ligands had been at a standstill, which may be partly related to the judgment that $[H_7P_8W_{48}O_{184}]^{33-}$ couldn't integrate divalent or trivalent TM ions to generate TMSTPs.[11n,15b] This situation was at a stalemate until Kortz *et al.* reported an unprecedented wheel-shaped Cu_{20}-anchoring tungstophosphate $[Cu_{20}Cl(OH)_{24}(H_2O)_{12}(P_8W_{48}O_{184})]^{25-}$ (Fig. 10b) by interacting $CuCl_2\cdot2H_2O$ with $K_{28}Li_5[H_7P_8W_{48}O_{184}]\cdot92H_2O$ in the ratio 24 : 1 in aqueous medium (pH 6) in 2005.[36a] Obviously, the template effect of $\{P_8W_{48}O_{184}\}$ induces the aggregation of twenty Cu^{2+} ions with inclusion of a chloride ion in the central cavity, leading to the formation of the $[Cu_{20}Cl(OH)_{24}(H_2O)_{12}(P_8W_{48}O_{184})]^{25-}$ cluster, in which twenty Cu^{2+} ions are linked to neighboring Cu^{2+} ions *via* μ_3-oxo atoms to generate a highly symmetrical, cage-like assembly.[36a] From then on, the poten-

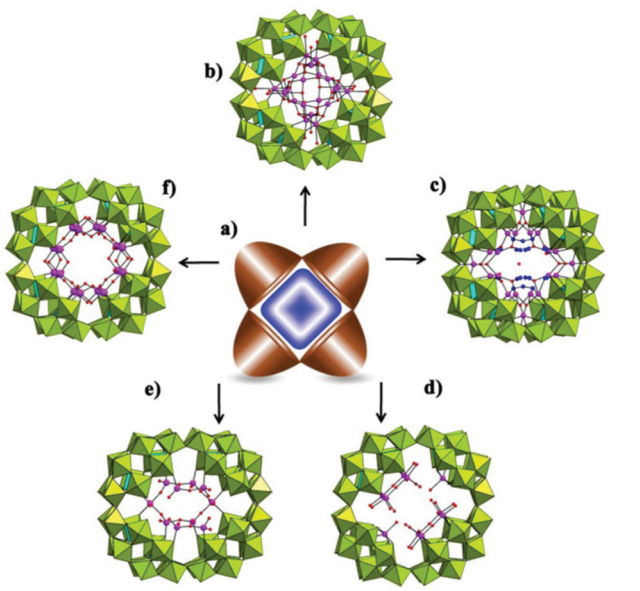

Fig. 10 (a) The schematic mode of wheel-shaped TMSPTs. (b) View of $[Cu_{20}Cl(OH)_{24}(H_2O)_{12}(P_8W_{48}O_{184})]^{25-}$. (c) The structure of $[P_8W_{48}O_{184}Cu_{20}(N_3)_6(OH)_{18}]^{24-}$. (d) The skeleton of $\{[Cu(H_2O)]_2[Cu_4(OH)_4(H_2O)_8]_2P_8W_{48}O_{184}\}^{28-}$. (e) View of $[K_8 \subset \{P_8W_{48}O_{184}\}\{V^V_4V^{IV}_2O_{12}(H_2O)_2\}_2]^{24-}$. (f) The structure of $[P_8W_{48}O_{184}Fe_{16}(OH)_{28}(H_2O)_4]^{20-}$. [$\{WO_6\}$: lime, $\{XO_4\}$: turquoise, TM: light lavender, O: red, N: blue].

tial of multi-vacant precursor $[H_7P_8W_{48}O_{184}]^{33-}$ integrating various TM ions has been constantly developed. For example, the analogues of $[Cu_{20}Cl(OH)_{24}(H_2O)_{12}(P_8W_{48}O_{184})]^{25-}$ with the central chloride guest substituted by bromide and iodide ions were also obtained by Bassil *et al.*[36b] Furthermore, an azido-bridging Cu_{20}-substituted hybrid $[P_8W_{48}O_{184}Cu_{20}(N_3)_6(OH)_{18}]^{24-}$ with two $\{Cu_5(OH)_4\}$ and two $\{Cu_5(OH)_2(\mu_{1,1,3,3}\text{-}N_3)\}$ groups connected through four μ-OH and four $\mu_{1,1}$-N_3 additional ligands was discovered by Mialane *et al.* and was the largest azido POT complex at that time (Fig. 10c).[23b] Subsequently, a Cu_{10}-encapusulated derivative $\{[Cu(H_2O)]_2[Cu_4(OH)_4(H_2O)_8]_2P_8W_{48}O_{184}\}^{28-}$ was also found, in which two $\{Cu_4\}$ clusters and two isolated Cu ions are co-trapped by $\{P_8W_{48}O_{184}\}$ units for the first time (Fig. 10d).[36c] When $VOSO_4{\cdot}5H_2O$ was introduced to this reaction in the CH_3COONa–CH_3COOH buffer, a mixed-valence V_{12}-encaplusted aggregate $[K_8 \subset \{P_8W_{48}O_{184}\}\{V^V_4V^{IV}_2O_{12}(H_2O)_2\}_2]^{24-}$ with two cyclic V_6-type $\{V^V_4V^{IV}_2O_{12}(H_2O)_2\}^{4+}$ capping groups closing in the central cavity (Fig. 10e) was separated.[36d] The application of Fe^{3+} ions and $[H_7P_8W_{48}O_{184}]^{33-}$ in the CH_3COOLi–CH_3COOH buffer made the isolation of an intriguing Fe^{II}_{16}-substituted PT nanocluster $[P_8W_{48}O_{184}Fe_{16}(OH)_{28}(H_2O)_4]^{20-}$ (Fig. 10f).[36e] Structurally, the unobserved $\{Fe_{16}(OH)_{28}(H_2O)_4\}$ core consisted of sixteen edge- and corner-sharing $\{FeO_6\}$ octahedra grafts to the inner surface of the wheel-shaped $\{P_8W_{48}O_{184}\}$ unit to form the major skeleton of $[P_8W_{48}O_{184}Fe_{16}(OH)_{28}(H_2O)_4]^{20-}$.[36e]

Moreover, tetrahedral species with more than twelve TM centers anchored by four lacunary Keggin or Dawson-type building blocks located on four vertices as an important subclass of tetrameric TMSPTs have made great progress over the past decade. The construction of such tetrahedral species is mostly relevant to the structure-stabilizing action of tetrahedral PO_4^{3-} groups and the structure templating functionality of lacunary POT building blocks. For example, by hydrothermal reaction of trilacunary Keggin-type precursor $[A\text{-}\alpha\text{-}PW_9O_{34}]^{9-}$ and Fe^{3+} ions at different temperatures, two kinds of novel tetrahedral TMSPTs $[\{Fe^{II}_{1.5}Fe^{III}_{12}(\mu_3\text{-}OH)_{12}(\mu_4\text{-}PO_4)_4\}(B\text{-}\alpha\text{-}PW_9O_{34})_4]^{21-}$ (Fig. 11b) and $[\{Fe^{II}Fe^{III}_{12}(\mu_3\text{-}OH)_{12}(\mu_4\text{-}PO_4)_4\}(B\text{-}\alpha\text{-}PW_9O_{34})_4]^{22-}$ (Fig. 11d) were synthesized by Yang *et al.* in 2007.[12c,37a] In the former, four tri-Fe^{III} substituted $\{Fe^{III}_3(\mu_3\text{-}OH)_3(B\text{-}\alpha\text{-}PW_9O_{34})\}$ units are connected together by a central $\{Fe^{II}_4O_4\}$ cubane core and four $\{\mu_4\text{-}PO_4\}$ bridges while in the latter four tri-Fe^{III} $\{Fe^{III}_3(\mu_3\text{-}OH)_3(\mu_4\text{-}PO_4)(B\text{-}\alpha\text{-}PW_9O_{34})\}$ units are combined together by a $\{Fe^{II}_2O_2\}$ unit and four μ_4-PO_4 bridges. The $Fe_{13.5}$-core in the former displays four exterior $\{Fe^{III}_3Fe^{II}O(OH)_3\}$ cubanes attaching to one interior $\{Fe^{II}_4O_4\}$ cubane by a corner-sharing mode (Fig. 11c), whereas two $\{Fe^{III}_3Fe^{II}O(OH)_3\}$ cubanes and two $\{Fe^{III}_3O(OH)_3\}$ truncated cubanes can be observed in the latter Fe_{13}-core (Fig. 11e). It should be emphasized that μ_4-PO_4 bridges in both TMSPTs are derived from the degradation of the precursors $[A\text{-}\alpha\text{-}PW_9O_{34}]^{9-}$. On the other hand, other tetrahedral TMSPTs can also be obtained from the reaction of trilacunary POM precursors, Fe^{3+} ions and PO_4^{3-} by virtue of CASSM, which include the Keggin- or Dawson-type Fe_{13}-substituted PT $[(B\text{-}\alpha\text{-}PW_9O_{34}Fe_3(OH)_3)_4(PO_4)_4Fe]$,[37b] and $[Fe_{13}P_8W_{60}O_{224}(OH)_{12}(PO_4)_4]^{33-}$ (Fig. 11f and g),[37c] two Keggin-type Fe_{14}-substituted POTs $[Na_2Fe_{14}(OH)_{12}(PO_4)_4(A\text{-}\alpha\text{-}XW_9O_{34})_4]^{20-}$ (X = Si^{IV}, Ge^{IV}) and a Dawson-type Fe^{III}_{14}-substituted PT $[Fe_{14}O_6(OH)_{13}(P_2W_{15}O_{56})_4]^{31-}$.[38b] All of them incorporate the arrangement of four exterior cubane units attaching to one interior cubane unit by a corner-sharing fashion, except for $[Na_2Fe_{14}(OH)_{12}(PO_4)_4(A\text{-}\alpha\text{-}XW_9O_{34})_4]^{20-}$ in which only one interior $\{Fe^{III}_4O_4\}$ cubane unit and four $\{Fe^{III}_4(OH)_3\}$ half-open cubane units can be detected (Fig. 11h and i),[37d] the main reason of which is that four $\{XW_9O_{34}\}$ fragments adopt the A-α-configuration rather than the B-α-configuration. Moreover, this efficient strategy also promoted the generation of four Co_{16}-substituted tetrahedral POTs with different heteroatoms $[\{Co_4(OH)_3(PO_4)\}_4(A\text{-}\alpha\text{-}XW_9O_{34})_4]^{28-}$ (X = P^V, As^V) and $[\{Co_4(OH)_3(PO_4)\}_4(A\text{-}\alpha\text{-}XW_9O_{34})_4]^{32-}$ (X = Si^{IV}, Ge^{IV}) (Fig. 11j), whose tetrahedral skeletons are all finished by four plenary $\{Co_3^{II}XW_9O_{34}\}$ units encapsulating a $\{Co^{II}_4O_4\}$ cubane and four PO_4^{3-} groups (Fig. 11k).[38] Notably, the structure of $\{Co^{II}_4O_4\}$ cubane is similar to the $\{Mn_3CaO_4\}$ core of the oxygen-evolving complex in photosystem II and their visible light-driven water oxidation properties will be discussed in the next section of application fields.[38a] Most interestingly, the assembly of Mn_{12}-acetate with $[A\text{-}\alpha\text{-}PW_9O_{34}]^{9-}$ in the participation of HPO_4^{2-} and en in aqueous solution produced a mixed-valence tetrahedral TMSPT $[Mn^{III}_{13}Mn^{II}O_{12}(PO_4)_4(PW_9O_{34})_4]^{31-}$ (Fig. 11l) with a $\{Mn^{III}_{13}Mn^{II}(\mu_2\text{-}O)_6(\mu_3\text{-}O)_6(\mu_4\text{-}PO_4)_2(\mu_5\text{-}PO_4)_2\}$ core (Fig. 11m),[39] which is very similar to the structure of $[\{Fe^{II}_{1.5}Fe^{III}_{12}(\mu_3\text{-}OH)_{12}(\mu_4\text{-}PO_4)_4\}(B\text{-}\alpha\text{-}$

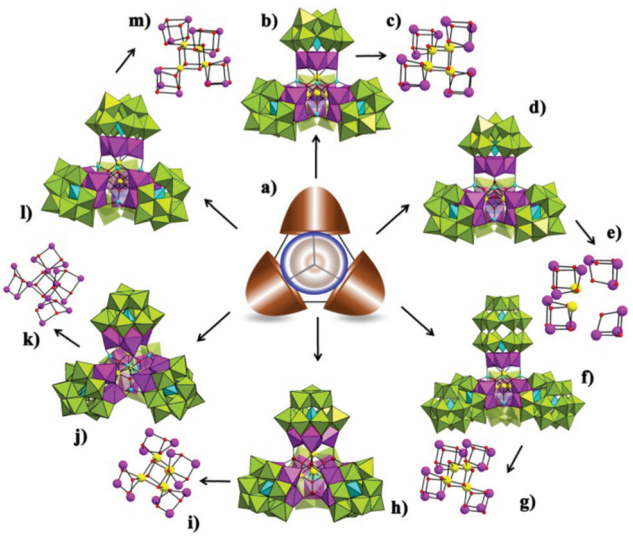

Fig. 11 (a) The schematic mode of tetrahedron-shaped TMSPTs. (b, c) View of $[\{Fe^{II}_{1.5}Fe^{III}_{12}(\mu_3\text{-}OH)_{12}(\mu_4\text{-}PO_4)_4\}(B\text{-}\alpha\text{-}PW_9O_{34})_4]^{21-}$ and its central core. (d, e) View of $[\{Fe^{II}Fe^{III}_{12}(\mu_3\text{-}OH)_{12}(\mu_4\text{-}PO_4)_4\}(B\text{-}\alpha\text{-}PW_9O_{34})_4]^{22-}$ and its central core. (f, g) View of $[Fe_{13}P_8W_{60}O_{224}(OH)_{12}(PO_4)_4]^{33-}$ and its central core. (h, i) View of $[Na_2Fe_{14}(OH)_{12}(PO_4)_4(A\text{-}\alpha\text{-}SiW_9O_{34})_4]^{20-}$ and its central core. (j, k) View of $[\{Co_4(OH)_3(PO_4)\}_4(PW_9O_{34})_4]^{28-}$ and the central core. (l, m) View of $[Mn^{III}_{13}Mn^{II}O_{12}(PO_4)_4(PW_9O_{34})_4]^{31-}$ and the central core. [{WO_6}: lime, {XO_4}: turquoise, TM and {TMO_x}: light lavender, disordered TM ion: yellow, O: red].

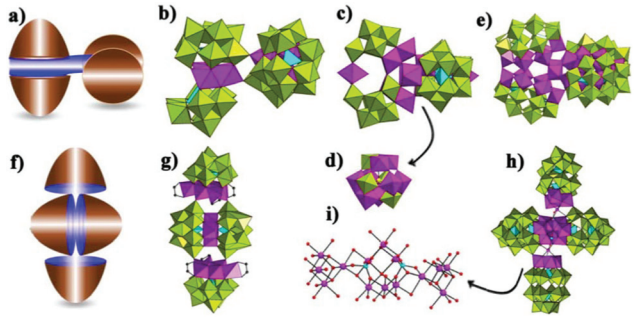

Fig. 12 (a) The schematic mode of stagger TMSPTs. (b) View of $[\{Co_3(B\text{-}\beta\text{-}SiW_9O_{33}(OH))(B\text{-}\beta\text{-}SiW_8O_{29}(OH)_2)\}_2]^{22-}$. (c) The structure of $[W_{36}Si_4O_{136}Mn^{II}_{10}(OH)_4(H_2O)_8]^{24-}$. (d) The skeleton of $\{H_4Mn_8W_4O_{40}\}$ fragment. (e) View of $[H_{55}P_8W_{49}Fe_{27}O_{248}]^{26-}$. (f) Scheme of cruciform TMSPTs. (g) View of $\{[Cu_6(\mu_3\text{-}OH)_3(en)_3(H_2O)_2(B\text{-}\alpha\text{-}PW_9O_{34})]_2[Cu_4(H_2O)_2(B\text{-}\alpha\text{-}PW_9O_{34})_2]\}^{6-}$. (h, i) View of $[Co_{14}P_{10}W_{60}O_{232}(OH)_9(H_2O)_6]^{35-}$ and its central Co_{14}-core. [$\{WO_6\}$: lime, $\{XO_4\}$: turquoise, TM, $\{TMO_x\}$ and $\{TMO_xN_y\}$: light lavender, O: red, C: cray-80%, N: blue].

$PW_9O_{34})_4]^{21-}$.[12c] Upon continuous research, several stagger tetrameric TMSPTs with distinctive structural features were also discovered. For example, by reaction of $[\gamma\text{-}SiW_{10}O_{36}]^{8-}$ with Co^{II} ions in the ratio of 1 : 2 in sodium acetate buffer (pH = 4.8), Kortz and collaborators found a Co^{II}_6-substituted stagger tetrameric ST $[\{Co_3(B\text{-}\beta\text{-}SiW_9O_{33}(OH))(B\text{-}\beta\text{-}SiW_8O_{29}(OH)_2)\}_2]^{22-}$ (Fig. 12b) constructed from two asymmetric sandwich-type units $[Co_3(B\text{-}\beta\text{-}SiW_9O_{33}(OH))(B\text{-}\beta\text{-}SiW_8O_{29}(OH)_2)]^{11-}$ with different spatial orientations linked *via* sharing to two terminal oxygen atoms,[40a] in which tri-vacant $\{B\text{-}\beta\text{-}SiW_9O_{33}(OH)\}$ and tetra-vacant $\{B\text{-}\beta\text{-}SiW_8O_{29}(OH)_2\}$ fragments are observed, suggesting the occurrence of the transformation of $\{\gamma\text{-}SiW_{10}O_{36}\} \rightarrow \{\beta\text{-}SiW_{10}O_{38}\}/\{\beta\text{-}SiW_{10}O_{37}\} \rightarrow \{B\text{-}\beta\text{-}SiW_9O_{34}\}/\{B\text{-}\beta\text{-}SiW_8O_{31}\} \rightarrow \{B\text{-}\alpha\text{-}SiW_9O_{34}\}$.[40a] The other example is Cronin's Mn_{10}-substituted ST $[W_{36}Si_4O_{136}Mn^{II}_{10}(OH)_4(H_2O)_8]^{24-}$ (Fig. 12c) with two crossed $\{(SiW_8O_{31})_2Mn\}$ subunits chelating an unique Keggin-type $\{H_4Mn_8W_4O_{40}\}$ core (Fig. 12d).[40b] Of special interest is that four $\{W_3\}$ units of the saturated Keggin-type moiety were all di-substituted by two Mn^{II} centers for the construction of this highly substituted central core $\{H_4Mn_8W_4O_{40}\}$. A more interesting case is Gouzerh's Fe_{27}-incorporated PT $[H_{55}P_8W_{49}Fe_{27}O_{248}]^{26-}$ (Fig. 12e) that was synthesized by $[H_2P_2W_{12}O_{48}]^{12-}$ with excess Fe^{3+} ions in a mixture of H_2O and CH_3COONa at 95 °C, *etc.*[15a] In $[H_{55}P_8W_{49}Fe_{27}O_{248}]^{26-}$, four hexa-substituted saturated $\{P_2W_{12}Fe_6\}$ subunits attach to a central adamantane $\{Fe_4O_6\}$ core *via* three Fe–O–Fe bridges. At that time, $[H_{55}P_8W_{49}Fe_{27}O_{248}]^{26-}$ is the second largest iron cluster including TMSPT, which is only surpassed by the reported $\{Mo^{VI}_{72}Fe^{III}_{30}\}$ keplerate.[41]

In contrast to other tetrameric TMSPT species, the cruciform TMSPTs are comparatively rare (Fig. 12f). In 2007, Yang *et al.* reported a cruciform Cu_{16}-substituted PT tetramer $\{[Cu_6(\mu_3\text{-}OH)_3(en)_3(H_2O)_2(B\text{-}\alpha\text{-}PW_9O_{34})]_2[Cu_4(H_2O)_2(B\text{-}\alpha\text{-}PW_9O_{34})_2]\}^{6-}$ (Fig. 12g) by hydrothermal reaction of $CuCl_2{\cdot}2H_2O$ and tri-vacant Keggin $Na_9[A\text{-}\alpha\text{-}PW_9O_{34}]{\cdot}7H_2O$ in the presence of en.[12b] Obviously, four terminal oxygen atoms on two $\{B\text{-}\alpha\text{-}PW_9O_{34}\}$ fragments in the $\{Cu_4(H_2O)_2(B\text{-}\alpha\text{-}PW_9O_{34})_2\}$ moiety substitute four water ligands on two $\{Cu_6(en)_3(H_2O)_2\}$ units in two $\{Cu_6(en)_3(H_2O)_2(B\text{-}\alpha\text{-}PW_9O_{34})\}$ moieties, resulting in an unprecedented double sandwich-type assembly. Therefore, the Cu_{16}-substituted PT tetramer can be viewed as the Cu_4-substituted sandwich-type $\{Cu_4(H_2O)_2(PW_9O_{34})_2\}$ moiety further sandwiched by two Cu_6-substituted $\{Cu_6(en)_3(H_2O)_2(PW_9O_{34})\}$ moieties.[12b] In 2012, Cronin *et al.* obtained a distorted cruciform tetramer $[Co_{14}P_{10}W_{60}O_{232}(OH)_9(H_2O)_6]^{35-}$ (Fig. 12h and i) exhibiting single-molecule-magnet (SMM) behavior, in which twelve Co^{II} centers are employed for completing the vacant sites of four $\{P_2W_{15}O_{56}\}$ units and two additional Co centers together with two PO_4^{3-} groups work as bridges to join four $\{Co_3P_2W_{15}\}$ units together.[27]

In the past decade, several rectangle tetrameric TMSPTs (Fig. 13a) were synthesized by different synthetic strategies. Dolbecq *et al.* firstly reported a simple rectangle Fe_8-substituted TMSPT $[(\alpha\text{-}PW_{10}Fe_2O_{39})_4]^{28-}$ (Fig. 13b) by reaction of $[A\text{-}\alpha\text{-}PW_9O_{34}]^{9-}$ and Fe^{III} ions in aqueous solution (pH = 8).[37b] Apparently, this rectangle tetramer is constituted by four di-Fe^{III} substituted $[\alpha\text{-}PW_{10}Fe_2O_{39}]^{7-}$ segments *via* four Fe–O–Fe bridges, in which eight Fe^{III} ions are situated in the lacunae of four Keggin-type $\{\alpha\text{-}PW_{10}O_{39}\}$ fragments. By the one-pot reaction of simple materials such as K_2WO_4, K_2SeO_3 and $Pd(NO_3)_2{\cdot}H_2O$ in an acidic solution, Cronin *et al.* obtained a pair of rectangle Pd_{10}-substituted POT isomers *trans*-$[Pd_{10}Se_{10}W_{52}O_{206}]^{40-}$ (Fig. 13c) and *cis*-$[Pd_{10}Se_{10}W_{52}O_{206}]^{40-}$

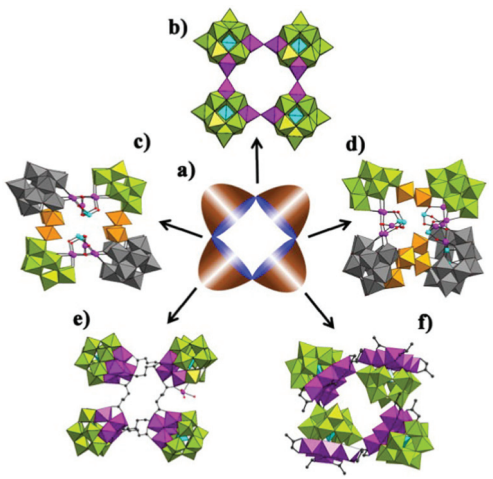

Fig. 13 (a) The schematic mode of rectangle TMSPTs. (b) View of $[(\alpha\text{-}PW_{10}Fe_2O_{39})_4]^{7-}$. (c) The structure of $[Pd_{10}Se_{10}W_{52}O_{206}]^{40-}$ [$\{WO_6\}$ in tetravacant Dawson moieties: gray; $\{WO_6\}$ in $\{W_3O_{10}\}$ trimers: orange]. (d) View of $[Pd_{10}Se_{10}W_{52}O_{206}]^{40-}$ [$\{WO_6\}$ in tetravacant Dawson moieties: gray; $\{WO_6\}$ in the $\{W_2O_7\}$ dimer and the $\{W_4O_{13}\}$ tetramer: orange]. (e) The structure of $[\{(A\text{-}\alpha\text{-}SiW_9O_{34})Ni^{II}_4(OH)_3\}_4(OOC(CH_2)_3COO)_6]^{32-}$. (f) The skeleton of $[H_2Ni_{24}P_4W_{36}(OH)_{12}O_{136}(enMe)_{12}(CH_3COO)_4(H_2O)_{12}]^{2-}$. [$\{WO_6\}$: lime, $\{XO_4\}$: turquoise, TM, $\{TMO_x\}$ and $\{TMO_xN_y\}$: light lavender, O: red, C: cray-80%, N: blue].

(Fig. 13d) with mixed Keggin- and Dawson-type building blocks.[42a] It is particularly interesting to note that the continued evaporation of the mother liquor of *trans*-$[Pd_{10}Se_{10}W_{52}O_{206}]^{40-}$ led to the isolation of *cis*-$[Pd_{10}Se_{10}W_{52}O_{206}]^{40-}$. The skeleton of *trans*-$[Pd_{10}Se_{10}W_{52}O_{206}]^{40-}$ is established by two $\{Se_3W_{26}O_{95}\}$ fragments connected by two $\{Pd_5Se_2O_8\}$ groups whereas the backbone of *cis*-$[Pd_{10}Se_{10}W_{52}O_{206}]^{40-}$ is built up of a $\{Se_2W_{20}O_{73}\}$ fragment and a $\{Se_2W_{32}O_{117}\}$ linked by two $\{Pd_5Se_2O_8\}$ groups. The $\{Se_3W_{26}O_{95}\}$ fragment in *trans*-$[Pd_{10}Se_{10}W_{52}O_{206}]^{40-}$ consists of a trivacant Keggin moiety $\{SeW_9O_{33}\}$ and a tetravacant Dawson moiety $\{Se_2W_{14}O_{52}\}$ sandwiching a $\{W_3O_{10}\}$ trimer, in contrast, the $\{Se_2W_{20}O_{73}\}$ fragment in *cis*-$[Pd_{10}Se_{10}W_{52}O_{206}]^{40-}$ contains two trivacant Keggin moieties $\{SeW_9O_{33}\}$ anchoring a $\{W_2O_7\}$ dimer and the $\{Se_2W_{32}O_{117}\}$ fragment in *cis*-$[Pd_{10}Se_{10}W_{52}O_{206}]^{40-}$ is composed of two tetravacant Dawson moieties $\{Se_2W_{14}O_{52}\}$ bridged together by a $\{W_4O_{13}\}$ tetramer.

Based on an effective strategy for the elaboration of TMSPOTs directly connected to organic groups, Mialane *et al.* discovered a Ni^{II}_{16}-substituted tetrameric oligomer $[\{(A\text{-}\alpha\text{-}SiW_9O_{34})Ni^{II}_4(OH)_3\}_4(OOC(CH_2)_3COO)_6]^{32-}$ (Fig. 13e) under heating at 80 °C starting from $[A\text{-}\alpha\text{-}SiW_9O_{34}]^{10-}$, Ni^{2+} and dicarboxylic glutaric acid at pH = 8.[42b] In its skeleton, six glutaric linkages connect four rectangular arranged $\{Ni_4SiW_9O_{34}\}$ fragments to construct an organic–inorganic tetrameric hybrid. Another organic–inorganic hybrid Ni_{24}-substituted rectangle tetrameric PT is $[H_2Ni_{24}P_4W_{36}(OH)_{12}O_{136}(enMe)_{12}(CH_3COO)_4(H_2O)_{12}]^{2-}$ (Fig. 13f), which possesses the largest Ni^{II} centers among the reported rectangular-shaped poly(POT) tetramers.[42c] In its skeleton, two types of hexa-Ni^{II} substituted POT units $\{Ni_6PW_9(H_2O)_2(enMe)_3(CH_3COO)\}$ and $\{Ni_6PW_9(H_2O)_4(enMe)_3(CH_3COO)\}$ with three enMe having different orientations and different water ligands can be recognized. The construction of this tetramer is driven by the formation of W–O–Ni linkages between neighboring hexa-Ni^{II} substituted POT units. This work demonstrates that the combination of HSM and lacunary POT SDAs is a useful strategy for manufacturing large or extra-large TM-cluster-substituted poly(POT)s.

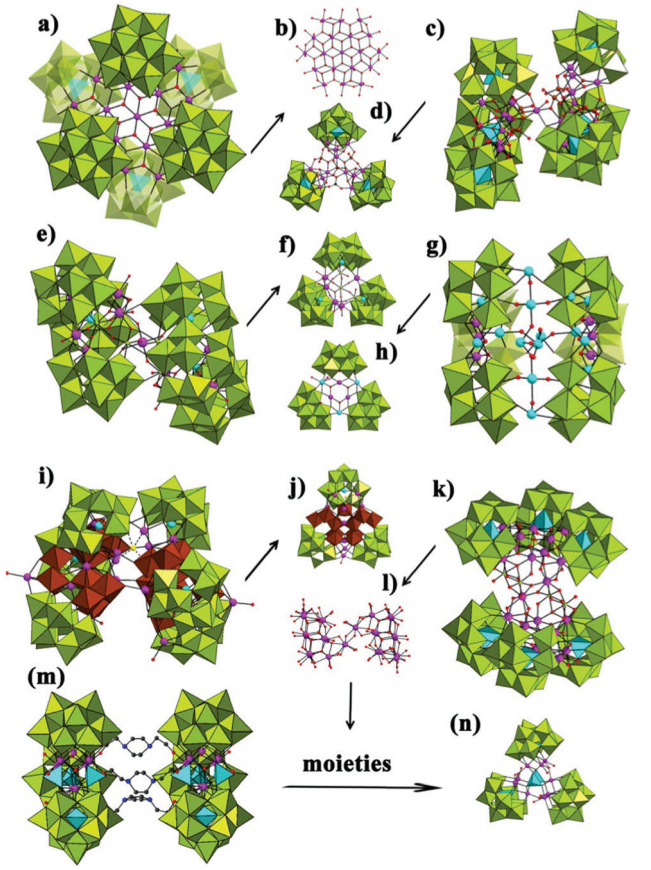

Fig. 14 (a, b) View of $[Mn_{19}(OH)_{12}(SiW_{10}O_{37})_6]^{34-}$ and its central $\{Mn_{19}(OH)_{12}\}$ core. (c) View of $[Ni_{25}(H_2O)_2(OH)_{18}(CO_3)_2(PO_4)_6(SiW_9O_{34})_6]^{50-}$. (d) View of $[Ni_{12}(OH)_9(CO_3)(PO_4)_3]^{4+}$. (e, f) View of $[Fe_{11}(H_2O)_{14}(OH)_2(W_3O_{10})_2(\alpha\text{-}SbW_9O_{33})_6]^{27-}$ and its half unit. (g, h) View of $[Pd_6Te_{19}W_{42}O_{190}]^{40-}$ and its half unit. (i) The skeleton of $[H_{10}Ag_{18}Cl(Te_3W_{38}O_{134})_2]^{29-}$ [$\{W_{11}O_{35}\}$ units: brown, Cl: yellow]. (j) View of superlacunary $\{Te_3W_{38}Ag_3O_{133}\}$ fragment [$\{W_{11}O_{35}\}$ units: brown]. (k, l) View of $[Zr_{24}O_{22}(OH)_{10}(H_2O)_2(W_2O_{10}H)_2(GeW_9O_{34})_4(GeW_8O_{31})_2]^{32-}$ and its $\{Zr_{24}O_{22}(OH)_{10}(H_2O)_2\}$ core. (m) The structure of $[\{Co_9(OH)_3(H_2O)_3(HPO_4)_2(B\text{-}\alpha\text{-}PW_9O_{34})_3\}_2\{C_8H_{18}N_2O_2\}_3]^{32-}$. (n) The skeleton of $[Co_9(OH)_3(H_2O)_6(HPO_4)_2(B\text{-}\alpha\text{-}PW_9O_{34})_3]^{16-}$. [$\{WO_6\}$: lime, $\{XO_4\}$: turquoise, TM: light lavender, O: red, C: cray-80%, N: blue].

2.5 Hexameric high-nuclear TMSPTs

Inspired by the interesting single-molecule magnet (SMM) behavior of Mn_{12}-acetate, Kortz *et al.* utilized the reaction of $[A\text{-}\alpha\text{-}SiW_9O_{34}]^{10-}$ and Mn^{2+} ions in alkaline solution (pH = 8) resulting in a Mn_{19}-substituted hexameric ST $[Mn_{19}(OH)_{12}(SiW_{10}O_{37})_6]^{34-}$ with S_6 point-group symmetry (Fig. 14a) and investigated its magnetic and electron paramagnetic resonance (EPR) properties.[43a] This architecture is constructed from a cationic $\{Mn_{19}(OH)_{12}\}$ cluster stabilized by six dilacunary $\{\alpha\text{-}SiW_{10}O_{37}\}$ segments through μ_4-, μ_3-, and μ_2-oxo bridges. Nineteen edge-sharing MnO_6 octahedra lie in the same plane forming a hexagonal alignment (Fig. 14b). More intriguingly, the combination of $[A\text{-}\alpha\text{-}SiW_9O_{34}]^{10-}$ precursors and Ni^{2+} ions with the assistance of PO_4^{3-} and CO_3^{2-} units can afford a Ni^{II}_{25}-substituted hexameric ST $[Ni_{25}(H_2O)_2(OH)_{18}(CO_3)_2(PO_4)_6(SiW_9O_{34})_6]^{50-}$ (Fig. 14c), in which a spectacular pentacosa-Ni^{II} core $\{Ni_{25}(H_2O)_2(OH)_{18}(CO_3)_2(PO_4)_6\}$ is observed and is constituted by two identical $\{Ni_{12}(OH)_9(CO_3)(PO_4)_3\}$ units connected together by a $\{Ni(H_2O)_2\}$. Therefore, the whole architecture of this Ni^{II}_{25}-substituted ST can be viewed as a $\{Ni(H_2O)_2\}$ linker connecting two $\{Ni_{12}(OH)_9(CO_3)(PO_4)_3(SiW_9O_{34})_3\}$ (Fig. 14d) moieties, which is similar to the previously reported Ni^{II}_{12}-substituted trimeric ST $[Ni_{12}(OH)_9(CO_3)_3(PO_4)(SiW_9O_{34})_3]^{24-}$ where two CO_3^{2-} units are substituted by two PO_4^{3-} units.[26b] Recently, the assembly of $[\alpha\text{-}SbW_9O_{33}]^{9-}$ precursor and Fe^{3+} ions gave rise to a hexameric Fe_{11}-substituted TMSPT $[Fe_{11}(H_2O)_{14}(OH)_2(W_3O_{10})_2(\alpha\text{-}SbW_9O_{33})_6]^{27-}$ (Fig. 14e) exhibiting efficient photocatalytic water oxidation and H_2 evolution activity, in which two $\{Fe_{5.5}(H_2O)_7(OH)(W_3O_{10})(\alpha\text{-}SbW_9O_{33})_3\}$ half units are fused together by the Fe^{III} center on an inversion (Fig. 14f).[43b,c] It is worth pointing out that one square pyramid Fe^{III} ion and five octahedral Fe^{III} ions coexist in the half unit.

On the other hand, its skeleton can be seen as six trilacunary Keggin-type $\{\alpha\text{-}SbW_9O_{33}\}$ units in the classical cyclohexane configuration encapsulating an electrophilic $\{Fe_{11}(H_2O)_{14}(OH)_2(W_3O_{10})_2\}$ cluster core. Except for 3d-metal ions, 4d-metal ions can also be implanted to hexameric TMSPTs. For instance, by the one-pot reaction of lone-electron-pair active TeO_3^{2-}, WO_4^{2-} and 4d metal ions in conventional aqueous solution, Cronin's group obtained a hexameric hexa-Pd^{II} substituted TMSPTs $[Pd_6Te_{19}W_{42}O_{190}]^{40-}$ (Fig. 14g).[42a] Three rarely observed $\{\alpha\text{-}TeW_7O_{27}\}$ fragments collectively encapsulate a $\{Pd_3Te_3O_3\}$ core to generate a triangle-shaped half unit (Fig. 14h), and then two half units are fused together by five pendant TeO_3^{2-} groups. In this skeleton, the Te^{IV} ions exhibit three distinct coordination modes: (a) the four-coordinate heteroatom templates within the $\{\alpha\text{-}TeW_7O_{27}\}$ fragments display the first unusual non-pyramidal, highly distorted tetrahedral geometries; (b) the Te^{IV} ions belong to two $\{Pd_3Te_3\}$ cores adopt the square pyramidal geometries; (c) three-coordinate pyramidal TeO_3^{2-} groups can also be observed. In 2014, they also communicated the interesting time-resolved supramolecular assembly of a series of nanoscale POT clusters $[H_{(10+m)}Ag_{18}Cl(Te_3W_{38}O_{134})_2]_n$ (n = 1 and m = 0 after 4 days, n = 2 and m = 3 after 10 days, n = 1 and m = 5 after 14 days), in which the innovative $\{Ag_{12}\}$-in-$\{W_{76}\}$ cluster could be recognized by detailed crystallography analysis.[43d] The complicated skeleton of $[H_{10}Ag_{18}Cl(Te_3W_{38}O_{134})_2]^{29-}$ with a virtual C_2 symmetry (Fig. 14i) can be described as a multi-layered assembly centered around a Cl^- anion that is inside the central $\{Ag_{12}\}$ cluster. That is, twelve Ag^+ ions in the $\{Ag_{12}\}$ cluster are connected by μ_3- and μ_4-oxo atoms to create three different $\{Ag_4\}$ units, which are connected together by the single Cl^- anion, constructing the $\{Ag_{12}Cl\}$ core. And then two well-defined high-vacant $\{Te_3W_{38}O_{134}\}$ half-units coordinate to the integrated $\{Ag_{12}Cl\}$ core in the face-to-face motif with a torsion angle of 65°. Finally, six additional Ag^+ ions are supported to two half-units, building the skeleton of $[H_{10}Ag_{18}Cl(Te_3W_{38}O_{134})_2]^{29-}$.[43d] Notably, the high-vacant $\{Te_3W_{38}O_{134}\}$ half-unit is constituted by an open-faced $\{W_{11}O_{35}\}$ fragment connecting three trilacunary $\{TeW_9O_{33}\}$ fragments. Apart from the above mono-/di-/tri-valence TM substituted hexameric POTs with ions, Yang and co-workers introduced tetravalent Zr^{4+} ions to the $[GeW_9O_{34}]^{10-}$ system under hydrothermal conditions to acquire an unprecedented Zr_{24}-cluster incorporated GT $[Zr_{24}O_{22}(OH)_{10}(H_2O)_2(W_2O_{10}H)_2(GeW_9O_{34})_4\ (GeW_8O_{31})_2]^{32-}$ (Fig. 14k), which represents the largest Zr-based poly(POT)s to date.[43e] In this POA skeleton, the central $\{Zr_{24}O_{22}(OH)_{10}(H_2O)_2\}$ core (Fig. 14l) is trapped by three types of different segments: $\{B\text{-}\alpha\text{-}GeW_9O_{34}\}$, $\{B\text{-}\alpha\text{-}GeW_8O_{31}\}$ and $\{W_2O_{10}\}$. Experimental results exhibit that this Zr_{24}-cluster incorporated GT can serve as an effective catalyst in the oxygenation reaction of thioethers.[43e] Moreover, an organic–inorganic hybrid hexameric Co^{II}_{18}-substituted PT $[\{Co_9(OH)_3(H_2O)_3(HPO_4)_2(B\text{-}\alpha\text{-}PW_9O_{34})_3\}_2\ \{C_8H_{18}N_2O_2\}_3]^{32-}$ (Fig. 14m) was reported by Cronin and co-workers by reaction of WO_4^{2-}, PO_4^{3-}, Co^{2+}, and *N*,*N*′-bis(2-hydroxyethyl)piperazine (bhep). The dimerization process of two triangular-shaped nonacobaltate containing cluster units $[Co_9(OH)_3(H_2O)_6(HPO_4)_2(B\text{-}\alpha\text{-}PW_9O_{34})_3]^{16-}$ (Fig. 14n) were accomplished by the coordination of the hydroxyl groups from three bhep ligands to the Co^{II} centers.[43f] In the triangle-shaped $[Co_9(OH)_3(H_2O)_6(HPO_4)_2(B\text{-}\alpha\text{-}PW_9O_{34})_3]^{16-}$ cluster unit, three tri-Co^{II} substituted $\{PW_9Co_3O_{40}\}$ moieties are connected together through three μ_3-hydroxyl groups and two capping monoprotonated phosphate ions.

2.6 Octameric high-nuclear TMSPTs

As discussed in the monomeric high-nuclear TMSPTs part, aqueous ligands on the hexa-Ni^{II} substituted POT $\{Ni_6(\mu_3\text{-}OH)_3(H_2O)_6(L)_3(B\text{-}\alpha\text{-}PW_9O_{34})\}$ (L = en, enMe, dien) fragment are highly active and can be efficaciously replaced by terminal oxygen atoms of POT segments, carboxylic groups of organic ligands, which have been affirmed by Yang's findings.[12] With further exploration, Yang *et al.* obtained a rod-shaped octameric Ni_{40}-based ferromagnetic poly(POT) $[H_4Ni_{40}P_8W_{72}(OH)_{18}O_{272}(en)_{18}(OAc)_2(WO_4)_2(H_2O)_{18}]^{12-}$ (Fig. 15a) representing the maximum number of Ni^{II} ions among the known poly(POT)s.[42c] Its featured structure can be understood as two acetate-en-stabilizing hexa-Ni^{II} substituted Keggin $\{Ni_6(\mu_3\text{-}OH)_3(H_2O)(en)_3(CH_3COO)(B\text{-}\alpha\text{-}PW_9O_{34})\}$ fragments, respectively, attached to both sides of a central tetra-Ni^{II} sandwiched Weakley-type $\{Ni_4(H_2O)_2(B\text{-}\alpha\text{-}PW_9O_{34})_2\}$ core *via* four terminal oxygen atoms from the $\{Ni_4(H_2O)_2(B\text{-}\alpha\text{-}PW_9O_{34})_2\}$ core replacing four aqueous ligands on two $\{Ni_6(\mu_3\text{-}OH)_3(H_2O)(en)_3(CH_3COO)(B\text{-}\alpha\text{-}PW_9O_{34})\}$ fragments, giving rise to a unique double-sandwich-type tetramer, which is very familiar to the Cu_{16}-based tetramer $\{[Cu_6(\mu_3\text{-}OH)_3\ (H_2O)_2(en)_3(B\text{-}\alpha\text{-}PW_9O_{34})]_2[Cu_4(H_2O)_2(B\text{-}\alpha\text{-}PW_9O_{34})_2]\}^{10-}$ also reported by Yang *et al.*[12b] And then two terminal oxygen atoms from the formed tetramer further substitute two aqueous ligands on two $\{Ni_6(\mu_3\text{-}OH)_3\ (H_2O)_3(en)_3(B\text{-}\alpha\text{-}PW_9O_{34})\}$ fragments to propagate an intriguing hexamer. Finally, each of two extraneous $\{Ni_6(\mu_3\text{-}OH)_3(H_2O)_4(en)_3(B\text{-}\alpha\text{-}PW_9O_{34})\}$ units respectively graft to two $\{Ni_6(\mu_3\text{-}OH)_3(H_2O)_3\ (en)_3(B\text{-}\alpha\text{-}PW_9O_{34})\}$ fragments in the hexamer *via* two additional $\{WO_4\}$ groups, resulting in an unprecedented octamer. Besides the rod-shaped octameric Ni_{40}

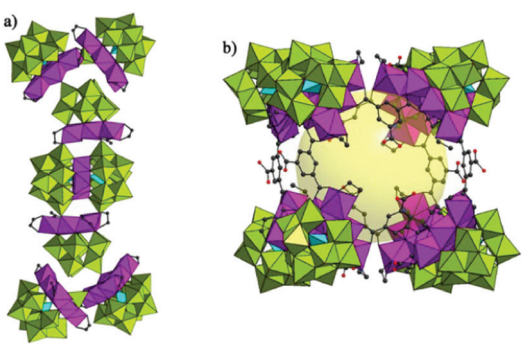

Fig. 15 (a) View of $[H_4Ni_{40}P_8W_{72}(OH)_{18}O_{272}(en)_{18}(OAc)_2(WO_4)_2(H_2O)_{18}]^{12-}$. (b) The cage structure of $\{[Ni_6(tris)(en)_3(BTC)_{1.5}(B\text{-}\alpha\text{-}PW_9O_{34})]_8\}^{12-}$. [$\{WO_6\}$: lime, $\{PO_4\}$: turquoise, $\{TMO_xN_y\}$: light lavender, O: red, C: cray-80%, N: blue].

comprising POT, the $\{Ni_6(\mu_3\text{-}OH)_3(H_2O)_6\ (L)_3(B\text{-}\alpha\text{-}PW_9O_{34})\}$ building unit can utilized as the construction of the molecular cage $[Ni(en)_2(H_2O)_2]_6\{Ni_6(Tris)(en)_3(BTC)_{1.5}(B\text{-}\alpha\text{-}PW_9O_{34})\}_8\cdot 12en\cdot 54H_2O$ (tris = tris(hydroxymethyl)aminomethane, BTC = 1,3,5-benzenetricarboxylate) (Fig. 15b).[44] In this POM–organic molecular cage, due to the existence of the tripod hydroxymethyl groups, Tris can function as an excellent tridentate ligand to covalently displace three hydroxyl groups on the $\{Ni_6(\mu_3\text{-}OH)_3(H_2O)_6(L)_3(B\text{-}\alpha\text{-}PW_9O_{34})\}$ building unit to enhance the stability. Simultaneously, the tricarboxylic BTC ligands were imported to serve as multi-functional connectors to integrate adjacent $\{Ni_6(\mu_3\text{-}OH)_3(H_2O)_6\ (L)_3(B\text{-}\alpha\text{-}PW_9O_{34})\}$ building units together in the establishment of a cage framework. Specifically, the skeleton of $[Ni(en)_2(H_2O)_2]_6\{Ni_6(Tris)(en)_3(BTC)_{1.5}(B\text{-}\alpha\text{-}PW_9O_{34})\}_8$ is composed of eight tris-grafted $\{Ni_6PW_9O_{34}\}$ building units and twelve BTC linkers.

2.7 Hexadecameric high-nuclear TMSPTs

Apart from the previously reported "S"-shaped Mn_{14}-substituted POT $[\{Mn_7O_4(OH)_2(H_2O)\}_2(W_6O_{22})(H_2W_8O_{32})_2(H_4W_{13}O_{46})_2]^{26-}$, tetrahedral $Mn^{III/II}_{14}$-substituted PT $[Mn^{III}_{13}Mn^{II}O_{12}(PO_4)_4(PW_9O_{34})_4]^{31-}$ and hexameric Mn_{19}-substituted ST $[Mn_{19}(OH)_{12}(SiW_{10}O_{37})_6]^{34-}$,[33,39,43a] by self-combination chemistry of metastable hexalacunary precursor $[\alpha\text{-}H_2P_2W_{12}O_{48}]^{12-}$ and Mn_{12}-acetate in a CH_3COOH–CH_3COOLi solution, Fang *et al.* obtained another representative Mn_{40}-substituted core–shell cluster aggregate $[(P_8W_{48}O_{184})\{(P_2W_{14}Mn^{III}_4O_{60})(P_2W_{15}Mn^{III}_3O_{58})_2\}_4]^{144-}$ (Fig. 16), which is formally built up from a total of sixteen corner-sharing Dawson-type units.[45] The total hexadecameric Dawson assembly has an idealized S_4 symmetry with the principal axis coinciding with the fourfold axis of the central $\{P_8W_{48}O_{184}\}$ wheel. The central hydrophilic cyclic $\{P_8W_{48}O_{184}\}$ core is encapsulated by an outer shell of twelve Mn^{III}-substituted Dawson units. Twelve Mn^{III}-substituted Dawson PT units on the outer shell can be divided into four of the self same semilune tri-Dawson PT subunits $\{(P_2W_{14}Mn^{III}_4O_{60})(P_2W_{15}Mn^{III}_3O_{58})_2\}$. The plane formed by two tri-Dawson PT subunits is perpendicular to the plane defined by two other tri-Dawson PT subunits. Two planes defined by the four tri-Dawson PT subunits are also perpendicular to the plane of the $\{P_8W_{48}O_{184}\}$ core. Interestingly, each tri-Dawson subunit only links to a single $\{P_2W_{12}O_{46}\}$ fragment of the $\{P_8W_{48}O_{184}\}$ core. It should be emphasized that this Mn_{40}-substituted core–shell cluster aggregate with dimensions of 43 × 43 × 34 Å contains the largest number of Mn ions in reported molecular TMSPTs to date.

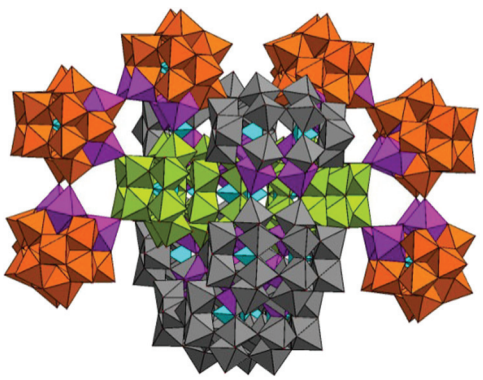

Fig. 16 The core–shell cluster architecture of $[(P_8W_{48}O_{184})\{(P_2W_{14}Mn_4O_{60})(P_2W_{15}Mn_3O_{58})_2\}_4]^{144-}$. [$\{WO_6\}$ in tri-Dawson PT subunits $\{(P_2W_{14}Mn^{III}_4O_{60})(P_2W_{15}Mn^{III}_3O_{58})_2\}$: lime or gray-50%, $\{WO_6\}$ in the $\{P_8W_{48}O_{184}\}$ wheel: orange, $\{PO_4\}$: turquoise, $\{MnO_6\}$: light lavender, O: red].

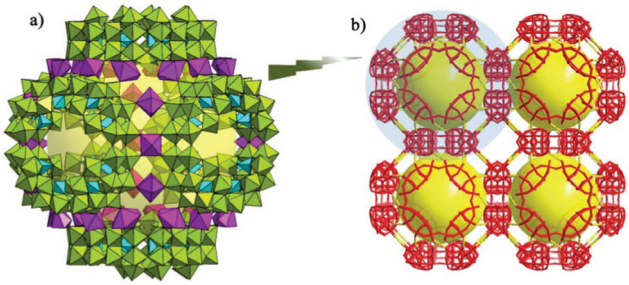

Fig. 17 (a) View of the truncated cuboctahedral principle building unit of $\{Mn_8(H_2O)_{48}P_8W_{48}O_{184}\}_6^{144-}$ [$\{WO_6\}$: lime, $\{PO_4\}$: turquoise, $\{MnO_6\}$: light lavender]. (b) The open framework constructed from truncated cuboctahedral principle building units *via* Mn^{2+} linkers. [copied from ref. 51].

2.8 Tetracosameric high-nuclear TMSPT

By means of the bridging role of Mn^{2+} ions and the face-directed assembly of a ring-shaped macrocyclic precursor $[P_8W_{48}O_{184}]^{40-}$, Cronin's group prepared an accessible open 3-D framework material based on truncated cuboctahedral $[Mn^{II}_8(H_2O)_{48}P_8W_{48}\ O_{184}]_6^{144-}$ principle building units (Fig. 17a).[46] In the 3-D framework architecture, each $[P_8W_{48}O_{184}]^{40-}$ fragment is combined with eight others by multiple Mn–O–W linkages and each isolated $[P_8W_{48}O_{184}]^{40-}$ fragment has a total of twenty-four Mn^{2+} ions located at its outer edges, however, because of the cubic sharing nature of the architecture, eight Mn^{2+} ions are related to each $[P_8W_{48}O_{184}]^{40-}$ fragment $[Mn^{II}_8(H_2O)_{48}P_8W_{48}O_{184}]^{24-}$ in the framework.[46] It can be seen clearly that Mn^{2+} ions not only direct the construction of the 3-D framework, but also transfer important electrochemical properties to the material.[46] Because the manganese-fused $[P_8W_{48}O_{184}]^{40-}$ anions form a truncated cuboctahedron-based framework with large internal voids of *ca.* 27% of the unit cell volume, the cation exchange properties of this material were performed through facile Cu^{2+} uptake experiments.

3. Application fields

3.1 Magnetic properties

It is well known that lacunary nonmagnetic POT fragments can function as remarkable inorganic nucleophilic polydentate ligands and induce nucleation aggregation of magnetic TM ions in the vacancies of POT fragments generating various

TMSPTs with diverse nuclearity and beautiful topology. Thus, the bulky diamagnetic POT matrixes guarantee an effective magnetic isolation of the magnetic cores, so that intermolecular interactions are usually negligible, which allows the quantitative determination of the intramolecular magnetic exchange interactions.[22a,47a,b] In addition, POA ligands have also been found sometimes to induce strong axial magnetic anisotropy, illustrated by Mn^{II}–POM complexes.[47c] Furthermore, an great breakthrough of SMMs, which shows slow relaxation of the magnetization at low temperatures and quantum effects, has triggered an important evolution in the molecular magnetism field.[47c–f] The discovery of a TM coordination cluster (Mn_{12}-acetate, a molecule that combines a very large easy-axis anisotropy and a high spin ground state) with SMM behavior has also stimulated the development of new SMMs.[47e] Notably, the POT fragments can facilitate the dilution of SMMs by removal of unwanted dipolar interactions, and the intrinsic redox activity of the POA fragments could control magnetic-exchange pathways through additional routes.[17d,48] From the perspective of magnetism research, TMSPTs enclosing high-nuclear (≥6) TM clusters are of great interest. Thus, in the past decade, the magnetic properties of many high-nuclear TMSPTs have been investigated.[12,15a,17a,19b,20b,d,21,22,24b,25b,c,26a,30a,c,31,33,34,36c–e,37a,b,39,43a,44] and several high-nuclear TMSPT-based SMMs were also discovered.[17d,18,27,29d,38b] Because the magnetic properties of many high-nuclear TMSPTs have been reported, herein, we select several representative high-nuclear TMSPTs to discuss their magnetic properties.

As demonstrated above, the hexa-Ni^{II} cluster fragments with six co-planar Ni^{II} ions in a triangle fashion have been observed in many high-nuclear TMSPTs,[12a,b,d,13b–e,14a,b,17a] moreover, these hexa-Ni^{II} cluster fragments all exhibit ferromagnetic coupling interactions, as a result, only the magnetic properties of the first Ni_6-substituted PT $[Ni_6(\mu_3\text{-}OH)_3(H_2O)_4(enMe)_3(CH_3COO)(B\text{-}\alpha\text{-}PW_9O_{34})]^-$ are described here.[12a] As illustrated in Fig. 18, increasing χ_mT upon cooling typifies the overall ferromagnetic interactions within Ni^{II} ions mediated by O and OH bridges, which is consolidated by the positive Weiss constant θ = 23.8 K. A sudden decrease of χ_mT below 11 K indicates the presence of obvious zero-field splitting (ZFS) effects in the ground state. The measurements of alternating current (ac) magnetic susceptibilities at 111, 511, 911, 1511 and 2511 Hz exhibit no frequency dependence, which excludes the possibility of the SMM behavior. Its magnetic behavior was also quantitatively analyzed by the MAGPACK software package. An exchange mode of the hexa-Ni^{II} cluster was established and an appropriate Hamiltonian for the hexa-Ni^{II} cluster can be written as $\hat{H} = -2J_1\hat{S}_1\hat{S}_2 - 2J_2\hat{S}_1\hat{S}_3 - 2J_3\hat{S}_2\hat{S}_3 - 2J_4\hat{S}_2\hat{S}_4 - 2J_5\hat{S}_2\hat{S}_5 - 2J_6\hat{S}_3\hat{S}_5 - 2J_7\hat{S}_3\hat{S}_6 - 2J_8\hat{S}_4\hat{S}_5 - 2J_9\hat{S}_5\hat{S}_6 + \sum D_i\hat{S}_{iz}^2$, where D represents the ZFS parameter and the contribution of the mononuclear Ni^{II} species is incorporated through the Curie law. The best-fit parameters are as follows: J_1 = 0.47 cm^{-1}, J_2 = 0.75 cm^{-1}, J_3 = 1.23 cm^{-1}, J_4 = 0.47 cm^{-1}, J_5 = 1.23 cm^{-1}, J_6 = 1.23 cm^{-1}, J_7 = 0.43 cm^{-1}, J_8 = 0.47 cm^{-1}, J_9 = 0.43 cm^{-1}, g = 2.24, D = 1.58 cm^{-1} and the agreement factor $R = 2.70 \times 10^{-4}$, which proves the overall ferromagnetic interactions within the hexa-Ni^{II} cluster.[12a] From the crystal data, the Ni–O–Ni angles vary between 90 and 104° and conform to the previous conclusion that the Ni···Ni ferromagnetic exchange interactions are predominant when the Ni–O–Ni angles lie in 90 ± 14°.[49a] In addition, the magnetic properties of the triangle hexa-Cu^{II} cluster fragments with six co-planar Cu^{II} ions have been investigated.[12c,13a] However, the triangle hexa-Cu^{II} cluster fragments display antiferromagnetic coupling interactions,[12c,13a] which are closely related to the Cu–O–Cu angles.[49b–d] In the above mentioned magnetic high-nuclear TMSPTs, the magnetic interactions between metal centers are mediated by O or OH^- groups. Actually, the azido ion is also a good electron transfer ligand for linking divalent metal centers (usually Cu^{II}, Ni^{II} and Mn^{II} ions) together, in which the azido ligand exhibits either μ-1,1- (end-on) or μ-1,3- (end-to-end) coordination modes.[50] A large number of experimental results reveal that the μ-1,1-azido ligand facilitates ferromagnetic couplings whereas the μ-1,3-azido ligand favors antiferromagnetic couplings.[50] For instance, Mialane *et al.* reported an interesting azido-including Cu_9^{II}-substituted trimeric ST $[\{SiW_8O_{31}Cu_3(OH)(H_2O)_2(N_3)\}_3(N_3)]^{19-}$, in which three equivalent $[\gamma\text{-}SiW_8O_{31}Cu_3(OH)(H_2O)_2(N_3)]^{6-}$ moieties are fused together by a C_3 axis through the exceptionally good μ-1,1,1,3,3,3-azido bridging ligand.[25b] Its magnetic behavior was been quantitatively probed. The value of χ_mT at 300 K of 4.03 cm^3 mol^{-1} K is consistent with the spin-only value expected for nine uncoupled copper(II) cations considering g = 2.17. The χ_mT increases gradually to a maximum value of 4.20 cm^3 mol^{-1} K at 40 K as temperature decreases, indicating weak ferromagnetic coupling interactions. The sudden decrease of the χ_mT value below 40 K reveals antiferromagnetic interactions. The quantitative magnetic fitting results indicate that relatively weak ferromagnetic coupling interactions (J_1 = +1.0 cm^{-1}, J_2 = +20.0 cm^{-1}, g = 2.17) exist within the $\{Cu_3\}$ units in $[\gamma\text{-}SiW_8O_{31}Cu_3(OH)(H_2O)_2(N_3)]^{6-}$ fragments whereas the dominant antiferromagnetic couplings are derived from the combined action of magnetic exchange interactions between the $\{Cu_3\}$ units mediated by the hexadentate μ-1,1,1,3,3,3-azido ligand (J_3 = –5.4 cm^{-1}, J_4 = +1.3 cm^{-1}).[25b]

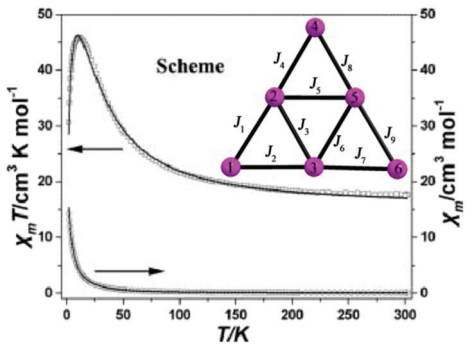

Fig. 18 Temperature dependence of χ_m and χ_mT for $[Ni_6(\mu_3\text{-}OH)_3(H_2O)_4(enMe)_3(CH_3COO)(B\text{-}\alpha\text{-}PW_9O_{34})]^-$ (inset: the exchange mode of the hexa-Ni^{II} cluster). [copied from ref. 12a].

Recently, construction of high-nuclear TMSPTs with SMM behavior has attracted much attention.[17d,18,27,29d,38b] For example, Fang *et al.* obtained a mixed-valence $\{Mn_6^{III}Mn^{IV}\}$-substituted Dawson-type TMSTP dimer $[(\alpha\text{-}P_2W_{15}O_{56})_2Mn_6^{III}Mn^{IV}O_6(H_2O)_6]^{14-}$ incorporating a heptanuclear $\{Mn_6^{III}Mn^{IV}O_8\}$ core, which displays an approximate D_{3d} symmetry with the Mn^{IV} ion at the inversion center.[18d] The $\{Mn_6^{III}Mn^{IV}O_8\}$ core resembles two corner-sharing cubanes such that it can be formally regarded as two Mn_4^{III} clusters sharing a common Mn^{IV} vertex. Magnetic susceptibility measurements indicate that χ_mT at 290 K (30.0 emu K mol^{-1}) is remarkably larger than the spin-only value (19.875 emu K mol^{-1}, g = 2.0) for non-interacting six Mn^{III} and one Mn^{IV} ions, suggesting ferromagnetic interactions within the heptanuclear $\{Mn_6^{III}Mn^{IV}O_8\}$ core (Fig. 19a). Moreover, the observation that increasing χ_mT upon cooling followed by a sudden decrease at 5 K also reveals dominant ferromagnetic interactions with the presence of ZFS effects. Based on the approximate D_{3d} symmetry of the structure, two magnetic exchange pathways exist in the $\{Mn_6^{III}Mn^{IV}O_8\}$ core (Mn^{III}–Mn^{IV}: J_1 and Mn^{III}–Mn^{III}: J_2) (Fig. 19b). Thus, an appropriate Hamiltonian for the heptanuclear $\{Mn_6^{III}Mn^{IV}O_8\}$ cluster can be written as $H_{ex} = -2[J_1(\hat{S}_1\cdot\hat{S}_2 + \hat{S}_1\cdot\hat{S}_3 + \hat{S}_1\cdot\hat{S}_4 + \hat{S}_1\cdot\hat{S}_5 + \hat{S}_1\cdot\hat{S}_6 + \hat{S}_1\cdot\hat{S}_7) + J_2(\hat{S}_2\cdot\hat{S}_3 + \hat{S}_3\cdot\hat{S}_4 + \hat{S}_4\cdot\hat{S}_2 + \hat{S}_5\cdot\hat{S}_6 + \hat{S}_6\cdot\hat{S}_7 + \hat{S}_7\cdot\hat{S}_5)]$.[18d] In addition, the deviation from isotropic Brillouin-type field-dependent magnetization curves at T = 1.8–5 K (Fig. 19c) shows the strong ZFS of the Mn^{III} ions in their Jahn–Teller elongated octahedral geometries ($^5B_{1g}$) while the Mn^{IV} ion is an isotropic spin-3/2 site ($^4A_2$). As a result, a precise magnetochemical explanation of the $\{Mn_6^{III}Mn^{IV}O_8\}$ spin polytope depends on simulating all associative single-ion effects and the Heisenberg-type exchange coupling interactions.[18d] The best fit affords J_1 = −18.75 cm^{-1}, J_2 = +12.5 cm^{-1} and leads to the S = 21/2 ground state, proving the prediction that the spins of the six Mn^{III} ions are all parallel, and antiparallel to the central Mn^{IV} ion (Fig. 19b), generating a molecular S = 21/2 ground state in the spin-only approximation.[18d] Interestingly, the ac susceptibility measurements indicate that the frequency-dependent results are characteristic of a SMM (Fig. 19d), because the m_S substates of the S = 21/2 ground state multiplet are ZFS to produce a parabolic energy barrier between the highest $\pm m_S$ (±21/2) substates, leading to a slowing of the magnetization relaxation upon a field change.[18d] Another SMM example is Cronin's $\{[GeW_9O_{34}]_2[Mn_4^{III}Mn_2^{II}O_4(H_2O)_4]\}^{12-}$ that consists of a mixed-valence $[Mn_4^{III}Mn_2^{II}O_4(H_2O)_4]^{8+}$ cluster core sandwiched by two trivacant GT $[GeW_9O_{34}]^{10-}$ fragments.[17d] The χ_mT value of 12.4 cm^3 K mol^{-1} at 300 K is lower than the expected value (20.75 cm^3 K mol^{-1}, taking g = 2) for four Mn^{III} and two Mn^{II} ions. Upon cooling to 120 K, the χ_mT value slowly declines to a minimum of 11 cm^3 K mol^{-1} and then rises to a maximum of 14.1 cm^3 K mol^{-1} at 10 K. Further cooling leads to the precipitous falling of the χ_mT value. This profile is suggestive of the coexistence of ferromagnetic and antiferromagnetic coupling interactions within the mixed-valence $[Mn_4^{III}Mn_2^{II}O_4(H_2O)_4]^{8+}$ cluster, which is also strongly consolidated by the least-squares fitting results of J_1 = 6.5 cm^{-1}, J_2 = 3.5 cm^{-1} and J_3 = −56.0 cm^{-1} with considering g = 2.0.[17d] Moreover, the low-temperature maximum implies the ground state with S = 5 and the χ_mT dropping of low-temperature (<10 K) is attributed to the zero-field splitting, intermolecular interactions and the Zeeman effects of the applied field, which are also supported by the fitting results (S = 5, g = 1.94, D = −0.67 cm^{-1}) of magnetization data collected in the range of 1–5 T and 1.8–7.0 K with the axial zero-field splitting plus Zeeman Hamiltonian.[51] Considering the magnitude of S and the sign of D, ac susceptibility measurements were carried out to examine the SMM characteristics. Below 5 K, the diverging of the $\chi'T$ curves at different frequencies and the frequency dependent χ'' signals demonstrate the SMM characteristic of $\{[GeW_9O_{34}]_2[Mn_4^{III}Mn_2^{II}O_4(H_2O)_4]\}^{12-}$. The Arrhenius simulation gives the energy barrier of $\Delta E/k_B$ = 14.8 K, which is smaller than the theoretical barrier of 24 K acquired from S and D parameters derived from the fitting of the reduced magnetization, the main reason of which is that the C_i point symmetry of the $[Mn_4^{III}Mn_2^{II}O_4(H_2O)_4]^{8+}$ cluster results in the transverse anisotropy terms in the zero-field splitting Hamiltonian, reducing the effective height of the energy barrier separating the $\pm M_S$ states, through quantum tunneling of magnetization.[17d]

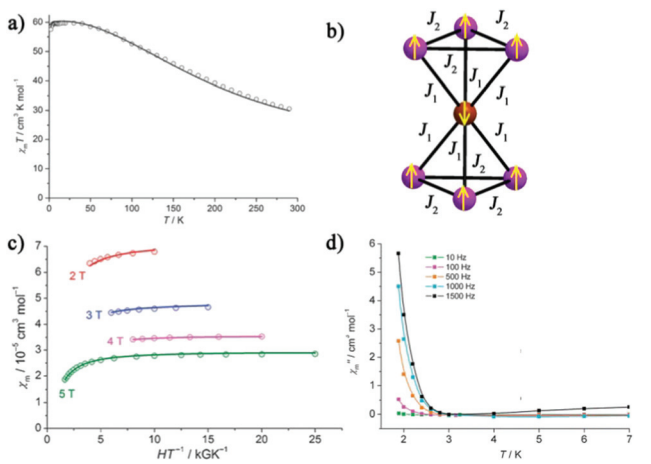

Fig. 19 (a) Temperature dependence of χ_mT for $[(\alpha\text{-}P_2W_{15}O_{56})_2Mn_6^{III}Mn^{IV}O_6(H_2O)_6]^{14-}$. (b) The magnetic exchange model and the ground state spin alignments of the $\{Mn_6^{III}Mn^{IV}O_8\}$ core. (c) The field-dependence of χ_m at low temperatures for $[(\alpha\text{-}P_2W_{15}O_{56})_2Mn_6^{III}Mn^{IV}O_6(H_2O)_6]^{14-}$. (d) Temperature dependence of the out-of-phase susceptibility χ''_m (H_{dc} = 0). [copied from ref. 18*d*]. Reprinted with permission from ref. 18*d*. Copyright The Royal Society of Chemistry 2012.

3.2 Catalytic properties

From the structural viewpoint, the abundant surface O atoms of POMs endow them with nucleophilic function that can donate electrons to acceptors, while the unoccupied orbitals of skeletal metal ions can work as Lewis acids to accept endogenous or exogenous electrons.[52a,b] Admittedly, the adaptable POMs can be bi-directional and feature functions of Lewis bases and acids. In addition, the bulky and highly negative charged POAs usually exhibit a strong capacity to bear and

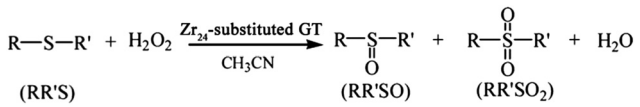

Scheme 1 The catalytic oxidation reaction of thioethers.

release electrons, which display their available redox natures.[52c] Thus POM-based materials with tunable acidity and redox properties, inherent resistance to oxidative decomposition, high stability and impressive sensitivity to electricity can be developed as robust catalysts. For instance, in 2014, Yang *et al.* reported the oxygenation reactions of thioethers by H_2O_2 (Scheme 1) in the presence of $Na_{10}K_{22}[Zr_{24}O_{22}(OH)_{10}(H_2O)_2(W_2O_{10}H)_2(GeW_9O_{34})_4(GeW_8O_{31})_2]\cdot 85H_2O$ (marked as Zr_{24}-GT) as a catalyst.[43e] In fact, most of the oxidation reactions of thioethers by H_2O_2 can occur in the absence of Zr_{24}-GT, however, the conversion and selectivity of most catalytic oxidation reactions are very low. When Zr_{24}-GT works as a catalyst to activate H_2O_2, the conversion and selectivity are vastly improved, illustrating that Zr_{24}-GT is an efficient catalyst for oxygenation of thioethers by H_2O_2. The driving force for the catalytic conversion from thioethers to sulfoxides/sulfones may be related to the combined action of the unique redox property of oxygen-enriched POT fragments and Lewis acidity of the encapsulated Zr cluster in Zr_{24}-GT. Moreover, the introduction of electron-donating groups on the aromatic ring of aryl–alkyl thioethers affords a higher ratio of sulfone than the introduction of electron-withdrawing groups.[43e] Furthermore, the recyclability tests show that the catalytic activity and the structure of Zr_{24}-GT can remain unchanged after six-run duplicate operations.[43e] So, the catalytic oxidation of thioethers in this work may be potentially useful for the removal of organic sulfur contents.

The oxidation of *n*-alkanes is an important reaction for the conversion of saturated hydrocarbons to their corresponding alcohols and ketones.[53a] Kortz and collaborators reported a heterogeneous catalyst system consisting of the wheel shaped Cu_{20}-substituted PT $[Cu_{20}Cl(OH)_{24}(H_2O)_{12}(P_8W_{48}O_{184})]^{25-}$ supported on 3-aminopropyltriethoxysilane-modified SBA-15 for solvent-free aerobic oxidation of *n*-hexadecane.[53a] This heterogeneous catalyst system can catalyze the solvent-free aerobic oxidation of *n*-hexadecane to alcohols and ketones by using air as the oxidant under room conditions, displaying a remarkably high turnover frequency (TOF) of 20 000 h^{-1} and is resistant to poisoning by CS_2.[53a] The catalytic reaction may be promoted by the Cu^{II} ions of the POM that activate the C–H bonds of the substrate at an early stage of the reaction, resulting in a shorter initial induction period required for *n*-hexadecanyl hydroperoxide mediated pathways. The formation of *n*-hexadecanyl hydroperoxide occurs predominantly through activation of CH bonds in RCH_2R^1 by $R(OO^{\bullet})R^1$ species.[53a] Therefore, this system can enhance the prospect of this type of heterogeneous catalyst for practical applications.[53a]

The excessive consumption of fossil fuels and the resulting serious environmental pollution has compelled researchers to exploit and search for green sustainable and safe energy sources as substitutes. Naturally, abundant solar energy has attracted increased attention, since it can be directly utilized to promote the generation of photocatalytic water splitting.[43b] Nevertheless, the development of efficient catalysts is the important topic. Under the irradiation of near-visible or UV light, electrons in POMs can leap from the ground state to their corresponding excited states and especially, the charge transfer transitions of O atoms to the d^0 TM ions may happen.[54] At this time, POMs are highly reactive species with the capability of oxidizing or reducing various substrates.[49] The recombination of photogenerated electrons with strong photoreductive ability and photogenerated holes with strong photooxidative ability can be inhibited by the well-defined HOMO–LUMO band gaps of POMs, which are efficient for evoking chemical reactions. On the other hand, oxygen-enriched surfaces of POMs can provide robust inorganic ligand systems to encapsulate active centers for catalyzing water splitting.[38b] Recently, several high-nuclear TMSPT-based photocatalysts for H_2 evolution and O_2 evolution were researched intensively.[17b,26b,38a,43b,c] Inspired by the special function of $\{Mn_3CaO_4\}$ cubane in PSII, Wang *et al.* designed and synthesized a series of purely inorganic high-nuclear cobalt–phosphate molecular catalysts $[\{Co_4(OH)_3(PO_4)\}_4(XW_9O_{34})_4]^{28-}$ ($X = P^V$, As^V) and $[\{Co_4(OH)_3(PO_4)\}_4(XW_9O_{34})_4]^{32-}$ ($X = Si^{IV}$, Ge^{IV}) (marked as Co_{14}-PT, Co_{14}-AT, Co_{14}-ST, Co_{14}-GT, respectively). Their structures all incorporate a $\{Co_4O_4\}$ cubane that is structurally similar to the $\{Mn_3CaO_4\}$ core of the oxygen/evolving complex in photosystem II.[38a] Photocatalytic water oxidation experiments in the borate buffer solution in the presence of $S_2O_8^{2-}$ as a sacrificial electron acceptor and $[Ru(bpy)_3]^{2+}$ as a photosensitizer. Upon visible light irradiation, these catalysts indicate high photocatalytic activity for water oxidation and the order of the maximum O_2 evolution is Co_{14}-PT $\leq$ Co_{14}-ST < Co_{14}-AT < Co_{14}-GT (Fig. 20).[38a] In addition, kinetics results of photocatalytic water oxidation indicate that the initial oxygen evolution rates of Co_{14}-ST and Co_{14}-GT in the first 300 s are first order to the concentration of the catalysts with high $[Ru(bpy)_3]^{2+}$ and $S_2O_8^{2-}$ concentrations.[38a] Furthermore, analytical results of laser flash photolysis, dynamic light-scattering, ^{31}P NMR, UV–vis absorption, POM extraction and ICP-MS collectively verify that these cobalt–phosphate molecular catalysts retain their structural integrity during the course of photocatalytic reactions. These findings offer not only a valuable molecular model of the cobalt–phosphate catalysts with well-defined structures, but also a great possibility to adjust and control high-nuclear TMSPTs for visible light-driven water splitting.[38a] Very recently, Ding and co-workers discovered an efficient photocatalyst $[Fe_{11}(H_2O)_{14}(OH)_2(W_3O_{10})_2(\alpha\text{-}SbW_9O_{33})_6]^{27-}$ for both H_2 evolution and O_2 evolution.[43b,c] Firstly, they found that this Fe_{11}-substituted POT is a stable photocatalyst for light driven H_2 evolution activity without any performed co-catalyst. The H_2 evolution rate in this work is 820 μmol h^{-1} g^{-1}, which is higher than that reported for POT photocatalysts.[43b] In the following work, the visible light-driven water oxidation experi-

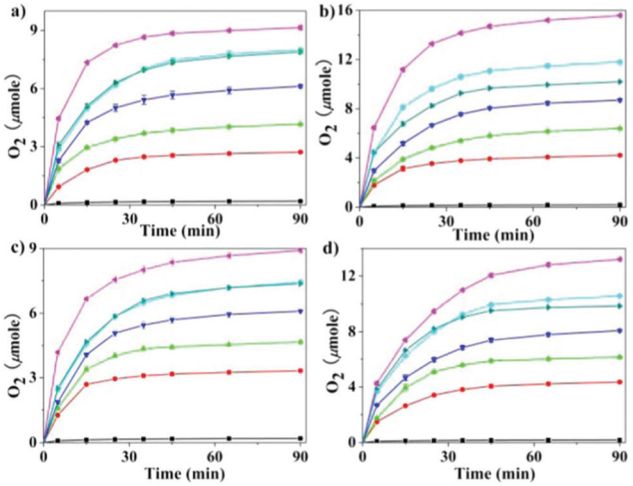

Fig. 20 (a–d) Kinetics of O_2 evolution in the photocatalytic system at different concentrations of Co_{14}-ST, Co_{14}-GT, Co_{14}-PT and Co_{14}-AT. [Concentrations: 0 μM, 3 μM, 5 μM, 10 μM, 15 μM, 20 μM, 30 μM. Conditions: 300 W Xe lamp, 420–800 nm; 1.0 mM $[Ru(bpy)_3]Cl_2$, 5.0 mM $Na_2S_2O_8$, sodium borate buffer pH 9.0 (80 mM); total reaction volume 20 mL; vigorous stirring (1.5×10^3 rpm)] [Fig. 21a–d is reprinted with permission from ref. 38*a*. Copyright 2014 American Chemical Society].

ments of this Fe_{11}-substituted POT were also investigated. The remarkable turn-over number (TON) of 1815 ± 50 and a turn-over frequency ($TOF_{initial}$) of 6.3 s^{-1} prove the efficient photocatalytic water oxidation activity of $[Fe_{11}(H_2O)_{14}(OH)_2(W_3O_{10})_2(\alpha\text{-}SbW_9O_{33})_6]^{27-}$.[43c] These findings not only fill a research gap in designing and developing water-splitting systems aimed at utilization in artificial photosynthetic schemes to enable efficient and sustainable solar fuel conversion and storage, but also offer the feasibility of iron-encapsulated inorganic clusters as efficient water oxidation catalysts, which can motivate the search and exploration of novel high-nuclear TMSPT water oxidation catalysts in the near future.[43b–c]

In addition, high-nuclear TMSPTs can also be applied to the electrocatalytic field.[17a,19a,23b,24d,25d,28c,32,37d] For example, in 2005, Kortz *et al.* reported the remarkable efficiency of the hexa-Fe^{III} substituted tungstogermanate $[Fe_6(OH)_3\text{-}(A\text{-}\alpha\text{-}GeW_9O_{34}(OH)_3)_2]^{11-}$ in the electrocatalytic reduction of nitrite, nitric oxide and nitrate.[17a] In 2015, his group probed the electrocatalytic activities of the tetradecanuclear iron(III)-oxo nanocluster $[Fe_{14}O_6(OH)_{13}(P_2W_{15}O_{56})_4]^{31-}$ towards O_2, H_2O_2, NO_3^- and NO in pH = 2 $Li_2SO_4 + H_2SO_4$ media, which indicate that this iron(III)-oxo nanocluster is effective for electrocatalytic reduction of O_2, H_2O_2, NO_3^- and NO.[37d] Furthermore, Cronin *et al.* also explored the interaction of a Keggin-based trimeric aggregate $[Rb \subset (GeW_{10}Mn_2O_{38})_3]^{17-}$ and a Wells–Dawson-based trimeric aggregate $[K \subset (P_2W_{16}Co_2O_{60})_3]^{23-}$ with nitrite in aqueous solution.[24d] Upon addition of $NaNO_2$, the cathodic currents of the second and third wave of both trimeric aggregates are apparently enhanced whereas the corresponding anodic currents decrease, which demonstrates their remarkable electrocatalytic behavior against the nitrite anion.[24d]

4. Conclusions and outlook

With the rapid explosion of the number of high-nuclear TMSPTs, TMSPT chemistry will enter into a new development stage. This perspective article has systematically compiled some important results on high-nuclear TMSPTs in the past decade with an emphasis on synthetic approaches, structural features and some selected properties. Undoubtedly, these neoteric high-nuclear TMSPTs not only enrich the structural chemistry and combinatorial chemistry of TMSPTs and contribute some meaningful and enlightening clues for exploring and preparing much more high-nuclear TMSPT-based new materials with innovative structures and interesting functionalities, but also to a larger extent establish and consolidate the dominating position of the TMSPT subfamily in the forefront of POM chemistry. However, although the Mn_{40}-substituted POT with the highest TM ions and the highest POM fragments per molecular unit to date has already been reported, the pursuit of discovering TMSPTs with much higher nuclearity of TM centers will never stagnate. Herein, some personal insights in exploiting much higher nuclear TMSPTs are supplied as follows. We hope that our humble opinions will provide some beneficial assistance for researchers who want to be dedicated to the field of TMSPTs even POMs.

(a) It is obvious that the adaptive POM precursors are always highly negative charged, but sometimes they still failed to meet the enormous requirements of negative charge in constructing higher nuclear TMSPTs with oligomeric, polymeric or extended structures. Therefore, appropriate multi-functional organic ligands (such as polycarboxylate ligands, *etc.*) or acid anions (such as AsO_3^{2-}, CO_3^{2-}, *etc.*) should be introduced to effectively increase the negative charges of the system, which will facilitate more TM ions and multi-functional organic ligands or acid anions to simultaneously insert to the skeletons of the resulting TMSPTs. This useful strategy has been already confirmed by Yang's illuminating work in POMOFs constructed from Ni_6-substituted Keggin POT units and carboxylate connectors and cubic POM–organic molecular cage,[12d,44] Niu's sandwich-type Cu_9-substituted arsenotungstate,[20d] and some carbonate including Ni_7^{II}-, Co_8^{II}- and Ni_9^{II}-substituted POTs.[17c,19] However, this useful strategy will still keep the great vitality in constructing high-nuclear TMSPTs in the following several years. Especially, judicious selection of appropriate multi-functional organic ligands will become increasingly important in designing and preparing organic–inorganic hybrid high-nuclear TMSPTs with special functionalities.

(b) In the in-depth exploration of high-nuclear TMSPTs, the step-by-step assembly strategy involving the targeted combination of adaptive lacunary POM precursors with preformed TM clusters is worthy of systematically exploring. In some cases, even if the structures of preformed TM clusters or POM precursors cannot be retained in the reaction procedures, but

in situ formed active species will provide excellent opportunities for creating novel TMSPTs. Sometimes, the step-by-step assembly reaction of preformed TM clusters with simple oxometalate (Na_2WO_4) can induce the more flexible assembly ability of simple oxometalate in the surrounding TM cluster cores, which is extremely conducive to the *in situ* generation of higher nuclear TMSPTs. On the other hand, the one-pot reaction of simple starting materials (TM ions, Na_2WO_4 and some auxiliary components) has been developed as one of the most flexible synthetic strategies in current synthetic chemistry, especially in the construction of high-nuclear POMs with nanosized shapes, which has been exemplified by Cronin's series of reports.[42a,43d,55] Thus, this strategy should be widely used in the synthesis of higher nuclear TMSPTs. With regard to this strategy, it should be pointed out that the selection of heteroatom sources with lone electron pair stereochemical effect can prevent the formation of saturated POM fragments offering the enormous probability of inserting TM centers to the POM skeletons.

(c) During the past decade, the most robust and efficient CASSM has been extensively employed in preparing TMSPTs and numerous merits have been stated in the Introduction. Meanwhile, the rational reactions of POM precursors with TM ions by HSM have also led to some innovative research fruits. However, new synthetic methods with unique advantages should be employed such as (i) the "superheating" microwave synthesis method, (ii) mixed solvent diffusion method, (iii) ionothermal synthesis method, (iv) solid-phase synthesis method, which may promote the discovery of higher nuclear TMSPTs.

Abbreviations

POM	Polyoxometalate
POT	Polyoxotungstate
POA	Polyoxoanion
TM	Transition-metal
SMM	Single molecule magnet
SBU	Secondary building unit
SDA	Structure-directing agent
SSA	Structure-stabilizing agent
en	Ethylenediamine
enMe	1,2-Diaminopropane
ST	Silicotungstate
PT	Phosphotungstate
dien	Diethylenetriamine
GT	Germanotungstate
Tris1	Tris(hydroxymethyl)aminomethane
Tris2	Pentaerythritol
Tris3	Dipentaerythritol
Tris4	Tripentaerythritol
oeen	*N*-(2-Hydroxyethyl)enediamine
tran	1,4,7-Triazonane
AT	Arsenotungstate
POMOF	POM–organic framework
CASSM	Conventional aqueous solution synthesis method
HSM	Hydrothermal synthesis method
H_5Ale	Alendronic acid
2,2′-bipy	2,2′-Bipyridine
phen	1,10-Phenanthroline
ITSM	Ionothermal synthesis method
IL	Ionic liquids
EMIM	1-Ethyl-3-methylimidazolium
bhep	*N*,*N*′-Bis(2-hydroxyethyl) piperazine
EPR	Electron paramagnetic resonance
Mn_{12}-acetate	$[Mn_8^{III}Mn_4^{IV}(CH_3COO)_{16}(H_2O)_4O_{12}]\cdot 4H_2O\cdot 2CH_3COOH$
BTC	1,3,5-Benzenetricarboxylate
dc	Directing current
ac	Alternating current

Acknowledgements

This work was supported by the Natural Science Foundation of China (21301049, U1304208, 21571048), Program for Science & Technology Innovation Talents in Universities of Henan Province (16HASTIT001), the Natural Science Foundation of Henan Province (142300410451), the Postdoctoral Foundation of Henan Province, 2014 Special Foundation for Scientific Research Project of Henan University (XXJC20140001), 2012 Young Backbone Teachers Foundation from Henan Province (2012GGJS-027) and the Students Innovative Pilot Plan of Henan University (15NA002).

Notes and references

1 L. Cronin and A. Müller, *Chem. Soc. Rev.*, 2012, **41**, 7333.
2 J. Berzelius, *Ann. Phys. Chem.*, 1826, **82**, 369.
3 (*a*) A. Müller and F. Peters, *Chem. Rev.*, 1998, **98**, 239; (*b*) M. T. Pope and A. Müller, *Angew. Chem., Int. Ed. Engl.*, 1991, **30**, 34; (*c*) B. S. Bassil and U. Kortz, *Z. Anorg. Allg. Chem.*, 2010, **636**, 2222; (*d*) S. Reinoso, *Dalton Trans.*, 2011, **40**, 6610.
4 D. L. Long and L. Cronin, *Chem. – Eur. J.*, 2006, **12**, 3698.
5 (*a*) T. B. Liu, E. Diemann, H. L. Li, A. W. M. Dress and A. Müller, *Nature*, 2003, **426**, 59; (*b*) D. Volkmer, B. Bredenkotter, J. Tellenbroker, P. Kögerler, D. G. Kurth, P. Lehmann, H. Schnablegger, D. Schwahn, M. Piepenbrink and B. Krebs, *J. Am. Chem. Soc.*, 2002, **124**, 10489; (*c*) S. Q. Liu, H. Mohwald, D. Volkmer and D. G. Kurth, *Langmuir*, 2006, **22**, 1949; (*d*) S. Q. Liu, D. G. Kurth, H. Mohwald and D. Volkmer, *Adv. Mater.*, 2002, **14**, 225; (*e*) E. Coronado, C. Gimenez-Saiz and C. J. Gomez-Garcia, *Coord. Chem. Rev.*, 2005, **249**, 1776; (*f*) T. Yamase, *J. Mater. Chem.*, 2005, **15**, 4773; (*g*) R. J. Errington, S. S. Petkar, B. R. Horrocks, A. Houlton, L. H. Lie and S. N. Patole, *Angew. Chem., Int. Ed.*, 2005, **44**, 1254; (*h*) S. Q. Liu, D. G. Kurth and D. Volkmer, *Chem. Commun.*, 2002, 976; (*i*) M. V. Vasylyev and R. Neumann,

J. Am. Chem. Soc., 2004, **126**, 884; (*j*) I. M. Mbomekalle, B. Keita, L. Nadjo, P. Berthet, K. I. Hardcastle, C. L. Hill and T. M. Anderson, *Inorg. Chem.*, 2003, **42**, 1163; (*k*) M. Luban, F. Borsa, S. Bud'ko, P. C. Canfield, S. Jun, J. K. Jung, P. Kögerler, D. Mentrup, A. Müller, R. Modler, D. Procissi, B. J. Suh and M. Torikachvili, *Phys. Rev. B: Condens. Matter*, 2002, **66**, 054407; (*l*) K. Kamata, K. Yonehara, Y. Sumida, K. Yamaguchi and N. Mizuno, *Science*, 2003, **300**, 964; (*m*) A. M. Khenkin and R. Neumann, *J. Am. Chem. Soc.*, 2002, **124**, 4198.

6 Y. Z. Li, J. Luo, L. J. Chen and J. W. Zhao, *RSC Adv.*, 2014, **4**, 50679.

7 V. E. Simmons and L. C. W. Baker, *Proc. VII I.C.C.C., Stockholm*, 1962, 195.

8 (*a*) M. T. Pope, *Compr. Coord. Chem. II*, 2003, **4**, 635; (*b*) C. L. Hill, *Compr. Coord. Chem. II*, 2003, **4**, 679; (*c*) J. J. Borras-Almenar, E. Coronado, A. Müller and M. T. Pope, *Polyoxometalate Molecular Science*, Kluwer, Dordrecht, The Netherlands, 2004.

9 S.-T. Zheng and G.-Y. Yang, *Chem. Soc. Rev.*, 2012, **41**, 7623.

10 D.-L. Long, E. Burkholder and L. Cronin, *Chem. Soc. Rev.*, 2007, **36**, 105.

11 (*a*) N. Haraguchi, Y. Okaue, T. Isobe and Y. Matsuda, *Inorg. Chem.*, 1994, **33**, 1015; (*b*) P. J. Domaille, *Inorganic Syntheses*, John Wiley and Sons, New York, 1990, vol. 27, p. 101; (*c*) A. Tézé and G. Hervé, *Inorganic Syntheses*, John Wiley and Sons, New York, 1990, vol. 27, p. 88; (*d*) N. H. Nsouli, B. S. Bassil, M. H. Dickman, U. Kortz, B. Keita and L. Nadjo, *Inorg. Chem.*, 2006, **45**, 3858; (*e*) U. Kortz, M. G. Savelieff, B. S. Bassil and M. H. Dickman, *Angew. Chem., Int. Ed.*, 2001, **40**, 3384; (*f*) P. J. Domaille, *Inorganic Syntheses*, John Wiley and Sons, New York, 1990, vol. 27, 100; (*g*) G. Hervé and A. Tézé, *Inorg. Chem.*, 1977, **16**, 2115; (*h*) A. J. Gaunt, I. Maya, R. Copping, A. I. Bhatt, D. Collison, O. D. Fox, K. T. Holman and M. T. Pope, *Dalton Trans.*, 2003, 3009; (*i*) C. Tourné, A. Revel, G. Tourné and M. Vendrell, *C. R. Seances Acad. Sci., Ser. C*, 1973, **277**, 643; (*j*) M. Bosing, I. Loose, H. Pohlmann and B. Krebs, *Chem. – Eur. J.*, 1997, **3**, 1232; (*k*) B. Botar, T. Yamase and E. Ishikawa, *Inorg. Chem. Commun.*, 2000, **3**, 579; (*l*) R. G. Finke, M. W. Droege and P. J. Domaille, *Inorg. Chem.*, 1987, **26**, 3886; (*m*) R. Contant, *Inorganic Syntheses*, John Wiley and Sons, New York, 1990, vol. 27, p. 108; (*n*) R. Contant, *Inorganic Syntheses*, John Wiley and Sons, New York, 1990, vol. 27, p. 110; (*o*) J. Fischer, L. Ricard and R. Weiss, *J. Am. Chem. Soc.*, 1976, **98**, 3050.

12 (*a*) S. T. Zheng, D. Q. Yuan, H. P. Jia, J. Zhang and G. Y. Yang, *Chem. Commun.*, 2007, 1858; (*b*) B. Li, J.-W. Zhao, S.-T. Zheng and G.-Y. Yang, *Inorg. Chem.*, 2009, **48**, 8294; (*c*) J. W. Zhao, H. P. Jia, J. Zhang, S. T. Zheng and G. Y. Yang, *Chem. – Eur. J.*, 2007, **13**, 10030; (*d*) S.-T. Zheng, J. Zhang and G.-Y. Yang, *Angew. Chem., Int. Ed.*, 2008, **47**, 3909.

13 (*a*) B. Li, J.-W. Zhao, S.-T. Zheng and G.-Y. Yang, *Chin. J. Struct. Chem.*, 2009, **28**, 519; (*b*) J.-W. Zhao, J. Zhang, Y. Song, S.-T. Zheng and G.-Y. Yang, *Eur. J. Inorg. Chem.*, 2008, 3809; (*c*) X.-X. Li, S.-T. Zheng, W.-H. Fang and G.-Y. Yang, *Inorg. Chem. Commun.*, 2011, **14**, 1541; (*d*) B. Cai, J.-W. Zhao, B.-F. Yang, H. He and G.-Y. Yang, *J. Cluster Sci.*, 2014, **25**, 1069; (*e*) B. Cai, J.-W. Zhao, B.-F. Yang and H. He, *J. Cluster Sci.*, 2014, **25**, 1047.

14 (*a*) Y.-C. Liu, C.-H. Fu, S.-T. Zheng, J.-W. Zhao and G.-Y. Yang, *Dalton Trans.*, 2013, **42**, 16676; (*b*) X.-X. Li, W.-H. Fang, J.-W. Zhao and G.-Y. Yang, *Chem. – Eur. J.*, 2014, **20**, 17324.

15 (*a*) B. Godin, Y.-G. Chen, J. Vaissermann, L. Ruhlmann, M. Verdaguer and P. Gouzerh, *Angew. Chem., Int. Ed.*, 2005, **44**, 3072; (*b*) R. Contant and A. Tézé, *Inorg. Chem.*, 1985, **24**, 4610; (*c*) T. M. Anderson, X. Zhang, K. I. Hardcastle and C. L. Hill, *Inorg. Chem.*, 2002, **41**, 2477; (*d*) A. Earnshaw and B. N. Figgis, *J. Chem. Soc. A*, 1966, 1656; (*e*) K. Anzenhofer and J. J. De Boer, *Recl. Trav. Chim. Pays-Bas*, 1969, **88**, 286.

16 T. J. R. Weakley, H. T. Jun Evans, J. S. Showell, G. F. Tourné and C. M. Tourné, *J. Chem. Soc., Chem. Commun.*, 1973, 139.

17 (*a*) L.-H. Bi, U. Kortz, S. Nellutla, A. C. Stowe, J. Tol, N. S. Dalal, B. Keita and L. Nadjo, *Inorg. Chem.*, 2005, **44**, 896; (*b*) W.-C. Chen, C. Qin, X.-L. Wang, Y.-G. Li, H.-Y. Zang, Y.-Q. Jiao, P. Huang, K.-Z. Shao, Z.-M. Su and E.-B. Wang, *Chem. Commun.*, 2014, **50**, 13265; (*c*) Z. M. Zhang, Y. G. Li, E. B. Wang, X. L. Wang, C. Qin and H. Y. An, *Inorg. Chem.*, 2006, **45**, 4313; (*d*) C. Ritchie, A. Ferguson, H. Nojiri, H. N. Miras, Y.-F. Song, D.-L. Long, E. Burkholder, M. Murrie, P. Kögerler, E. K. Brechin and L. Cronin, *Angew. Chem., Int. Ed.*, 2008, **47**, 5609; (*e*) C. Lydon, C. Busche, H. N. Miras, A. Delf, D.-L. Long, L. Yellowlees and L. Cronin, *Angew. Chem., Int. Ed.*, 2012, **51**, 2115.

18 (*a*) X. Fang, M. Speldrich, H. Schilder, R. Cao, K. P. O'Halloran, C. L. Hill and P. Kögerler, *Chem. Commun.*, 2010, **46**, 2760; (*b*) X. Fang and P. Kögerler, *Angew. Chem., Int. Ed.*, 2008, **47**, 8123; (*c*) X. Fang and P. Kögerler, *Chem. Commun.*, 2008, 3396; (*d*) X. K. Fang, P. Kögerler, M. Speldrich, H. Schilderb and M. Luban, *Chem. Commun.*, 2012, **48**, 1218; (*e*) H. Moll, A. Dolbecq, J. Marrot, G. Rousseau, M. Haouas, F. Taulelle, G. Rogez, W. Wernsdorfer, B. Keita and P. Mialane, *Chem. – Eur. J.*, 2012, **18**, 3845.

19 (*a*) L. Lisnard, P. Mialane, A. Dolbecq, J. Marrot, J. Clemente-Juan, E. Coronado, B. Keita, P. Oliveira, L. Nadjo and F. Sécheresse, *Chem. – Eur. J.*, 2007, **13**, 3525; (*b*) C. Pichon, P. Mialane, A. Dolbecq, J. Marrot, E. Rivière, B. S. Bassil, U. Kortz, B. Keita, L. Nadjo and F. Sécheresse, *Inorg. Chem.*, 2008, **47**, 11120.

20 (*a*) J. P. Wang, P. T. Ma, Y. Shen and J. Y. Niu, *Cryst. Growth Des.*, 2007, **7**, 603; (*b*) T. Yamase, K. Fukaya, H. Nojiri and Y. Ohshima, *Inorg. Chem.*, 2006, **45**, 7698; (*c*) Z. M. Zhang, E. B. Wang, Y. F. Qi, Y. G. Li, B. D. Mao and Z. M. Su, *Cryst. Growth Des.*, 2007, **7**, 1305; (*d*) Z. Zhou, D. D. Zhang, L. Yang, P. T. Ma, Y. N. Si, U. Kortz, J. Y. Niu and J. P. Wang, *Chem. Commun.*, 2013, **49**, 5189.

21 (*a*) S.-T. Zheng, D.-Q. Yuan, J. Zhang and G.-Y. Yang, *Inorg. Chem.*, 2007, **46**, 4569; (*b*) J.-W. Zhao, C.-M. Wang, J. Zhang, S.-T. Zheng and G.-Y. Yang, *Chem. – Eur. J.*, 2008, **14**, 9223; (*c*) J.-W. Zhao, J. Zhang, S.-T. Zheng and G.-Y. Yang, *Chem. Commun.*, 2008, 570.

22 (*a*) J. P. Wang, J. Du and J. Y. Niu, *CrystEngComm*, 2008, **10**, 972; (*b*) J. P. Wang, P. T. Ma, Y. Shen and J. Y. Niu, *Cryst. Growth Des.*, 2008, **8**, 3130.

23 (*a*) T. M. Anderson, W. A. Neiwert, K. I. Hardcastle and C. L. Hill, *Inorg. Chem.*, 2004, **43**, 7353; (*b*) C. Pichon, P. Mialane, A. Dolbecq, J. Marrot, E. Rivire, B. Keita, L. Nadjo and F. Sécheresse, *Inorg. Chem.*, 2007, **46**, 5292; (*c*) Y.-Y. Zheng, R. Wen, X.-J. Kong, L.-S. Long, R.-B. Huang and L.-S. Zheng, *Dalton Trans.*, 2012, **41**, 9871; (*d*) L. Yang, Y. Huo and J. Y. Niu, *Dalton Trans.*, 2013, **42**, 364.

24 (*a*) B. Botar, Y. V. Geletii, P. Kögerler, D. G. Musaev, K. Morokuma, I. A. Weinstock and C. L. Hill, *J. Am. Chem. Soc.*, 2006, **128**, 11268; (*b*) S. G. Mitchell, P. I. Molina, S. Khanra, H. N. Miras, A. Prescimone, G. J. T. Cooper, R. S. Winter, E. K. Brechin, D.-L. Long, R. J. Cogdell and L. Cronin, *Angew. Chem., Int. Ed.*, 2011, **50**, 9154; (*c*) B. S. Bassil, M. H. Dickman and U. Kortz, *Inorg. Chem.*, 2006, **45**, 2394; (*d*) S. G. Mitchell, S. Khanra, H. N. Miras, T. Boyd, D.-L. Long and L. Cronin, *Chem. Commun.*, 2009, 2712; (*e*) P. I. Molina, H. N. Miras, D.-L. Long and L. Cronin, *Inorg. Chem.*, 2013, **52**, 9284.

25 (*a*) S. G. Mitchell, C. Ritchie, D.-L. Long and L. Cronin, *Dalton Trans.*, 2008, 1415; (*b*) P. Mialane, A. Dolbecq, J. Marrot, E. Rivière and F. Sécheresse, *Chem. – Eur. J.*, 2005, **11**, 1771; (*c*) B. S. Bassil, S. Nellutla, U. Kortz, A. C. Stowe, J. Tol, N. S. Dalal, B. Keita and L. Nadjo, *Inorg. Chem.*, 2005, **44**, 2659; (*d*) S. W. Lin, W. L. Liu, Y. G. Li, Q. Wu, E. B. Wang and Z. M. Zhang, *Dalton Trans.*, 2010, **39**, 1740.

26 (*a*) H.-M. Zhang, Y.-G. Li, Y. Lu, R. Clérac, Z.-M. Zhang, Q. Wu, X.-J. Feng and E.-B. Wang, *Inorg. Chem.*, 2009, **48**, 10889; (*b*) X.-B. Han, Y.-G. Li, Z.-M. Zhang, H.-Q. Tan, Y. Lu and E.-B. Wang, *J. Am. Chem. Soc.*, 2015, **137**, 5486.

27 C. Lydon, M. Sabi, M. D. Symes, D.-L. Long, M. Murrie, S. Yoshii, H. Nojiri and L. Cronin, *Chem. Commun.*, 2012, **48**, 9819.

28 (*a*) Z. Zhang, S. Yao, Y. Li, Y. Wang, Y. Qi and E. Wang, *Chem. Commun.*, 2008, 1650; (*b*) S. Yao, Z. Zhang, Y. Li, Y. Lu, E. Wang and Z. Su, *Cryst. Growth Des.*, 2010, **10**, 135; (*c*) S. Yao, Z. M. Zhang, Y. G. Li and E. B. Wang, *Dalton Trans.*, 2010, **39**, 3884; (*d*) A. S. Assran, N. V. Izarova and U. Kortz, *CrystEngComm*, 2010, **12**, 2684.

29 (*a*) I. M. Mbomekalle, B. Keita, M. Nierlich, U. Kortz, P. Berthet and L. Nadjo, *Inorg. Chem.*, 2003, **42**, 5143; (*b*) M. D. Ritorto, T. M. Anderson, W. A. Neiwert and C. L. Hill, *Inorg. Chem.*, 2004, **43**, 44; (*c*) R. Tong, L. Chen, Y. Liu, B. Liu, G. Xue, H. Hu, F. Fu and J. Wang, *Inorg. Chem. Commun.*, 2010, **13**, 1281; (*d*) J.-D. Compain, P. Mialane, A. Dolbecq, I. Mbomekallé, J. Marrot, F. Sécheresse, E. Rivière, G. Rogez and W. Wernsdorfer, *Angew. Chem., Int. Ed.*, 2009, **48**, 3077.

30 (*a*) N. H. Nsouli, A. H. Ismail, I. S. Helgadottir, M. H. Dickman, J. M. Clemente-Juan and U. Kortz, *Inorg. Chem.*, 2009, **48**, 5884; (*b*) S. G. Mitchell, H. N. Miras, D.-L. Long and L. Cronin, *Inorg. Chim. Acta*, 2010, **363**, 4240; (*c*) J. W. Zhao, Q. X. Han, D. Y. Shi, Li. J. Chen, P. T. Ma, J. P. Wang and J. Y. Niu, *J. Solid State Chem.*, 2011, **184**, 2756.

31 L. J. Chen, D. Y. Shi, J. W. Zhao, Y. L. Wang, P. T. Ma, J. P. Wang and J. Y. Niu, *Cryst. Growth Des.*, 2011, **11**, 1913.

32 (*a*) R. S. Winter, J. M. Cameron and L. Cronin, *J. Am. Chem. Soc.*, 2014, **136**, 12753; (*b*) Z. M. Zhang, Y. F. Qi, C. Qin, Y. G. Li, E. B. Wang, X. L. Wang, Z. M. Su and L. Xu, *Inorg. Chem.*, 2007, **46**, 8162.

33 X. K. Fang and M. Luban, *Chem. Commun.*, 2011, **47**, 3066.

34 S.-T. Zheng, J. Zhang, J. Clemente-Juan, D. Q. Yuan and G. Y. Yang, *Angew. Chem., Int. Ed.*, 2009, **48**, 7176.

35 (*a*) J. W. Zhao, D. Y. Shi, L. J. Chen, P. T. Ma, J. P. Wang and J. Y. Niu, *CrystEngComm*, 2011, **13**, 3462; (*b*) X.-X. Li, S.-T. Zheng, J. Zhang, W.-H. Fang, G.-Y. Yang and J. M. Clemente-Juan, *Chem. – Eur. J.*, 2011, **17**, 13032; (*c*) L. J. Chen, J. W. Zhao, P. T. Ma, Q. X. Han, J. P. Wang and J. Y. Niu, *Inorg. Chem. Commun.*, 2010, **13**, 50.

36 (*a*) S. Mal and U. Kortz, *Angew. Chem., Int. Ed.*, 2005, **44**, 3777; (*b*) S. Mal, B. S. Bassil, M. Ibrahim, S. Nellutla, J. Tol, N. S. Dalal, J. A. Fernández, X. López, J. M. Poblet, R. Ngo Biboum, B. Keita and U. Kortz, *Inorg. Chem.*, 2009, **48**, 11636; (*c*) Z.-J. Liu, Z.-M. Zhang, H. Fu, Y.-G. Li, W.-L. Chen, H.-H. Wu and E.-B. Wang, *Dalton Trans.*, 2012, **41**, 11700; (*d*) A. Müller, M. T. Pope, A. Todea, H. Bögge, J. Slageren, M. Dressel, P. Gouzerh, R. Thouvenot, B. Tsukerblat and A. Bell, *Angew. Chem., Int. Ed.*, 2007, **46**, 4477; (*e*) S. Mal, M. H. Dickman, U. Kortz, A. Todea, A. Merca, H. Bçgge, T. Glaser, A. Müller, S. Nellutla, N. Kaur, J. Tol, N. S. Dalal, B. Keita and L. Nadjo, *Chem. – Eur. J.*, 2008, **14**, 1186.

37 (*a*) J.-W. Zhao, J. Zhang, S.-T. Zheng and G.-Y. Yang, *Inorg. Chem.*, 2007, **46**, 10944; (*b*) C. Pichon, A. Dolbecq, P. Mialane, J. Marrot, E. Riviere and F. Sécheresse, *Dalton Trans.*, 2008, 71; (*c*) P. I. Molina, H. N. Miras, D.-L. Long and L. Cronin, *Dalton Trans.*, 2014, **43**, 5190; (*d*) M. Ibrahim, A. Haider, Y. X. Xiang, B. S. Bassil, A. M. Carey, L. Rullik, G. B. Jameson, F. Doungmene, I. M. Mbomekalé, P. de Oliveira, V. Mereacre, G. E. Kostakis, A. K. Powell and U. Kortz, *Inorg. Chem.*, 2015, **54**, 6136.

38 (*a*) X.-B. Han, Z.-M. Zhang, T. Zhang, Y.-G. Li, W. B. Lin, W. S. You, Z.-M. Su and E.-B. Wang, *J. Am. Chem. Soc.*, 2014, **136**, 5359; (*b*) M. Ibrahim, Y. H. Lan, B. S. Bassil, Y. X. Xiang, A. Suchopar, A. K. Powell and U. Kortz, *Angew. Chem., Int. Ed.*, 2011, **50**, 4708.

39 Q. Wu, Y.-G. Li, Y.-H. Wang, E.-B. Wang, Z.-M. Zhang and R. Clérac, *Inorg. Chem.*, 2009, **48**, 1606.

40 (*a*) B. S. Bassil, U. Kortz, A. S. Tigan, J. M. Clemente-Juan, B. Keita, P. Oliveira and L. Nadjo, *Inorg. Chem.*, 2005, **44**, 9360; (*b*) R. S. Winter, J. Yan, C. Busche, J. S. Mathieson, A. Prescimone, E. K. Brechin, D.-L. Long and L. Cronin, *Chem. – Eur. J.*, 2013, **19**, 2976.

41 A. Müller, S. Sarkar, S. Q. N. Shah, H. Bögge, M. Schmidtmann, S. Sarkar, P. Kögerler, B. Hauptfleisch, A. X. Trautwein and V. Shnemann, *Angew. Chem., Int. Ed.*, 1999, **38**, 3238.

42 (*a*) J. M. Cameron, J. Gao, D.-L. Long and L. Cronin, *Inorg. Chem. Front.*, 2014, **1**, 178; (*b*) G. Rousseau, O. Oms, A. Dolbecq, J. Marrot and P. Mialane, *Inorg. Chem.*, 2011, **50**, 7376; (*c*) L. Huang, J. Zhang, L. Cheng and G.-Y. Yang, *Chem. Commun.*, 2012, **48**, 9658.

43 (*a*) B. S. Bassil, M. Ibrahim, R. Al-Oweini, M. Asano, Z. X. Wang, J. Tol, N. S. Dalal, K.-Y. Choi, R. Biboum, B. Keita, L. Nadjo and U. Kortz, *Angew. Chem., Int. Ed.*, 2011, **50**, 5961; (*b*) X. Q. Dua, J. L. Zhao, J. Q. Mi, Y. Ding, P. P. Zhou, B. C. Ma, J. W. Zhao and J. Song, *Nano Energy*, 2015, **16**, 247; (*c*) X. Q. Du, Y. Ding, F. Y. Song, B. C. Ma, J. W. Zhao and J. Song, *Chem. Commun.*, 2015, **51**, 13925; (*d*) C. H. Zhan, J. M. Cameron, J. Gao, J. W. Purcell, D.-L. Long and L. Cronin, *Angew. Chem., Int. Ed.*, 2014, **53**, 10362; (*e*) L. Huang, S.-S. Wang, J.-W. Zhao, L. Cheng and G.-Y. Yang, *J. Am. Chem. Soc.*, 2014, **136**, 7637; (*f*) C. Ritchie, T. Boyd, D.-L. Long, E. Ditzel and L. Cronin, *Dalton Trans.*, 2009, 1587.

44 S.-T. Zheng, J. Zhang, X.-X. Li, W.-H. Fang and G.-Y. Yang, *J. Am. Chem. Soc.*, 2010, **132**, 15102.

45 X. K. Fang, P. Kögerler, Y. Furukawa, M. Speldrich and M. Luban, *Angew. Chem., Int. Ed.*, 2011, **50**, 5212.

46 S. G. Mitchell, C. Streb, H. N. Miras, T. Boyd, D.-L. Long and L. Cronin, *Nat. Chem.*, 2010, **2**, 308.

47 (*a*) J. M. Clemente-Juan, E. Coronade, A. Forment-Aliaga, J. R. Galán-Mascarós, C. Giménez-Saiz and C. J. Gómez-García, *Inorg. Chem.*, 2004, **43**, 2689; (*b*) N. Zamstein, A. Tarantul and B. Tsukerblat, *Inorg. Chem.*, 2007, **46**, 8851; (*c*) C. Pichon, P. Mialane, E. Rivière, G. Blain, A. Dolbecq, J. Marrot, F. Sécheresse and C. Duboc, *Inorg. Chem.*, 2007, **46**, 7710; (*d*) A. Dolbecq, E. Dumas, C. R. Mayer and P. Mialane, *Chem. Rev.*, 2010, **110**, 6009; (*e*) J. M. Clemente-Juan, E. Coronado and A. Gaita-Ariño, *Chem. Soc. Rev.*, 2012, **41**, 7464; (*f*) D. Gatteschi and R. Sessoli, *Angew. Chem., Int. Ed.*, 2003, **42**, 268.

48 J. Lehmann, A. Gaita-Arino, E. Coronado and D. Loss, *Nat. Nanotechnol.*, 2007, **2**, 312.

49 (*a*) J. A. Bertrand, A. P. Ginsberg, R. I. Kaplan, C. E. Kirkwood, R. L. Martin and R. C. Sherwood, *Inorg. Chem.*, 1971, **10**, 240; (*b*) V. H. Crawford, H. V. Richardson, J. R. Wason, D. J. Hodgson and W. E. Hatfield, *Inorg. Chem.*, 1976, **15**, 2107; (*c*) L. Merz and W. Haase, *J. Chem. Soc., Dalton Trans.*, 1980, 875; (*d*) M. Handa, N. Koga and S. Kida, *Bull. Chem. Soc. Jpn.*, 1988, **61**, 3853.

50 J. Ribas, A. Escuer, M. Monfort, R. Vicente, R. Cortés, L. Lezama and T. Rojo, *Coord. Chem. Rev.*, 1999, **193–195**, 1027.

51 S. Piligkos, E. Bill, D. Collison, E. J. L. McInnes, G. A. Timco, H. Weihe, R. E. P. Winpenny and F. Neese, *J. Am. Chem. Soc.*, 2007, **129**, 760.

52 (*a*) Y. Izumi, K. Matsuo and K. Urabe, *J. Mol. Catal.*, 1983, **18**, 299; (*b*) I. V. Kozhevnikov, *Chem. Rev.*, 1998, **98**, 171; (*c*) S.-S. Wang and G.-Y. Yang, *Chem. Rev.*, 2015, **115**, 4893.

53 (*a*) L. F. Chen, J. C. Hu, S. Mal, U. Kortz, H. Jaensch, G. Mathys and R. M. Richards, *Chem. – Eur. J.*, 2009, **15**, 7490.

54 Y. H. Guo and C. W. Hu, *J. Mol. Catal. A: Chem.*, 2007, **262**, 136.

55 (*a*) J. Gao, J. Yan, S. Beeg, D.-L. Long and L. Cronin, *J. Am. Chem. Soc.*, 2013, **135**, 1796; (*b*) J. Yan, J. Gao, D.-L. Long, H. N. Miras and L. Cronin, *J. Am. Chem. Soc.*, 2010, **132**, 11410.

